NASA/TP—2018–219855

Summary Report on Phase I and Phase II Results From the 3D Printing in Zero-G Technology Demonstration Mission, Volume II

T.J. Prater and N.J. Werkheiser
Marshall Space Flight Center, Huntsville, Alabama

F.E. Ledbetter III
Wheelhouse Consulting, LLC, Marshall Space Flight Center, Huntsville, Alabama

March 2018

The NASA STI Program…in Profile

Since its founding, NASA has been dedicated to the advancement of aeronautics and space science. The NASA Scientific and Technical Information (STI) Program Office plays a key part in helping NASA maintain this important role.

The NASA STI Program Office is operated by Langley Research Center, the lead center for NASA's scientific and technical information. The NASA STI Program Office provides access to the NASA STI Database, the largest collection of aeronautical and space science STI in the world. The Program Office is also NASA's institutional mechanism for disseminating the results of its research and development activities. These results are published by NASA in the NASA STI Report Series, which includes the following report types:

- TECHNICAL PUBLICATION. Reports of completed research or a major significant phase of research that present the results of NASA programs and include extensive data or theoretical analysis. Includes compilations of significant scientific and technical data and information deemed to be of continuing reference value. NASA's counterpart of peer-reviewed formal professional papers but has less stringent limitations on manuscript length and extent of graphic presentations.

- TECHNICAL MEMORANDUM. Scientific and technical findings that are preliminary or of specialized interest, e.g., quick release reports, working papers, and bibliographies that contain minimal annotation. Does not contain extensive analysis.

- CONTRACTOR REPORT. Scientific and technical findings by NASA-sponsored contractors and grantees.

- CONFERENCE PUBLICATION. Collected papers from scientific and technical conferences, symposia, seminars, or other meetings sponsored or cosponsored by NASA.

- SPECIAL PUBLICATION. Scientific, technical, or historical information from NASA programs, projects, and mission, often concerned with subjects having substantial public interest.

- TECHNICAL TRANSLATION. English-language translations of foreign scientific and technical material pertinent to NASA's mission.

Specialized services that complement the STI Program Office's diverse offerings include creating custom thesauri, building customized databases, organizing and publishing research results…even providing videos.

For more information about the NASA STI Program Office, see the following:

- Access the NASA STI program home page at <http://www.sti.nasa.gov>

- E-mail your question via the Internet to <help@sti.nasa.gov>

- Phone the NASA STI Help Desk at 757–864–9658

- Write to:
  NASA STI Information Desk
  Mail Stop 148
  NASA Langley Research Center
  Hampton, VA 23681–2199, USA

NASA/TP—2018–219855

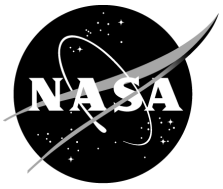

Summary Report on Phase I and Phase II Results From the 3D Printing in Zero-G Technology Demonstration Mission, Volume II

T.J. Prater and N.J. Werkheiser
Marshall Space Flight Center, Huntsville, Alabama

F.E. Ledbetter III
Wheelhouse Consulting, LLC, Marshall Space Flight Center, Huntsville, Alabama

National Aeronautics and
Space Administration

Marshall Space Flight Center • Huntsville, Alabama 35812

March 2018

Acknowledgments

The authors would like to acknowledge the following personnel at NASA Marshall Space Flight Center for leading the testing effort for the 3D Printing in Zero-G Technology Demonstration Mission: Dr. Ron Beshears and Dr. Terry Rolin (computed topography analysis), Cameron Bosley, Howard Gibson, and Catherine Bell (mechanical testing), John Ivester (structured light scanning), and Ellen Rabenberg and Dr. Richard Grugel (microscopy).

TRADEMARKS

Available from:

NASA STI Information Desk
Mail Stop 148
NASA Langley Research Center
Hampton, VA 23681–2199, USA
757–864–9658

This report is also available in electronic form at
<http://www.sti.nasa.gov>

TABLE OF CONTENTS

TABLE OF CONTENTS (Continued)

LIST OF FIGURES

LIST OF FIGURES (Continued)

LIST OF FIGURES (Continued)

LIST OF FIGURES (Continued)

LIST OF FIGURES (Continued)

LIST OF FIGURES (Continued)

LIST OF TABLES

LIST OF TABLES (Continued)

LIST OF ABBREVIATIONS AND ACRONYMS

3DP	three-dimensional printer
ABS	acrylonitrile butadiene styrene
AMF	Additive Manufacturing Facility
ANOVA	analysis of variance
ASTM	American Society of Materials Testing
ATR	attenuated total reflectance
BSE	backscatter electron
CAD	computer-aided design
CT	computed tomography
ETU	engineering test unit
FDM	fused deposition modeling
FTIR	Fourier transform infrared spectroscopy
IR	infrared
ISM	in-space manufacturing
ISS	International Space Station
LED	light-emitting diode
MSFC	Marshall Space Flight Center
MSG	Microgravity Science Glovebox
SBIR	Small Business Innovative Research
SEM	scanning electron microscopy

TP	Technical Publication
UTS	ultimate tensile strength
zero-G	zero gravity

NOMENCLATURE

E	modulus of elasticity
n	number
z	build direction
ρ	gravimetric density
σ_{max}	maximum stress
σ_{uts}	ultimate tensile strength
σ_{ys}	yield strength

TECHNICAL PUBLICATION

SUMMARY REPORT ON PHASE I AND PHASE II RESULTS FROM THE 3D PRINTING IN ZERO-G TECHNOLOGY DEMONSTRATION MISSION, VOLUME II

1. INTRODUCTION: SUMMARY OF PHASE I OF THE 3D PRINTING IN ZERO-G TECHNOLOGY DEMONSTRATION MISSION

Manufacturing in space is one method proposed to reduce the logistics associated with long-duration human spaceflight and address key challenges of supportability for these extended missions. The International Space Station (ISS) has been continuously crewed since its completion in 2011, but has depended on regular resupply from Earth-based rockets for cargo, spare parts, and consumables. Logistics analyses strongly indicate this model, which depends on increasing reliability of systems and manifesting extensive suites of spares, will not be feasible for the long-duration, long-endurance missions NASA seeks to undertake beyond the proposed decommissioning of the ISS in the 2020s.[1] In these scenarios, cargo resupply is not readily available and a return to Earth in the event of a failure may not be possible. The mass of spares required and the large uncertainty associated with precisely which spares will be needed and when quickly drive up the cost, number of launches, and reliability required for space systems to levels that may not be feasible.[2] Logistics analyses for this class of missions point toward a new logistics paradigm, one where the crew has manufacturing capabilities to supply parts on demand (the space-based equivalent of 'just in time' manufacturing) and adapt rapidly to unforeseen scenarios which otherwise may result in a loss of mission.

1.1 Phase I Objectives and Analysis

The first step in enabling this new paradigm for human spaceflight was taken in 2014, when NASA, in cooperation with Made in Space, Inc., launched the first three-dimensional printer (3DP) to the ISS as part of the 3D Printing in Zero-G Technology Demonstration Mission. The printer, a fused deposition modeling (FDM) system capable of making small parts of acrylonitrile butadiene styrene (ABS) plastic, was the first proof-of-concept demonstration of three dimensional printing in the space environment. The printer, pictured in figure 1, operated inside the Microgravity Science Glovebox (MSG), which provided containment and air circulation to the outside of the printer and the electronics box. The 3DP from the technology demonstration mission also has its own environmental control unit to provide filtration of air within the printer volume. Following the printer's launch in September 2014 on the SpaceX cargo resupply mission 3, the printer was installed in the MSG and completed its first round of printing operations in November and December 2014. Phase I prints consisted of 42 total specimens: 21 ground prints made with the printer prior to its launch to the ISS (inside the MSG mockup facility at NASA Marshall Space Flight Center (MSFC)) and 21

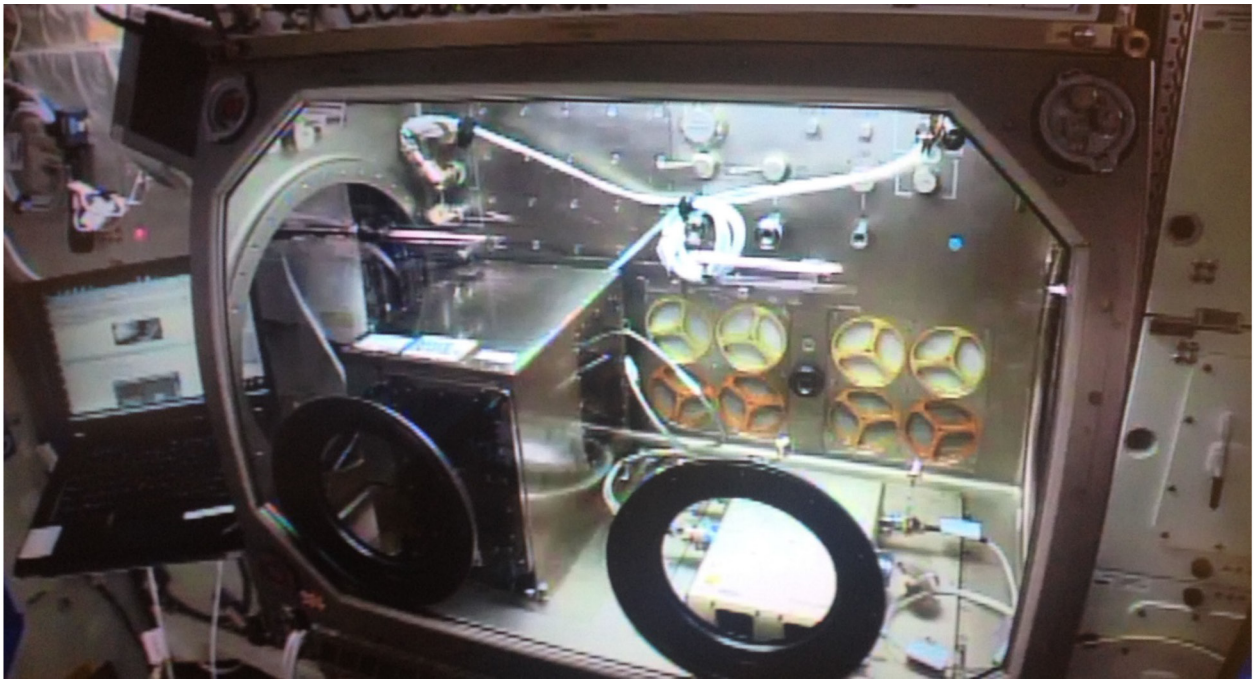

Figure 1. The printer, built and operated by Made in Space, Inc., from the 3D Printing in Zero-G Technology Demonstration Mission. The printer is integrated into the MSG on the ISS.

flight prints completed on orbit during the 2 weeks of operation in 2014. The specimen set consisted of mechanical test coupons (type IV tensile specimens from the American Society of Testing Materials ASTM) D6380-14,[3] standard compression specimens from ASTM D695-15,[4] flexural coupons from ASTM D790[5]), an extruder head casing (a side plate of the extruder which is a replacement part for the printer itself), layer quality specimens (square column specimens used to assess adhesion between successive layers and material structure), range coupons (specimens with holes and features to assess the performance, geometric accuracy, and tolerances of the 3DP unit), and some functional tools (torque tool, crowfoot, structural clip for avionics in CubeSats, a sample container, a wire tie, and a ratchet). The file for the ratchet printed on orbit was uplinked to the printer from the ground, demonstrating an important capability for long-duration spaceflight.

The phase I prints were returned to Earth in February 2015 on SpaceX 5 and underwent analysis at MSFC's Materials and Processes Laboratory from April to October 2015. Phase I specimens underwent mass measurement, structured light scanning to assess dimensional differences between analogous flight and ground prints with respect to the specimen's computer-aided design (CAD) geometry, 2D radiography and 3D computed tomography (CT) to examine the internal specimen structures, mechanical testing (for the compression, tensile, and flexure specimens), optical microscopy, and scanning electron microscopy (SEM)). Data and analysis from this test regime are summarized in the Technical Publication (TP), "Summary Report on Phase I Results from the 3D Printing in Zero-G Technology Demonstration Mission, Volume I."[6] Some significant differences in mechanical properties, internal structure, and dimensional variation were noted for the corresponding phase I ground and flight specimen sets. Flight tensile and flexural specimens were significantly denser and stronger than their ground counterparts, while the opposite trend was observed for the

compression specimens. (Flight specimens were weaker than ground specimens.) Some specimens also exhibited a visually apparent change in densification on CT images. This was more pronounced for the flight tensile specimens, where material was denser in the bottom half of the specimen and abruptly changed to a more open structure at approximately the midpoint in the *z* (build) direction. Flight tensile specimens also exhibited more often deviation from the CAD model than the analogous ground specimens.

Potential explanations for these discrepancies (microgravity effects, differences in manufacturing process settings between ground and flight printer operations, and aging of the filament feedstock) were considered and follow-on studies of the phase I specimens were developed to further investigate the potential sources of variability between the ground and flight data sets. The results of these additional analyses, which include Fourier transform infrared spectroscopy (FTIR) to compare functional chemical groups present in the specimens and their relative concentrations and SEM to more closely examine material cross sections, are published in reference 7. FTIR analysis was unable to detect significant chemical differences between the ground- and ISS-manufactured specimens (flight feedstock was 6 months older than ground feedstock at the time of printing) and largely ruled out any aging effects on the observed discrepancies in material performance. SEM analysis of representative material cross sections failed to show differences in filament slump—the degree to which the filament sags under its own weight—between flight and ground specimens and was not, in general, indicative of a substantive microgravity effect on internal material structure (fig. 2). However, comparative SEM analysis noted greater material buildup at the base of the flight tensile specimens (mirrored in the structured light scanning data) and dramatic differences in fiber structure between the ground and flight specimens. These differences are suggestive of differences in the way the ground and flight specimens were manufactured.

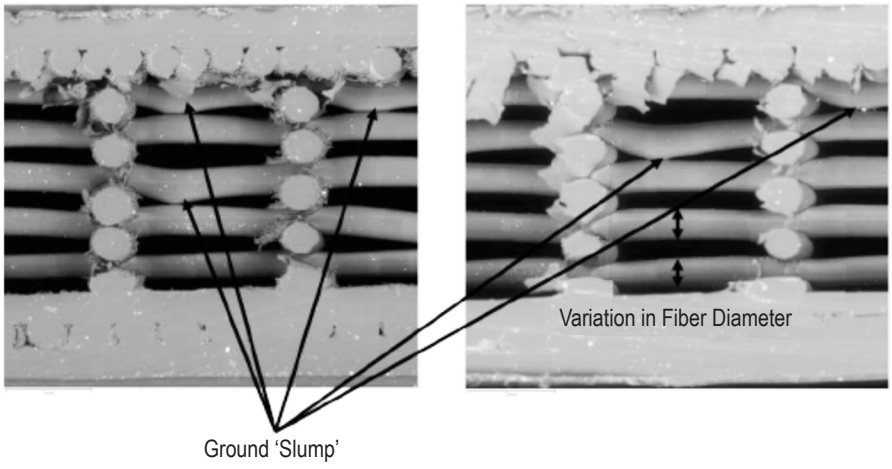

Figure 2. Cut section view comparison of fiber slump for a (a) ground (G001) and (b) flight (F001C) specimen from phase I (image from ref. 7).

1.2 Interim Ground-Based Study of Manufacturing Process Variability Using the Flight Backup Unit

One known source of process variability in the 3DP phase I data set stemmed from differences in the calibration setting for the printer during flight and ground prints. The *z*-calibration value, which in turn determines the distance of the extruder head from the build tray that the extruded material is deposited on, was adjusted based on visual feedback during phase I on-orbit operations of the 3DP unit. This value was held constant for the ground-based prints. Figure 3 illustrates the relationship between the *z*-calibration value—commanded by the user prior to printing—and the extruder standoff distance, the distance from the tip of the extruder to the build tray. The *z*-calibration distance for the ground-manufactured 3DP specimens was held constant at 2.2 mm. For flight prints, this tip-to-tray distance (also referred to as the extruder standoff distance) is not directly measurable since the printer does not have closed-loop positional feedback. The commanded value for the flight prints ranged from 2.39 mm to 2.84 mm. No two flight prints had the same process setting.

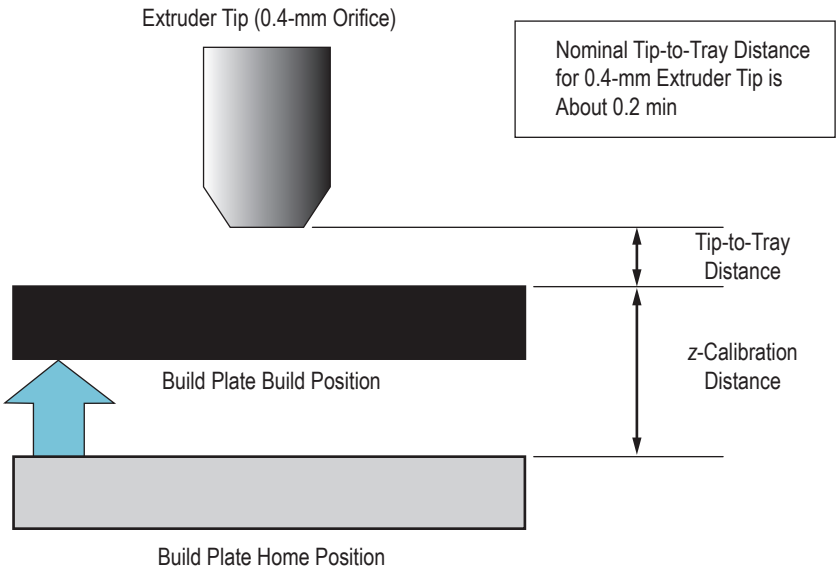

Figure 3. Illustration of relationship between *z*-calibration and extruder standoff distance.

Based on data from structured light scanning (and corroborated by SEM analysis of the phase I prints), the extruder tip was positioned too close to the tray during flight prints, resulting in specimens with protrusions along the geometric boundaries. The discrepancy in this machine setting for ground and flight settings may explain why flight specimens were slightly denser than their ground counterparts in the initial layers, a key finding documented in the phase I results. The extruder standoff distance hypothesis developed based on the 3DP phase I data set postulated that the closer position of the extruder tip to the specimen during flight prints (and subsequent variation of this distance) potentially explains some of the measured variability in material properties for ground and flight specimens. While no consistent correlation was detected between the *z*-calibration

value (or the subsequently derived tip-to-tray distance) and density or mechanical properties for the flight prints, literature on manufacturing process optimization for FDM indicates this distance is a parameter which influences thermal flow and cooling rate, deposition rate, and interlayer configuration. Rodriguez et al. found significant changes in stiffness and strength of materials produced with FDM as a result of small variations in process parameters during the extrusion process.[8] Variation in processing conditions are closely linked to variations in microstructure, which can in turn exert immense influence over mechanical performance of the resulting part.[9]

In the time between phase I and phase II prints on the ISS, a separate study was undertaken using the engineering test unit (ETU), the flight-like unit for 3DP. A matrix of tensile coupons, layer quality specimens, and compression coupons were printed at *z*-calibration values which encompass the ground and flight operational settings of 3DP phase I. A series of multiple prints was performed at four distinct manufacturing process settings:

(1) Optimal calibration. The 'Goldilocks' extruder standoff distance for a particular specimen geometry.

(2) –0.02 mm. The build tray is moved –0.02 mm downward from its optimal setting, resulting in a print where the extruder is slightly too far away from the specimen, mimicking the manufacturing process settings for phase I ground prints.

(3) 0.05 mm. The build tray is translated 0.05 mm upward from its optimal setting, resulting in a print where the extruder is slightly too close to the specimen.

(4) 0.1 mm. The build tray is moved 0.1 mm upward from its optimal setting, resulting in a print where the extruder is much too close to the specimen. This condition is closest to the flight print settings for phase I.

Tensile, compression, and layer quality specimens produced at each setting were compared with other specimens in their respective geometry class. The extruder standoff distance study was not a precise replicate of ground or flight operations of 3DP, but an attempt to broadly recreate the ground and flight manufacturing conditions and evaluate the sensitivity of material outcomes to changes in this process setting. Print trays must be periodically replaced due to material adhesion over the course of a series of builds; e.g., four print tray changes took place during the printing of the 21 flight parts for 3DP phase I operations. Tray-to-tray surface variability and differences in the extruder are variables that will slightly change the *z*-calibration value. To compound these issues, *z*-calibration can also vary based on the location of the specimen on the print tray. The trays themselves are not flat and, in some instances, extruded material tends to fill the grooves of the tray, making it harder for the part to adhere and artificially decreasing the tip-to-tray distance. These issues are inherent limitations of the 3DP hardware and difficult to control without substantial modifications/upgrades to both the flight and ground units.

Despite the aforementioned limitations, the results of the study, summarized in reference 10, indicated that the position of the extruder tip relative to the build plate does impact the structure and properties of the tensile specimens to some extent. Overall, ultimate tensile strength (UTS) and

elastic modulus improve as the specimens are built closer to the extruder tip. This finding mirrors the phase I results, where flight specimens built with the extruder closer to the build tray exhibited slightly enhanced mechanical performance relative to the ground prints. SEM analysis, structured light scanning, and CT show protrusions at the base of the tensile specimens made at the closer extruder standoff distances that contribute to an artificial strengthening of the part. These features likely enhance mechanical performance relative to specimens built farther away from the extruder tip, which do not possess reinforcing structural features to align with the load path during tensile testing. Results suggest that discrepancies in tensile performance between flight and ground prints can likely be explained by differences in manufacturing process settings. The reduced extruder standoff distance for the flight prints thus likely resulted in protrusions at the base of the specimen and densification of the lower layers that contribute to enhanced mechanical strength relative to other (ground-manufactured) specimens, a phenomenon which was largely replicated through the ground study.

A clear relationship between extruder standoff distance and material performance in compression was not detected by these experiments. The stronger mechanical behavior noted for the ground prints (built at a greater standoff distance) and comparatively weaker behavior of the flight prints (built at a smaller standoff distance) was not replicated in this data set. Overall results of this study also indicate some build-to-build variability for the ETU, and by extension, the 3DP flight unit. Significant structural differences in the builds across a given manufacturing processing condition were observed; e.g., the layer spacing and internal structural features of the specimen may be different for each sample in a series, despite being made at exactly the same process setting. This creates scatter in the data set.

The full report on the extruder standoff distance study is summarized in NASA TP, "A Ground-Based Study on Extruder Standoff Distance for the 3D Printing in Zero-G Technology Demonstration Mission."[10] Overall, this study is suggestive that variations between the ground and flight specimen sets from phase I are largely an artifact of differences in manufacturing process settings rather than microgravity effects or other factors. The study was intended to provide interim data for assessment until phase II prints—conducted with the flight unit on the ISS—could be tested to provide more definitive data related to sources of variability.

2. PHASE II OF THE TECHNOLOGY DEMONSTRATION MISSION: OBJECTIVES AND OPERATIONS

Phase II operations for the 3D printing in zero-G technology demonstration mission took place between June 28 and July 12, 2016. Results of the phase I data analyses, summarized in NASA/TP—2016–219101[6] and an article published in the *Rapid Prototyping Journal*,[7] were unable to definitively ascertain whether there is an engineering significant effect on properties of materials produced by operating the FDM manufacturing process in microgravity. As discussed in section 1.2, the effect of microgravity in the phase I data set may have been overwhelmed by other variables, such as the distance between the extruder tip and the build plate, which were varied nonsystematically. In phase I, flight operations of the printer, the *z*-calibration value, which in turn drives the tip-to-tray distance, was varied slightly after every print, based on visual feedback.

Since phase I data were inconclusive with regard to microgravity effects, additional specimens were needed to create a more structured data set that, to the greatest extent possible, isolate the impact of microgravity on the FDM process. For phase II prints, the physical distance between the extruder tip and the build plate was locked after printing a calibration coupon to assess the functionality of the printer hardware. Following a series of 25 prints in phase II at an optimal setting, the *z*-calibration value, which drives the tip-to-tray distance, was changed to recreate the 'too close' condition of phase I. Nine additional prints were produced at this suboptimal condition. A separate ground-based study, discussed in section 1.2, was previously undertaken by the in-space manufacturing (ISM) team using the ETU/backup flight unit to quantify the degree to which changes in the extruder standoff distance can explain variability between ground and flight specimens in the phase I data set.[10] Phase II prints will also provide greater insight into the sources of process variability.

Testing of the phase II prints will also assess the extent to which age of the feedstock impacts mechanical properties and part performance. For all specimens produced as part of phases I and II, the filament feedstock used was undyed ABS plastic at 1.75-mm diameter extruded through a 0.4-mm orifice at 230 to 235 °F. In phase I, flight feedstock, while still within the shelf life recommended by the manufacturer, was 6 months older than ground feedstock at the time of printing. FTIR indicated no substantial chemical differences between analogous ground and flight specimens, but the effect of offgassing of feedstock and moisture absorption from exposure to the environment on subsequently measured mechanical properties in the printed part has not been systematically evaluated. While the filament feedstock is stored in a sealed container with desiccant, approximately 4 inches of the feedstock is exposed to the surrounding air as it traverses between the feedstock canister and the printer head. If material aging does impact mechanical properties in the manner observed for the 3DP phase I specimens, aging would be expected to manifest itself in subsequent specimens printed using the same (now older) feedstock as the phase I prints. At the time of phase II prints, the flight feedstock was approximately 18 months older than feedstock for phase I flight prints and 24 months older than the feedstock for phase I ground prints. All feedstocks are the same material and derived from the same manufacturing lot.

Additional data obtained from mechanical testing of phase II tensile and compression specimens will provide insight into whether trends, biases, and characteristic mechanical properties reported based on phase I testing are consistent with further flight operation of the printer. Whether confirmatory or disparate from the original data set, phase II prints will lend additional clarity to sources of variability in the phase I data and identify which concepts/hypotheses are best poised to explain property differences noted between flight and ground specimens. Phase II prints will also enable the ISM team to assess reliability and repeatability of the FDM process using the 3DP hardware and help to define requirements for future printers.

Phase II print operations will help to answer questions related to microgravity effects on the FDM process by implementing better manufacturing process controls, based on lessons learned from phase I operations. 'Locking' the manufacturing process—in particular, control of the extruder standoff distance—will allow the ISM team to better isolate the effect of microgravity on the material produced. Additionally, phase II print operations were needed to fulfill project level III programmatic requirements imposed by the Advanced Exploration Systems program.

2.1 Phase II Print Matrix and Notes on Printer Operations

Table 1 lists the phase II print matrix. Thirty-four total specimens were printed as part of phase II operations: 1 calibration coupon, 14 compression specimens, 7-layer quality (square column) specimens, and 12 tensile specimens. The *z*-offset corresponds to the commanded *z*-calibration value for the hardware. (*z*-calibration distance is the distance between the build plate home position and the commanded position as illustrated in fig. 1.) This value in turn drives the tip-to-tray distance (distance between tip where ABS plastic is extruded and the build surface). For phase II, the initial *z*-calibration value (2.64 mm) was determined to be too close based on visual feedback; the part exhibited protrusions around the edges. A specimen at the 2.54-mm *z*-calibration value was printed using a ground-equivalent printer at Made in Space's Mountain View, CA, facility following this print. Based on visual inspection of this part, the 2.54-mm value was selected for continued operation. The *z*-calibration value of 2.54 mm was used for manufacturing of the next 25 specimens, at which point it was changed back to 2.64 mm. This change was intended to create specimens that mimicked the manufacturing processing conditions of the phase I flight prints, which were built with the extruder tip too close to the build platform. The specimen set built at 2.64 mm will provide greater statistical sampling for the phase I print data set and provide some additional indication as to whether *z*-calibration distance explains some of the variability in the flight and ground specimens observed over the course of phase I specimen testing and evaluation.

Table 1. Phase II operations print matrix.

Specimen ID No.	Part Type	Offsets (*x*,*y*,*z*)			Date	Notes
F022	Calibration coupon	–	–	2.64	6/28/2016	Too close
F024	Compression	–	–	2.54	6/28/2016	Optimal z–calibration
F025	Layer quality specimen	–	–	2.54	6/29/2016	
F026	Tensile	–	–	2.54	6/29/2016	
F027	Compression	–	–	2.54	7/1/2016	
F028	Tensile	–	4	2.54	7/1/2016	
F029	Compression	–	–	2.54	7/1/2016	
F030	Tensile	19	–	2.54	7/2/2016	
F031A	Compression	–20	–	2.54	7/5/2016	
F031B	Compression	20	–	2.54	7/5/2016	
F031C	Compression	–20	45	2.54	7/5/2016	
F032	Tensile	–	4	2.54	7/5/2016	
F033	Tensile	–5	4	2.54	7/6/2016	
F034A	Layer quality specimen	–20	–	2.54	7/6/2016	
F034B	Layer quality specimen	20	–	2.54	7/6/2016	
F034C	Layer quality specimen	–20	43	2.54	7/6/2016	
F035A	Compression	–20	–	2.54	7/6/2016	
F035B	Compression	20	–	2.54	7/6/2016	
F035C	Compression	–20	45	2.54	7/6/2016	
F036	Tensile	–5	–	2.54	7/7/2016	
F037	Tensile	–5	–	2.54	7/7/2016	
F038A	Tensile	–5	4	2.54	7/7/2016	
F038B	Compression	20	15	2.54	7/7/2016	
F039	Tensile	–5	4	2.54	7/8/2016	
F040A	Tensile	–5	4	2.54	7/8/2016	
F040B	Compression	20	15	2.54	7/8/2016	
F041A	Compression	–20	–	2.64	7/11/2016	Too close
F041B	Compression	20	–	2.64	7/11/2016	
F041C	Compression	–20	45	2.64	7/11/2016	
F042A	Layer quality specimen	–20	–	2.64	7/12/2016	
F042B	Layer quality specimen	–20	43	2.64	7/12/2016	
F042C	Layer quality specimen	20	30	2.64	7/12/2016	
F043A	Tensile	–20	–	2.64	7/12/2016	Left on print tray
F043B	Tensile	5	–	2.64	7/12/2016	Left on print tray

In some cases, multiple specimens were produced in the same build. The (x,y) offset indicates the position of a particular part on the build tray. The final two specimens were not separated from the build tray and were downmassed in this condition. Table 2 summarizes the specimen counts for phase II.

Table 2. Specimen summary from phase II operations.

	Total	Optimal *z*-Calibration	Suboptimal *z*-Calibration (too close)
Total calibration coupons	1	–	1
Total tensile coupons	12	10	2
Compression coupons	14	11	3
Layer quality specimens	7	4	3
Total number of samples	34	25	9

2.2 Overview of Test Plan for Phase II Samples

The phase II flight samples underwent several phases of testing following their receipt at MSFC. These included photographic/visual inspection, mass measurement, structured light scanning, 2D x-ray and 3D CT, optical microscopy, SEM, mechanical testing, and FTIR. Nondestructive tests are a precursor to destructive testing. Then possible, sets of specimens were processed in parallel to expedite testing. This approach proved effective for phase I and was also followed for phase II.

Table 3 summarizes the data obtained from each test and the specific questions from the 3D Printing in Zero-G Technology Demonstration Mission phase I results addressed by each test. Phase II prints are intended to ascertain whether differences noted in phase I prints between flight and ground specimens were a result of microgravity effects on the FDM process, the difference in age of the feedstock material, and/or differences in processing conditions between ground and flight prints. While additional analysis of 3DP flight and ground specimens (published in ref. 7) and subsequent ground-based studies using a ground-equivalent printer are not suggestive of an engineering significant microgravity effect,[10] phase II prints, with greater manufacturing process controls, are better poised to provide definitive insight into this question.

Table 3. Data obtained and open question(s) addressed with each test.

Test	Data Obtained	Questions Addressed
Photographic/visual inspection	Identification of interesting physical features or damage to specimens	Part damage due to overadhesion to build tray and subsequent removal
Mass measurement	Mass of specimen used to calculate gravimetric density	Variations in density observed between flight and ground specimens for phase I (both magnitude of difference and bias between ground and flight)
Structured light scanning	Measurement of closed part volume used in density calculation; geometric variation of specimen from CAD model; geometric variations between specimens of the same type	Greater deviation in circularity observed for flight compression specimens from phase I; greater protrusions/larger base buildup observed for some flight specimens relative to ground from phase I; manufacturing repeatability of 3DP hardware
CT	Density of specimen that can be compared against gravimetric density derived from mass measurement and structured light scanning as well as bulk (injection molded) ABS; qualitative assessment of internal structure; size and frequency of voids	Density variation in through thickness of parts noted from phase I; density variation between ground and flight specimens from phase I
Optical microscopy	Layer height, features of interest or evidence of damage to specimens	Features or part damage that may influence results of mechanical test
Tensile test (ASTM D638)	Ultimate strength, elastic modulus, elongation to failure	Property variation between and within ground and flight specimen sets from phase I
Compression test (ASTM D695)	Compressive strength, compressive modulus	Property variation between and within ground and flight specimen sets from phase I
SEM	Layer height, differences in internal structure, pore sizes	Microgravity effects; source of differences in densification, internal structure, and fracture surfaces noted for ground and flight prints from phase I
FTIR	Presence and relative concentration of functional chemical groups present in the specimen	Chemical changes in feedstock and printed part (potentially due to aging)

It is important to note that there are no pass/fail criteria for these test samples. All specimens for phase II are flight samples. Unlike phase I, there were no ground-printed samples to directly compare against for this phase of operations. The phase I ground prints, made using the printer in the MSG ground-based facility prior to the hardware's launch to the ISS, represent the closest analog. The data obtained from the phase II samples will be compared against data from the phase I flight and ground samples with the knowledge that the manufacturing process settings across these data sets are not entirely consistent.

Table 4 identifies which samples underwent specific tests. Information on specific test procedures is detailed in subsequent sections of this TP. All specimens underwent photographic and visual inspection after being unboxed and the mass of each specimen is measured using a precision scale in the metrology laboratory. A representative mass value is used in conjunction with the closed volume of the part obtained from structured light scanning to calculate the part's gravimetric density. All specimens were structured light scanned to obtain a closed volume estimate for the part and derive a density value. A subset of the specimens were analyzed further to characterize dimensional variation from the CAD model and other parts in the same specimen class. For CT, the calibration coupon along with a subset of the compression, layer quality, and tensile specimens were analyzed. All tensile and compression specimens were destructively tested per the relevant ASTM standard. Optical microscopy and SEM were performed on a subset of specimens following destructive testing. Layer quality specimens were also part of the SEM analysis. FTIR analyses were conducted on a subset of phase II flight specimens to assess potential chemical differences/changes in feedstock over time.

Table 4. Testing matrix for phase II specimens.

Testing Phase	Specimens
Photographic/visual inspection	All
Mass measurement	All
Structured light scanning	All
CT	Tensile: F028, F033, F038A, F043A, F043B Compression: F031B, F035B, F041A, F041B, F041C
Tensile testing	F026, F028, F030, F032, F033, F036, F037, F038A, F039, F040A, F043A, F043B
Compression testing	F024, F027, F029, F031A, F031B, F031C, F035A, F035B, F035C, F038B, F040B, F041A, F041B, F041C
Optical microscopy and SEM	Tensile: F026, F030, F033, F036, F040A, F043A, F043B Compression: F027, F029, F035A, F035C, F041A, F041B, F041C Layer quality: F034A, F034B, F042A, F042B
FTIR	F029, F042C

3. PHASE II RESULTS: MASS AND DENSITY

3.1 Mass Measurements

3.1.1 Summary of Mass Measurements

Following receipt and unboxing of the flight specimens from the 3DP phase II prints at MSFC in August 2017, ground and flight specimens were weighed in the precision metrology laboratory at MSFC. Each specimen was weighed five times using a calibrated laboratory scale (Mettler analytical balance) with a capacity of 261 g and a resolution of 1×10^{-5} g. The weighing pan was enclosed in an isolation chamber. Specimen weights range from 1.3 g (sparse fill calibration coupon) to ≈5 g (tensile specimen) and are summarized in table 5. These measurements were used to obtain a characteristic value for the mean weight of each specimen. Uncertainty in the reported values was generally on the order of 10^{-5}.

Table 5. Weights of phase II specimens.

Specimen ID No.	Specimen Type	Specimen Weight (g)
F022	Calibration coupon	1.4
F024	Compression	2.94
F025	Layer quality specimen	2.58
F026	Tensile	4.99
F027	Compression	2.95
F028	Tensile	4.98
F029	Compression	2.9
F030	Tensile	4.18
F031A	Compression	2.86
F031B	Compression	2.87
F031C	Compression	2.87
F032	Tensile	5
F033	Tensile	4.99
F034A	Layer quality specimen	2.65
F034B	Layer quality specimen	2.7
F034C	Layer quality specimen	2.65
F035A	Compression	2.79
F035B	Compression	2.92
F035C	Compression	2.94
F036	Tensile	4.98
F037	Tensile	4.99
F038A	Tensile	4.99

Table 5. Weights of phase II specimens (Continued).

Specimen ID No.	Specimen Type	Specimen Weight (g)
F038B	Compression	2.89
F039	Tensile	5
F040A	Tensile	4.99
F040B	Compression	2.84
F041A	Compression	2.89
F041B	Compression	2.83
F041C	Compression	2.87
F042A	Layer quality specimen	2.66
F042B	Layer quality specimen	2.68
F042C	Layer quality specimen	2.67
F043A	Tensile	5.01
F043B	Tensile	4.96

3.1.2 Comparative Analysis of Mass Measurements

Five groups of specimens were compared across each specimen geometry:

(1) The phase II specimen set includes all phase II flight specimens of a particular geometry; e.g., all phase II tensile specimens.

(2) The phase II optimal set includes only specimens of a particular geometry produced at the optimal manufacturing process setting (*z*-calibration value of 2.54 mm). Per specimen group (3), this means the build tray was commanded to translate upward of 2.54 mm prior to the print. This distance was chosen based on visual feedback from the phase II calibration print, which was manufactured at 2.64-mm *z*-calibration, but the specimen showed some evidence of protrusions and was designated as too close.

(3) The phase II off-nominal set designates specimens produced at the suboptimal manufacturing setting (*z*-calibration value of 2.64 mm). This means that the build tray was translated upward 2.64 mm relative to its home position for the print. This places the extruder tip 0.1 mm closer to the build tray than in the optimal specimen sets. Suboptimal in this context designates a manufacturing condition that is different from the normal value and does not imply problems with the 3DP hardware or its operation during phase II.

(4) Ground phase I specimens were specimens produced as part of phase I operations using the flight printer prior to its launch to the ISS. The commanded calibration setting for these prints was 2.2 mm.

(5) Flight phase I specimens refer to specimens produced in November and December 2014 on the ISS as part of phase I operations. The *z*-calibration value for every print in the flight print

matrix was varied based on real-time visual feedback from cameras inside the MSG. Values ranged from 2.39 mm to 2.84 mm.

Suboptimal specimens for phase II are intended to approximate the conditions of the phase I flight prints, where the extruder tip was too close to the build tray during specimen manufacture. While other data from specimens produced with the 3DP unit are plotted for comparative analysis, the key comparison for the phase II prints is the optimal versus suboptimal conditions within the phase II specimen set. These represent the most controlled data set since they were produced during the same phase of operations and only a single process setting (the extruder standoff distance) was varied systematically.

The comparison of the mass data across specimen sets for specific geometries are summarized in this section. Figure 4 compares the mass of the tensile specimens across the five specimen sets. Analysis of variance (ANOVA) shows there is not a statistically significant difference between the means of the five variables at the 95% confidence level. The average mass is remarkably consistent for the tensile specimens (fig. 5, table 6) despite the differences in manufacturing process settings. This finding is consistent with phase I data and the follow-on extruder standoff distance study using the ground equivalent printer.

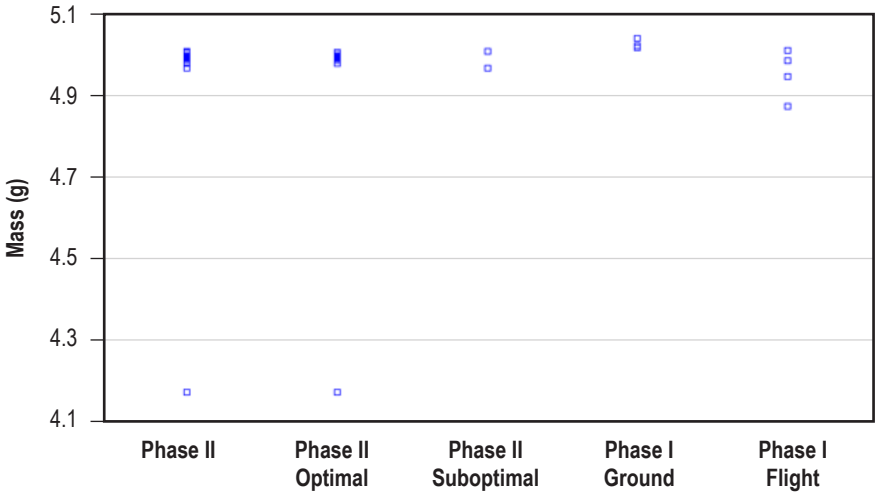

Figure 4. Scatterplot comparison of tensile specimen masses from phases II and I.

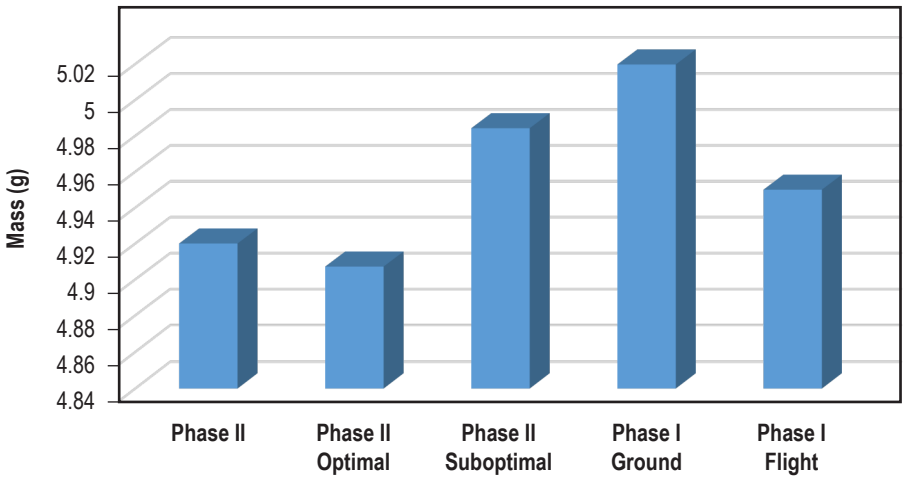

Figure 5. Bar chart comparison of average tensile specimen masses.

Table 6. Average mass of tensile specimens.

Specimen Set	Average Mass of Tensile Specimens (g)	Coefficient of Variation (%)
Phase II	4.92	4.77
Phase II optimal	4.91	5.24
Phase II suboptimal	4.98	0.59
Phase I ground	5.02	0.21
Phase I flight	4.95	1.2

Figure 6 compares the compression specimen mass across the five specimen sets. ANOVA indicates there is a statistically significant difference in the mass of specimens for some data sets. The masses of the compression phase I flight prints are distinct from all specimen sets except specimens produced at the phase II off-nominal condition. However, specimen sets for phase II off-nominal, phase I ground, and phase I flight are small. Little is known about the distribution these samples originate from and the validity of the statistical test for these specimen sets, which assumes normality, cannot be robustly assessed. Figure 7 and table 7 summarize the average mass comparisons.

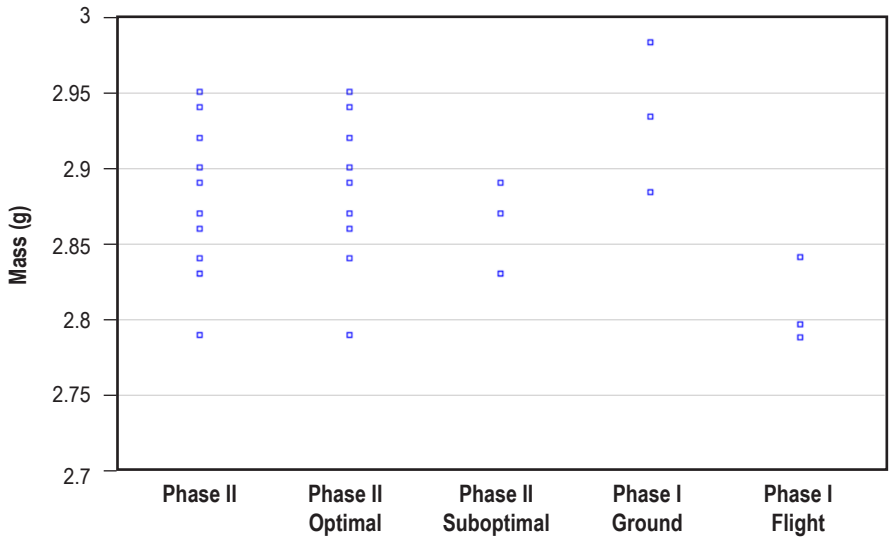

Figure 6. Scatterplot comparison of compression specimen masses from phases II and I.

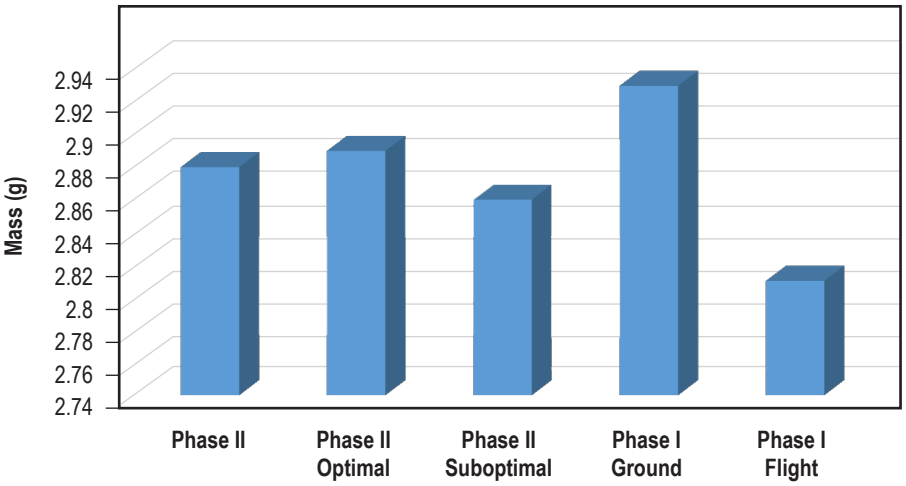

Figure 7. Bar chart of average compression specimen masses.

Table 7. Average mass of compression specimens.

Specimen Set	Average Mass of Compression Specimens	Coefficient of Variation (%)
Phase II	2.88	1.58
Phase II optimal	2.89	1.7
Phase II subtopimal	2.86	0.01
Phase I ground	2.93	1.69
Phase I flight	2.81	1.01

Group comparisons of layer quality with phase I are considered for completeness but are not particularly meaningful since phase I ground and flight specimen sets only contained one of these specimens. To the extent a comparison is possible, the mass data appear to be part of the same family. Figure 8 is a scatterplot comparison of individual specimen masses; figure 9 and table 8 show average masses.

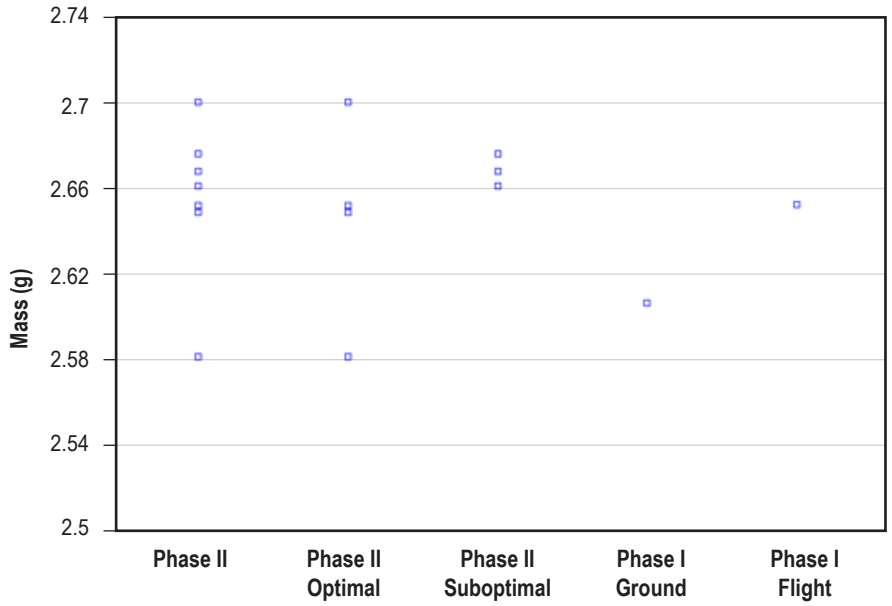

Figure 8. Scatterplot comparison of layer quality specimen masses from phases II and I.

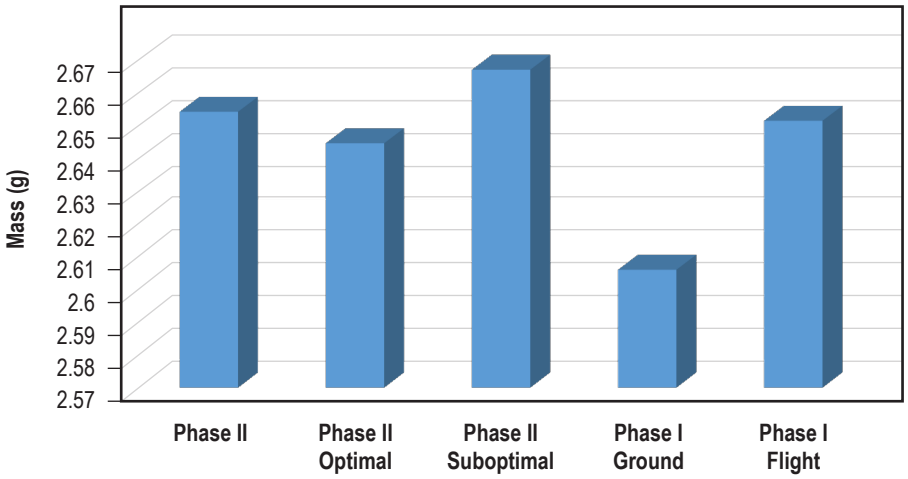

Figure 9. Bar chart of average layer quality specimen masses.

Table 8. Average mass of layer quality specimens.

Specimen Set	Average Mass of Layer Quality Specimens (g)	Coefficient of Variation (%)
Phase II	2.65	1.83
Phase II optimal	2.65	1.83
Phase II suboptimal	2.67	0.28
Phase I ground	2.61	–
Phase I flight	2.65	–

Although calibration coupons are not test specimens but rather a means to verify hardware health and manufacturing process conditions prior to printing, the masses of this class of specimen were also compared for completeness. For phases I and II ground prints, only a single calibration specimen was produced in each specimen set. For phase I flight prints, five specimens were generated prior to printing other specimens in an effort to optimize the extruder standoff distance, which was subsequently varied throughout the phase I flight print matrix based on visual feedback. Figure 10 is a scatterplot of the calibration coupon masses and figure 11 is a bar chart of average masses. For phases I and II ground, the average represents only a single print value. Table 9 summarizes the mass comparison. Reduced mass relative to other specimen geometries stems from the reduced size of the part and it is built with only a 50% infill.

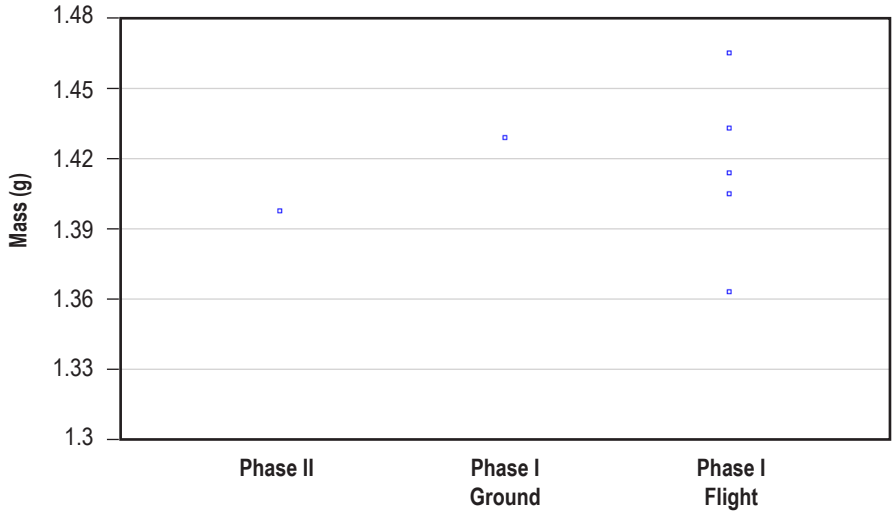

Figure 10. Scatterplot comparing calibration specimen masses from phases II and I.

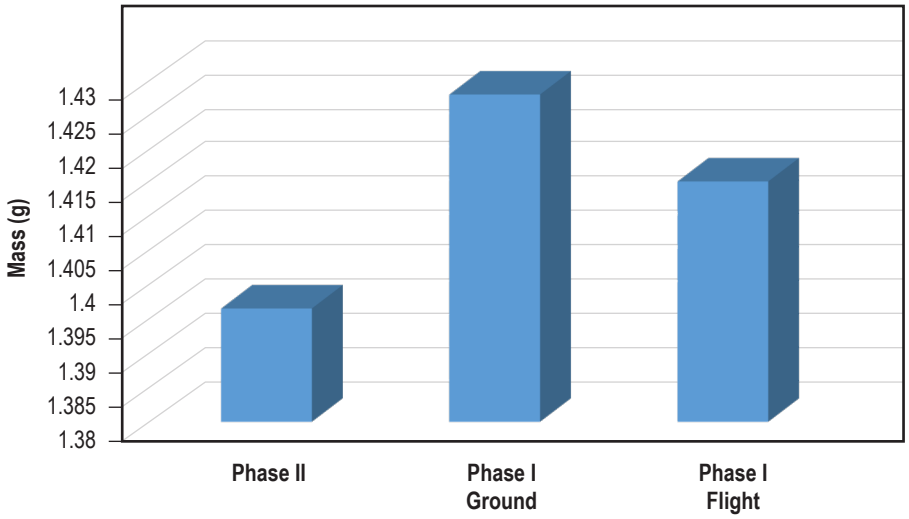

Figure 11. Bar chart comparing calibration specimen masses. (Only one calibration specimen was printed for phase II and phase I ground. Phase I flight represents an average of five specimens.)

Table 9. Masses of calibration specimens.

Specimen Set	Average Mass of Calibration Specimen (g)	Coefficient of Variation (%)
Phase II	1.4	–
Phase I ground	1.43	–
Phase I flight	1.42	2.65

3.1.3 Key Findings

No substantive mass differences were noted in comparison of the tensile, layer quality, and calibration prints across manufacturing settings. The total mass of extrudate across a range of manufacturing conditions for a particular specimen geometry is remarkably consistent. This is largely in agreement with phase I findings. One interesting note is that the flight compression specimens, which were distinct from all previously analyzed specimen sets prior to phase II operations, have a mass that is in family with only the phase II flight prints manufactured at the too close setting. The sample sizes of the phase I flight compression specimen set ($n = 3$) and the off-nominal compression specimen set from phase II ($n = 3$), however, are small. Since the small sample size precludes an assessment of the distribution the data originate from, this may limit the validity of the statistical test applied to compare the data sets, which assumes normality. Limiting the comparative analysis to only phase II specimen sets, the change in the extruder standoff distance does not seem to substantively impact the mass of the specimens produced for any specimen geometry considered in the microgravity environment. The ground specimens from 3DP phase I are also in family with phase II across all specimen geometries.

3.2 Density

3.2.1 Summary of Density Measurements

The gravimetric density ρ was subsequently calculated for each specimen by dividing the mean mass value by the corresponding volume obtained from structured light scanning. The scanner has an accuracy of ±12.7 mm at the scale of the 3DP specimens. Point cloud data from the structured light scan are imported into a software program, Geomagic® Control™. Surface fill operations allow the user to create a complete surface and execute a volume calculation. This volume is representative of the as-built part. The surface fill algorithm creates high-quality surfaces that are representative of the part geometry. Average volumes for the phase II specimens for each specimen class are tabulated in table 10. Gravimetric density for each specimen in the phase II print matrix is summarized in table 11. Since the volume for each specimen represents a single calculation based on structured light scan data rather than repeated measurements, an uncertainty value is not reported for the density values.

Table 10. Average volumes (based on structured light scan data) for phase II specimens.

Specimen Type	Average Volume (cm^3)
Tensile	5.32
Compression	3.08
Layer quality	2.88
Calibration*	2.72

*Only one specimen printed in phase II operations.

Table 11. Density measurements for phase II specimens.

Specimen ID No.	Specimen Type	Specimen Density (g/cm^3)
F022	Calibration coupon	0.513
F024	Compression	0.951
F025	Layer quality specimen	0.902
F026	Tensile	0.93
F027	Compression	0.954
F028	Tensile	0.918
F029	Compression	0.945
F030	Tensile	0.906
F031A	Compression	0.93
F031B	Compression	0.93
F031C	Compression	0.936
F032	Tensile	0.934
F033	Tensile	0.923

Table 11. Density measurements for phase II specimens (Continued).

Specimen ID No.	Specimen Type	Specimen Density (g/cm^3)
F034A	Layer quality specimen	0.912
F034B	Layer quality specimen	0.934
F034C	Layer quality specimen	0.929
F035A	Compression	0.916
F035B	Compression	0.94
F035C	Compression	0.946
F036	Tensile	0.925
F037	Tensile	0.922
F038A	Tensile	0.92
F038B	Compression	0.939
F039	Tensile	0.926
F040A	Tensile	0.921
F040B	Compression	0.929
F041A	Compression	0.935
F041B	Compression	0.93
F041C	Compression	0.927
F042A	Layer quality specimen	0.926
F042B	Layer quality specimen	0.931
F042C	Layer quality specimen	0.918
F043A	Tensile	0.939
F043B	Tensile	0.937

3.2.2 Comparative Analysis of Density

As with the mass measurements, five groups of specimens were compared across each specimen geometry:

(1) The phase II specimen set includes all phase II flight specimens of a particular geometry; e.g., all phase II tensile specimens.

(2) The phase II optimal set includes only specimens of a particular geometry produced at the optimal manufacturing process setting (z-calibration value of 2.54 mm). Per specimen group (3), this means the build tray was commanded to translate upward of 2.54 mm prior to the print. This distance was chosen based on visual feedback from the phase II calibration print which was manufactured at 2.64-mm z-calibration, but the specimen showed some evidence of protrusions and was designated as too close, at which point the z-calibration was adjusted to 2.54 mm.

(3) The phase II off-nominal set designates specimens produced at the off-nominal manufacturing setting (z-calibration value of 2.64 mm). This means that the build tray was translated upward 2.64 mm relative to its home position for the print. This places the extruder tip 0.1 mm closer to the build tray than in the optimal specimen sets.

(4) Ground phase I specimens were specimens produced as part of phase I operations using the flight printer prior to its launch to the ISS. The commanded calibration setting for these prints was 2.2 mm.

(5) Flight phase I specimens refer to specimens produced in November and December 2014 on the ISS as part of phase I operations. The *z*-calibration value for every print in the flight print matrix was varied based on real-time visual feedback from cameras inside the MSG. Values ranged from 2.39 mm to 2.84 mm.

As noted in figure 12, figure 13, and table 12, tensile density shows some small variation across all specimen sets evaluated for 3DP phases I and II. Specimen sets that clearly are in family with one another are (a) the complete set of phase II specimens and the phase II optimal specimen subset and (b) the phase II suboptimal set and the flight phase I set (built at similar but not identical processing conditions; in both sets, the extruder tip was positioned too close to the build plate). The ground phase I tensile prints, which were manufactured with the extruder tip too far from the build tray, have an overall slightly lower density. Mean densification increases slightly in the optimal distance set (phase II optimal) and increases further with the suboptimal and flight phase I prints, which were manufactured with the extruder too close to the build tray. This too close distance was also hypothesized to create protrusions, evident on structured light scans and SEM in phase I prints and the ground-manufactured analogous specimens evaluated in reference 10, which serve to artificially strengthen the part under tensile loading.

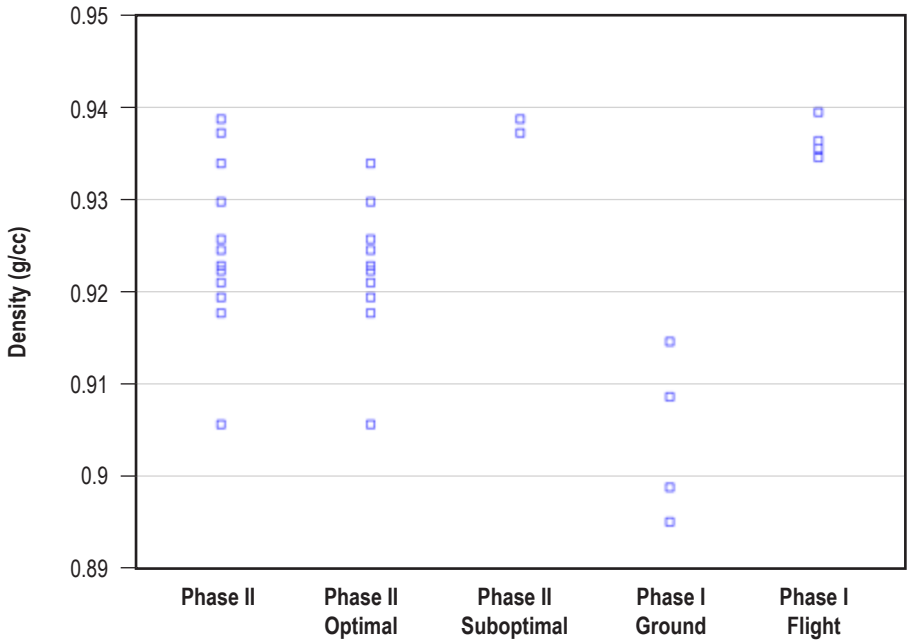

Figure 12. Scatterplot comparison of density data for tensile specimens from phases II and I.

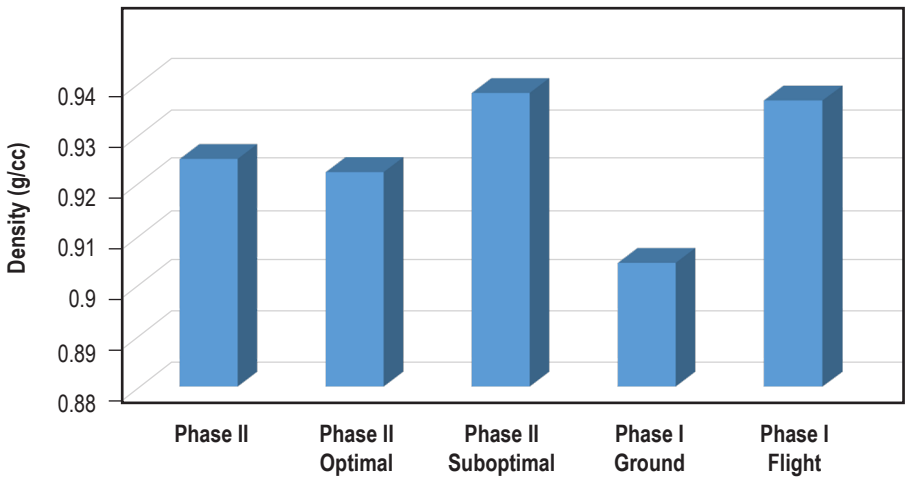

Figure 13. Bar chart comparison of average density data for tensile specimens.

Table 12. Average density of tensile specimens by specimen class.

Specimen Set	Average Density of Tensile Specimens (g/cc)	Coefficient of Variation (%)
Phase II	0.93	0.99
Phase II optimal	0.92	0.91
Phase II suboptimal	0.94	0.11
Phase I ground	0.9	0.98
Phase I flight	0.94	0.22

The compression data are similar and largely appear to be part of the same data family. However, the flight phase I prints have a slightly lower mean density than the other specimen sets and also contain the lowest density specimen. The mean of the flight phase I specimen set lies close enough to be considered in family with the phase II suboptimal prints, which were also built with the extruder at a standoff distance that is closer to the build tray. The scatterplot of the data is in figure 14, the averages for the data sets are plotted in the bar chart in figure 15, and table 13 also summarizes the data.

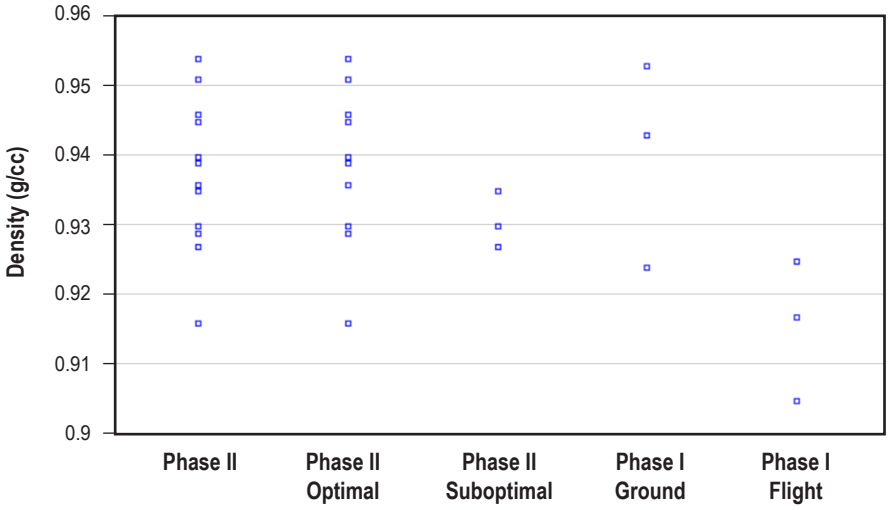

Figure 14. Scatterplot comparing compression specimen densities.

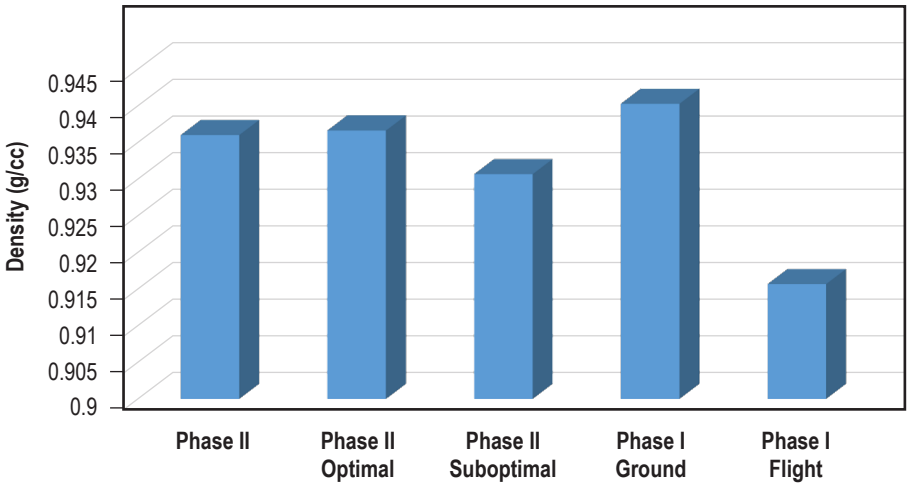

Figure 15. Bar chart comparing average compression specimen densities.

Table 13. Average density comparison for compression specimens.

Specimen Set	Average Density of Compression Specimens (g/cc)	Coefficient of Variation (%)
Phase II	0.94	1.13
Phase II optimal	0.94	1.27
Phase II off-nominal	0.93	0.39
Phase I ground	0.94	1.55
Phase I flight	0.92	1.11

For the layer quality specimens, the densities across manufacturing process settings for phases I and II operations appear to be in family with one another, as illustrated in figures 16 and 17 and table 14. Comparing the subgroups of the phase II data, movement of the extruder head closer to the build tray does not result in an accompanying increase in densification for these specimens. The ground-based extruder standoff distance study using the ground-equivalent 3D print unit (ref. 10) also failed to show any relationship between density and extruder standoff distance for this specimen class.

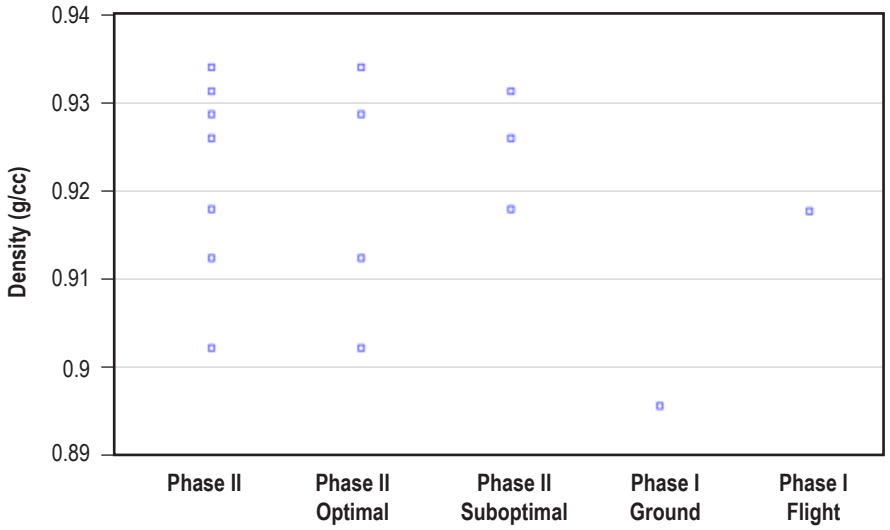

Figure 16. Scatterplot comparing layer quality specimen densities of phases II and I.

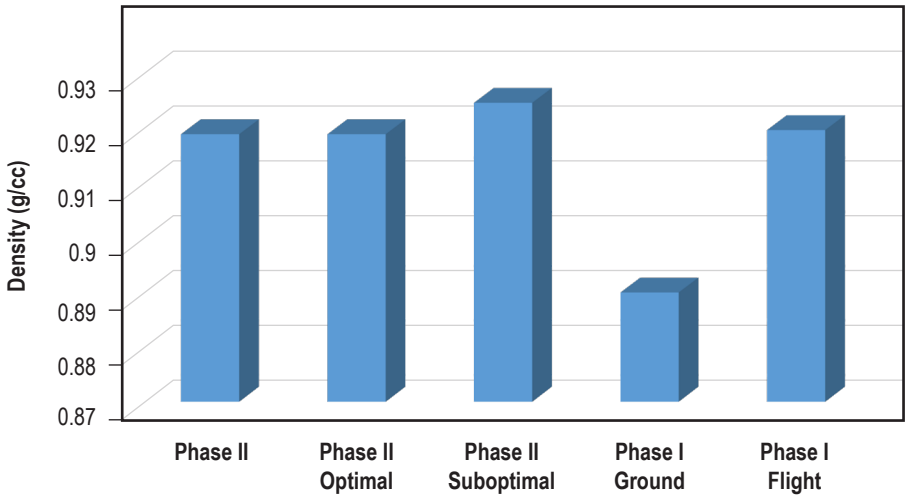

Figure 17. Bar chart comparing average layer quality specimen densities.

Table 14. Average density comparison for layer quality specimens.

Specimen Set	Average Density of Compression Specimens (g/cc)	Coefficient of Variation (%)
Phase II	0.92	1.25
Phase II optimal	0.92	1.6
Phase II off-nominal	0.93	0.72
Phase I ground	0.89	–
Phase I flight	0.92	–

Only a single calibration print was produced as part of phase II operations. This print was at the 2.64-mm *z*-calibration value. Due to visible protrusions on the specimens (observed via the camera feed from inside the MSG), the distance was set to 2.54 mm for optimal phase II operations. For phase I, only one ground calibration specimen was produced. Phase I flight prints required production of five calibration coupons to determine an appropriate *z*-calibration setting, but this distance was changed throughout operations based on visual feedback. Density for these specimens is about 50% relative to injection molded material since they were built with a sparser infill. Density data are summarized in figures 18 and 19 and table 15.

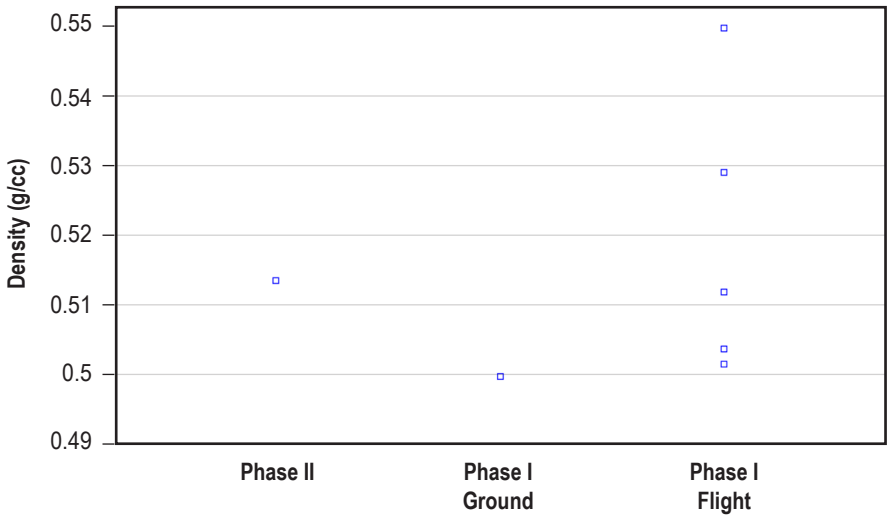

Figure 18. Scatterplot comparing calibration coupon densities of phases II and I.

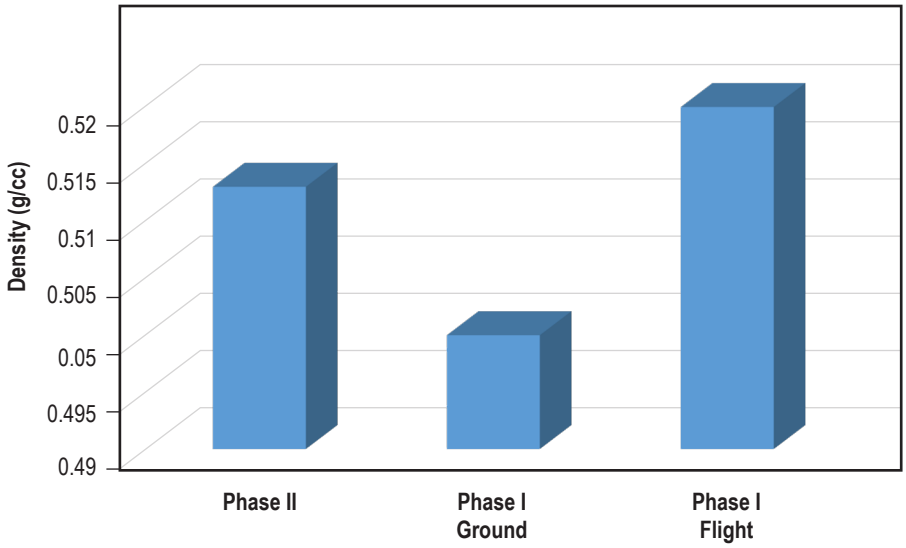

Figure 19. Bar chart comparing calibration specimen densities. (Only one calibration coupon was printed for phases II and I ground operations. Phase I flight represents an average of five specimens.)

Table 15. Calibration specimen densities.*

Specimen Set	Average Density of Compression Specimens (g/cc)	Coefficient of Variation (%)
Phase II	0.51	–
Phase I ground	0.5	–
Phase I flight	0.52	3.89

* Since only one calibration coupon was printed for phase II and phase I ground operations, only a single value is reported with no associated coefficient of variation.

3.2.3 Key Findings

An apparent engineering significant difference between specimen classes is not evident. Tensile specimens become slightly denser as the extruder tip is moved closer to the build tray. Flight compression phase I specimens are slightly less dense than other specimen sets, but are in family with the flight compression phase II suboptimal specimens that were built at a sufficiently similar extruder standoff distance.

Ground prints for tensile and compression are both in family with phase II prints. Despite the differences in manufacturing process conditions, the similarity in the means of these sample sets for density is not suggestive of a significant microgravity impact on part density. Overall, the density calculations across all specimen sets suggest that the data are part of a single family.

4. MECHANICAL TESTING

This section summarizes the results of mechanical testing of tensile and compression specimens for phase II and compares them back to phase I data.

4.1 Methodology

Tensile tests followed a standard method defined in ASTM D638-14 and measured the tensile strength, yield strength, elastic modulus, and fracture elongation of the printed material.[3] A type I specimen would generally be chosen for this application due to the reduced stress concentration at the fillet, but the dimensions prescribed by the ASTM standard were almost too large for the printer build volume to accommodate. This limitation drove the alternate choice of the type IV specimen. The compression test, ASTM D695-15, was used to determine the characteristic compressive stress and modulus of the specimens.[4] The compression tests for phase II specimens were stopped at 20% strain in order to preserve the internal structure of the specimen for microscope evaluation. In phase I, compression specimens were tested to 100% strain, rendering analysis of the tested specimens via microscopy more difficult.

For mechanical testing, specimens were initially compared across five specimen sets:

(1) The phase II specimen set includes all phase II flight specimens of a particular geometry; e.g., all phase II tensile specimens.

(2) The phase II optimal set includes only specimens of a particular geometry produced at the optimal manufacturing process setting (z-calibration value of 2.54 mm). Per figure 3, this means the build tray was commanded to translate upward of 2.54 mm prior to the print. This distance was chosen based on visual feedback from the phase II calibration print, which was manufactured at 2.64-mm z-calibration, but the specimen showed some evidence of protrusions and was designated as too close, at which point the z-calibration was adjusted to 2.54 mm.

(3) The phase II off-nominal set designates specimens produced at the off-nominal manufacturing setting (z-calibration value of 2.64 mm). This means that the build tray was translated upward of 2.64 mm relative to its home position for the print. This places the extruder tip 0.1 mm closer to the build tray than in the optimal specimen sets.

(4) Ground phase I specimens were specimens produced as part of phase I operations using the flight printer prior to its launch to the ISS. The commanded calibration setting for these prints was 2.2 mm.

(5) Flight phase I specimens refer to specimens produced in November and December 2014 on the ISS as part of phase I operations. The *z*-calibration value for every print in the flight print matrix was varied based on real-time visual feedback from cameras inside the MSG. Values ranged from 2.39 mm to 2.84 mm.

4.2 Tensile Test Results

Mechanical Test Facility personnel performed tensile tests of ABS plastic 'dogbone' specimens produced as part of phase II operations for 3DP under ambient (75 °F, 0 psig) conditions. Test procedures were identical to those for phase I specimens. Nominal dimensions for the tensile specimens were based on type IV specimens in ASTM D638-10.5. Width of the reduced section was 0.25 in with a length of 1.3 in and a thickness of 0.13 in. A 1-in-gauge-length extensometer, calibrated per the B-2 classification for determining modulus of elasticity, measured tensile strain up to 100%. Tensile specimens were preloaded to a minimum of 1 ft-lb at 0.05 in/min, then pulled at a failure rate of 0.2 in/min. All of the equipment used during these tests was calibrated per applicable ASTM standards. Data derived from each tensile test include the following:

- Ultimate tensile strength (σ_{uts}) is the load at fracture divided by the original cross-sectional area of the test specimen.

- Yield strength (σ_{ys}) is the point at which the material begins to deform plastically (per ASTM D638-10, the "first point on the stress-strain curve at which an increase in strain occurs without an increase in stress"[5]).

  – Some classes of materials exhibit behavior that makes it difficult to determine the yield stress. In these cases, yield stress may be defined as the stress that coincides with some specific amount of plastic deformation; e.g., 0.2% of the stressed length.

  – For the 3DP specimens, no yield is reported because the maximum and yield stresses are virtually coincident for ABS plastic.

- Modulus of elasticity (E) is the ratio of tensile stress to tensile strain, the slope of the line that represents the linear elastic portion of the stress-strain curve.

- Fracture elongation (%) is the ratio of the initial length of the specimen to the change in the length of the specimen measured following fracture. Elongation to failure is a measure of ductility.

The consolidated plot of all tensile data from phases I and II is shown in figure 20. Figure 21 plots the ground and flight tensile specimens from phase I on the same axis. Figure 22 shows the stress-strain curves for phase II specimens only. Specific group comparisons are detailed in the next section.

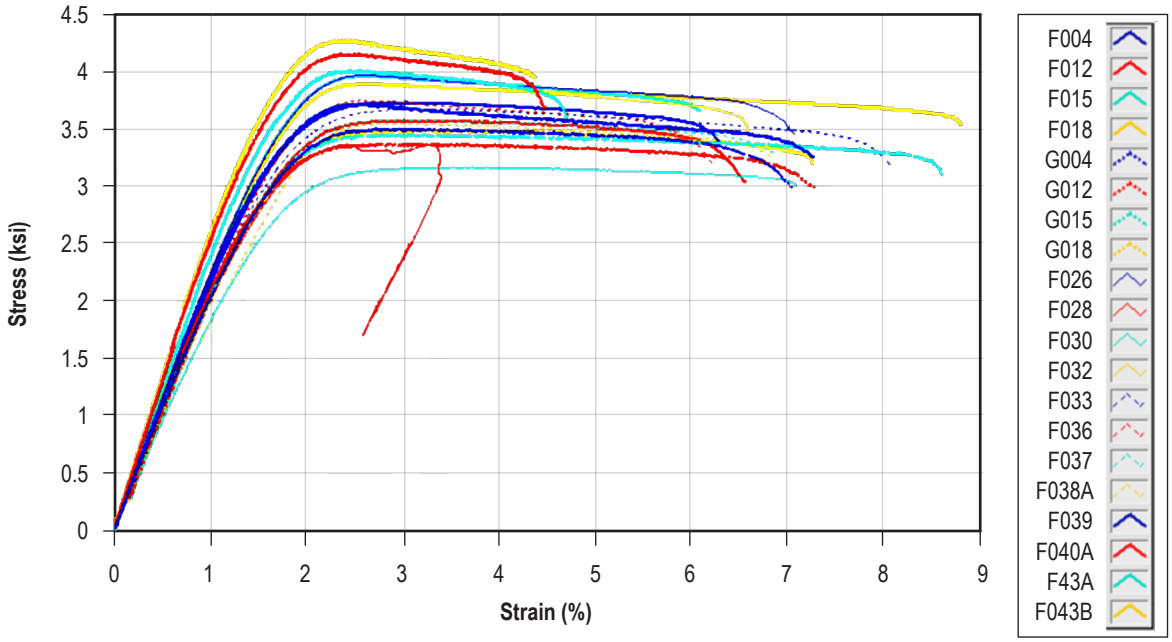

Figure 20. Consolidated plot of stress/strain curves from phases I and II.

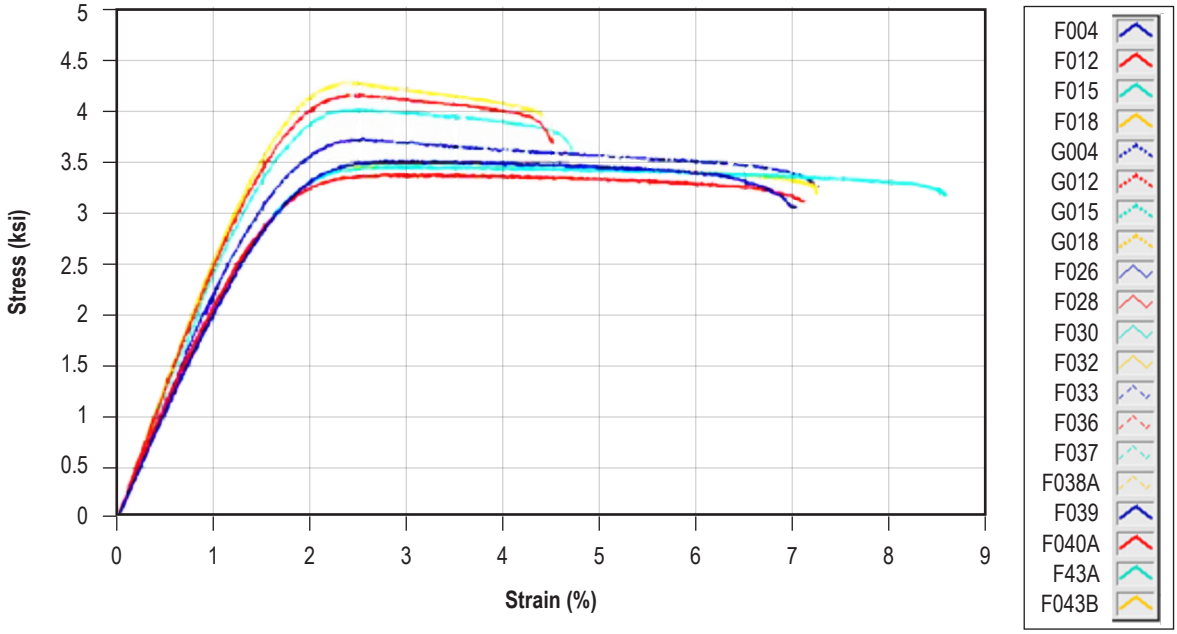

Figure 21. Plot of phase I ground and flight tensile specimens.

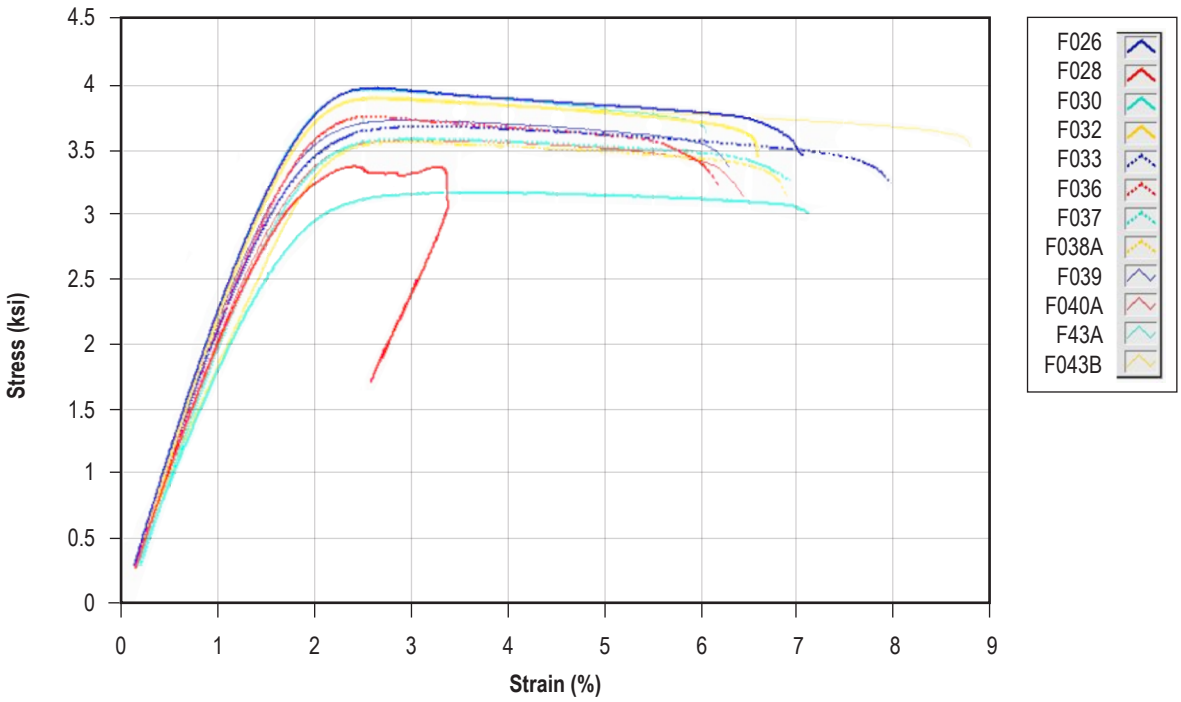

Figure 22. Plot of phase II tensile specimens.

4.2.1 Comparative Analysis of Tensile Data

4.2.1.1 Ultimate Tensile Strength Comparison. The UTS corresponds to the strength at which the specimen breaks. Comparing the data sets using the scatterplot in figure 23 and the bar chart in figure 24 as a visual aid, it is apparent that phase I flight specimen UTS is slightly greater than all other groups. However, phase I flight specimens do exhibit some overlap with the phase II optimal data set (upper regions) and, specifically, the suboptimal phase II specimens, which suggests that mechanical performance data may be part of a single large, albeit variable, data set. Table 16 gives a summary of UTS data.

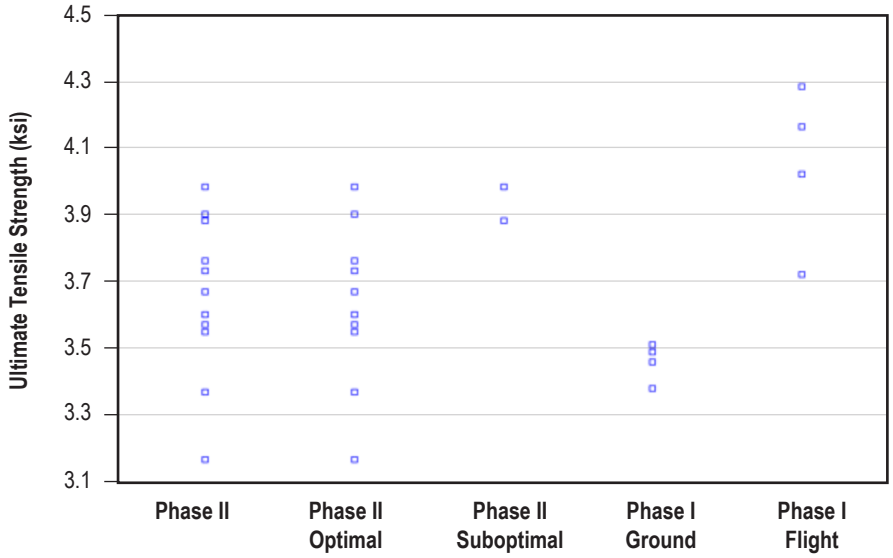

Figure 23. Scatterplot comparing UTS for phases II and I tensile specimens.

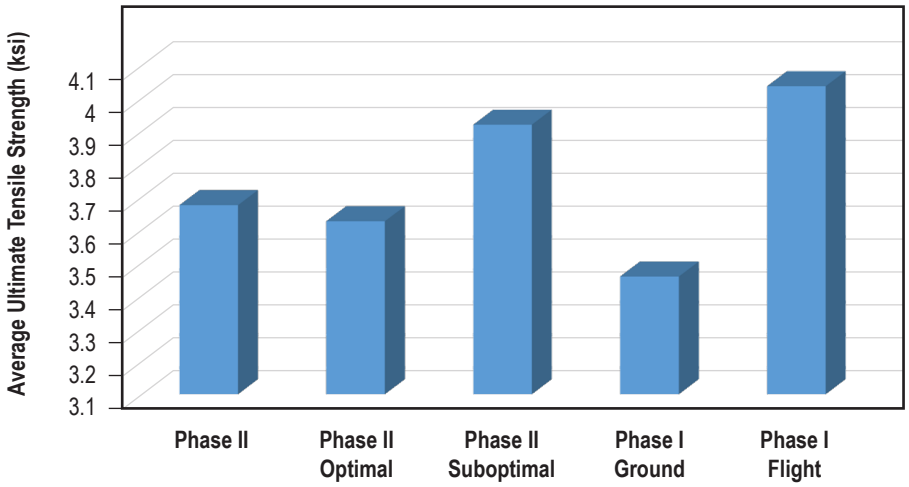

Figure 24. Bar chart comparing the average UTS of all specimen groups.

Table 16. Summary of UTS data.

Specimen Set	Average Ultimate Tensile Strength (ksi)	Coefficient of Variation (%)
Phase II	3.68	6.71
Phase II optimal	3.63	6.61
Phase II suboptimal	3.93	0.07
Phase I ground	3.46	1.71
Phase I flight	4.04	5.95

4.2.1.2 Elastic Modulus Comparison. Comparing the specimen group means for elastic modulus, the flight specimens from phase I again seem distinct but also show some overlap with the suboptimal condition and the upper moduli ranges for the other specimen sets. The means of the phase II flight specimens on the modulus metric are in family with the ground specimens. Since values within a specimen class tend to be closely clustered (and in some cases, values repeat), points within specimen classes have been 'jittered' (slightly offset) to render them distinct from other data points. Figures 25, 26, and table 17 summarize the modulus data.

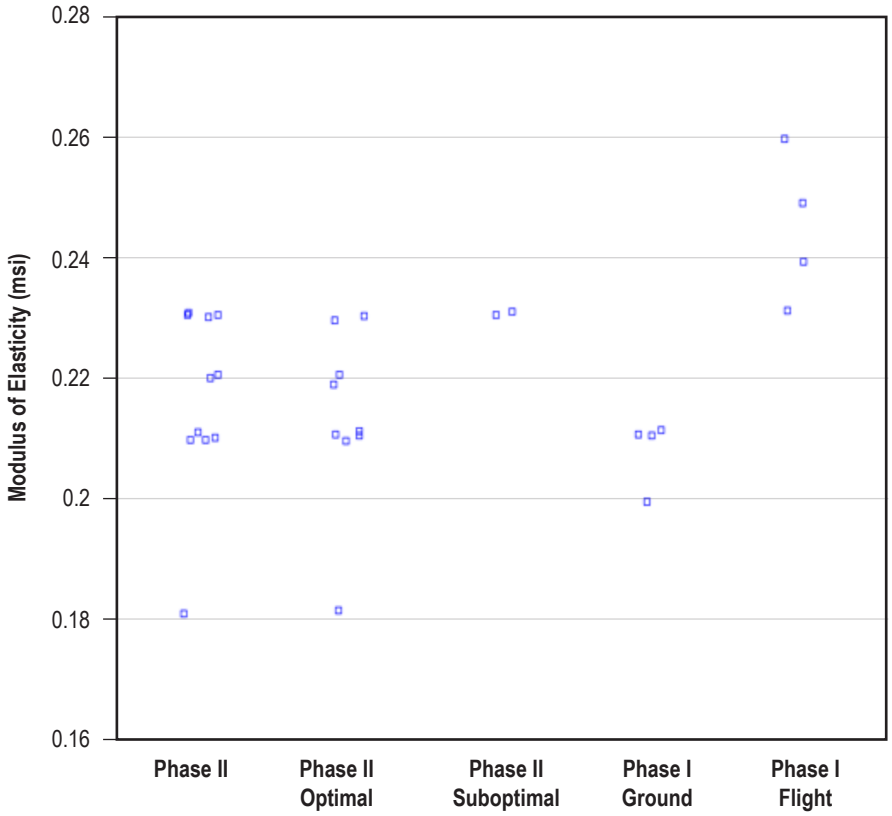

Figure 25. Scatterplot of elastic modulus values from phases II and I tensile testing.

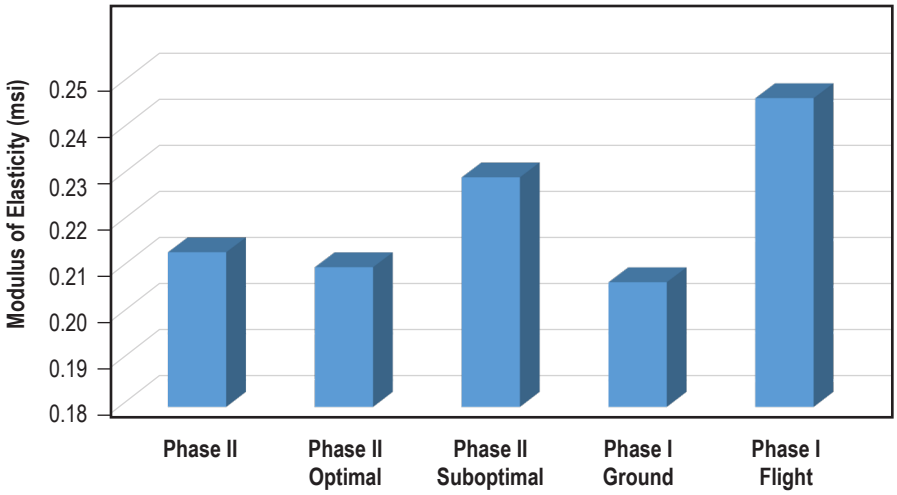

Figure 26. Bar chart of average elastic modulus values.

Table 17. Summary of elastic modulus data.

Specimen Set	Average Modulus (msi)	Coefficient of Variation (%)
Phase II	0.21	8.11
Phase II optimal	0.21	8.17
Phase II suboptimal	0.23	1.68
Phase I ground	0.21	0.95
Phase I flight	0.25	4.94

4.2.1.3 Comparison of Fracture Elongation. Phase I flight specimens exhibit a lower fracture elongation than other data sets. Fracture elongation, however, is a metric which typically exhibits a very high degree of scatter for 3D printed polymer materials. In phase I, it was initially thought flight specimens exhibiting characteristically lower fracture elongation values may have become embrittled due to moisture absorption or other aging mechanisms, such as radiation effects. However, chemical analysis showed no differences in functional chemical groups or relative concentrations between the flight and ground specimens for phase I.[7] Fracture elongation data are summarized in figures 27, 28, and table 18.

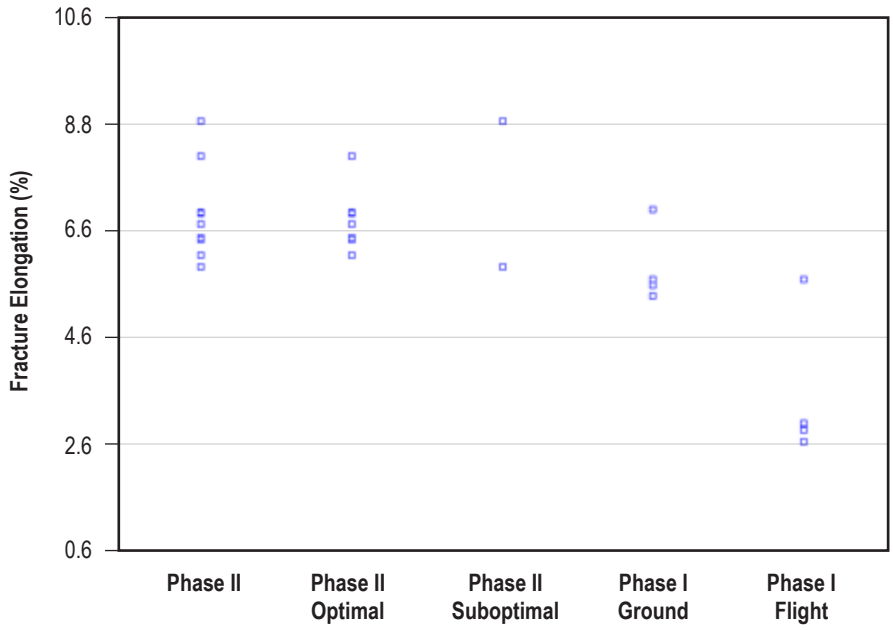

Figure 27. Scatterplot of fracture elongation values for phases II and I. For specimen F028, the exetensometer slipped and did not record failure. Measurements are accurate up to a maximum stress. Therefore, this fracture elongation was not used in analysis.

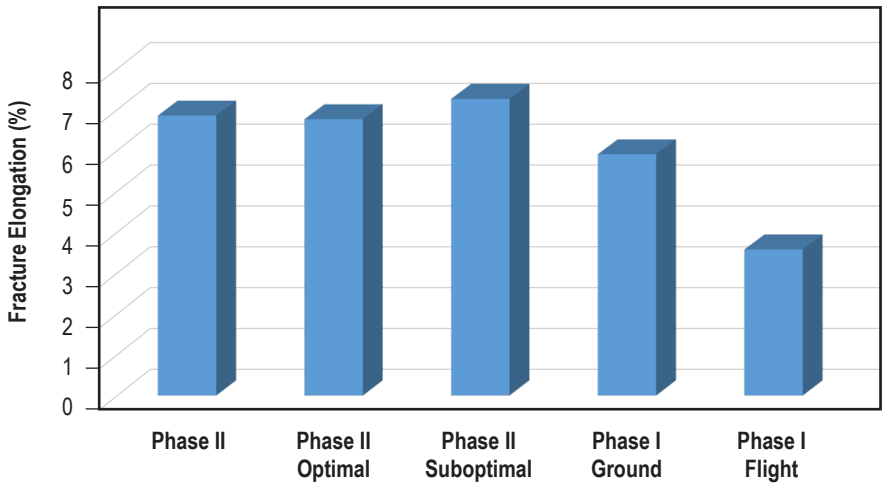

Figure 28. Bar chart of average fracture elongation values.

Table 18. Summary of fracture elongation data.

Specimen Set	Fracture Elongation (%)	Coefficient of Variation (%)
Phase II	6.88	11.6
Phase II optimal	6.79	7.8
Phase II suboptimal	7.29	26.5
Phase I ground	5.93	12.3
Phase I flight	3.58	39.9

4.3 Compression Test Results

Mechanical Test Facility personnel performed compression tests for the phase II ABS plastic cylinders (dimensions 0.5 in diameter by 1 in long) under ambient (75 ºF, 0 psig) conditions. Specimens were placed between the platens of a 'birdcage' compression fixture and pulled in tension to create a compressive load on the specimen. A 1-in-gauge-length extensometer, calibrated to the required B-2 classification for estimating modulus of elasticity, was chosen to measure compressive strain up to 20%. Test conditions were identical to phase I, but in this case, the test was truncated at 20% strain in order to preserve the structure of the specimen for further analysis. In phase I compression testing, data were truncated at 20% strain, but the specimens were tested until reaching a local maximum or at least 80% compressive strain, whichever occurred first. Material properties based on 20% compressive strain are reported across all data sets. All of the equipment used during these tests was calibrated per applicable ASTM standards. Properties derived from the compression test include the following:

- Maximum stress (σ_{max}, 20%) (ksi) is the value of compressive stress that corresponds to 20% strain.

- Yield strength (σ_{ys}) (ksi) is the point at which the material begins to deform plastically (the first point on the stress-strain curve at which an increase in strain occurs without an increase in stress).

  – Yield stress is defined as the stress that coincides with some specific amount of plastic deformation. (ASTM D695-107 does not specify a yield offset; an offset of 0.6% of the stressed length was selected.)

- Compressive modulus of elasticity (E) (msi) is the ratio of the compressive stress applied to a material to the resulting compression.

The consolidated plot of all compression data from phases I and II is shown in figure 29. Figure 30 plots the ground and flight tensile specimens from phase I on the same axis. Figure 31 shows the stress-strain curves for phase II specimens only. Specific group comparisons are detailed in the next section.

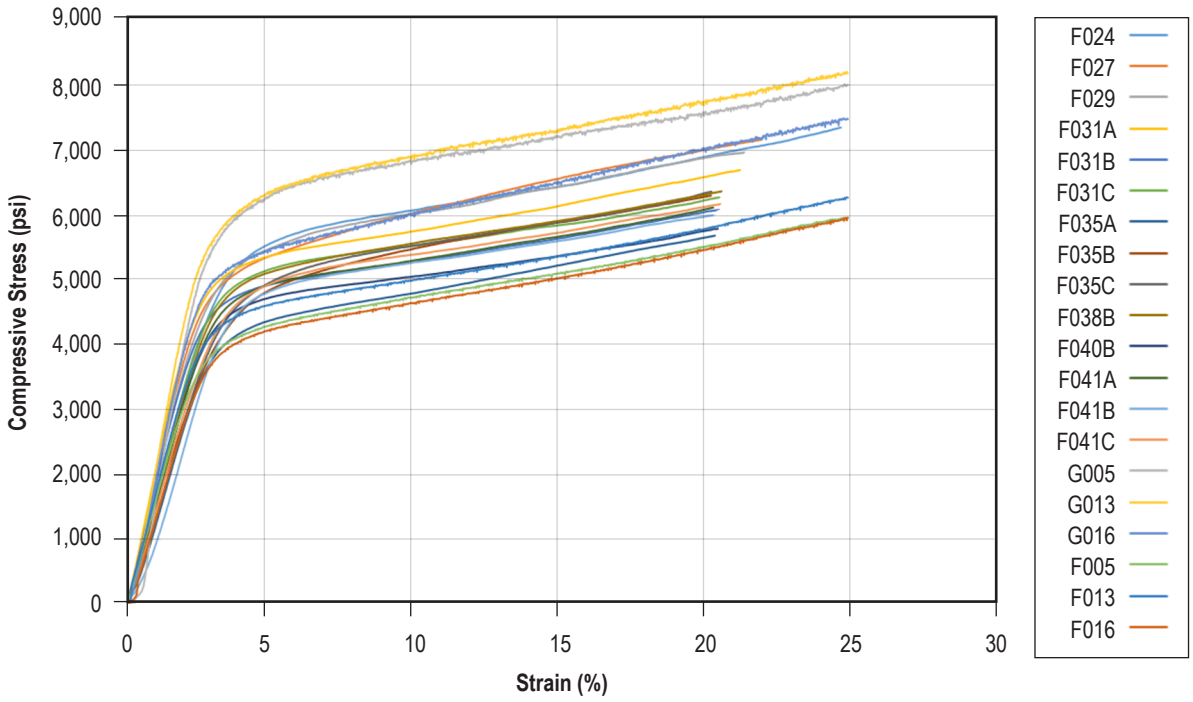

Figure 29. Consolidated plot of phases I and II compression stress/strain curves.

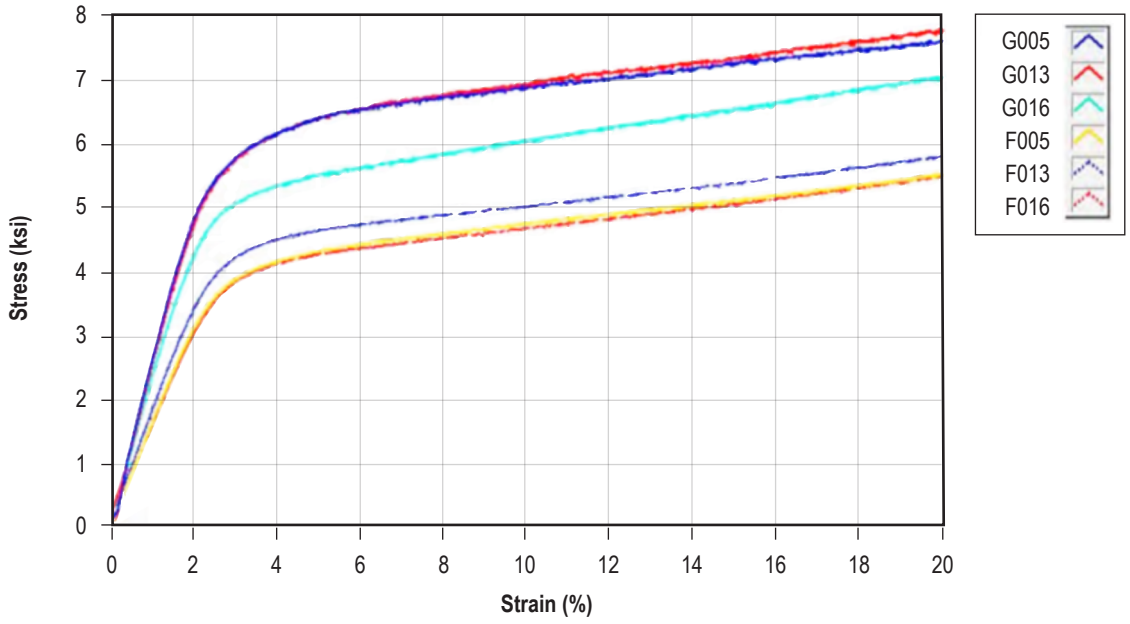

Figure 30. Plot of phase I ground and flight compression specimens.

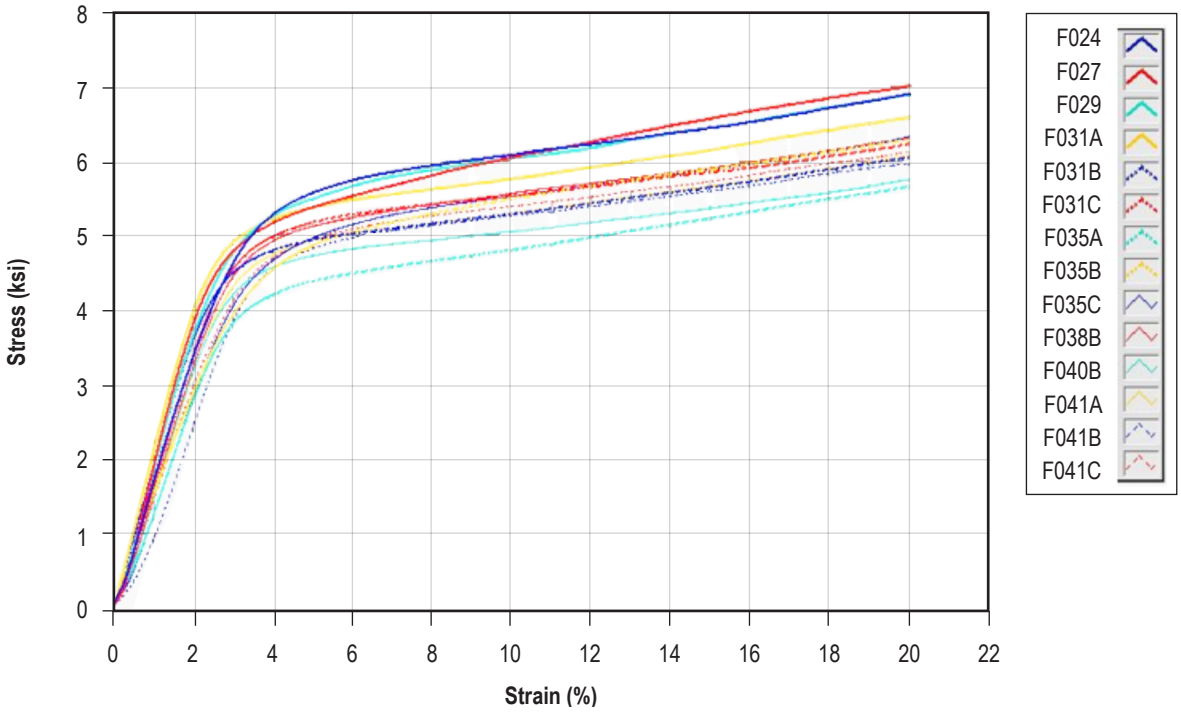

Figure 31. Plot of phase II compression specimens.

4.3.1 Comparative Analysis of Compression Data

4.3.1.1 Comparison of Maximum Compressive Stress. Figures 32, 33, and table 19 compare maximum compressive stress at 20% strain across phases I and II data sets. Testing of phase II specimens was truncated at 20% strain, while the phase I data set was run to 100% strain. (Only the values up to 20% are considered here.) Strengths are somewhat variable across groups and ground and flight specimens from phase I are somewhat distinct from all other groups considered. However, both phase I ground and flight exhibit overlap with the phase II data.

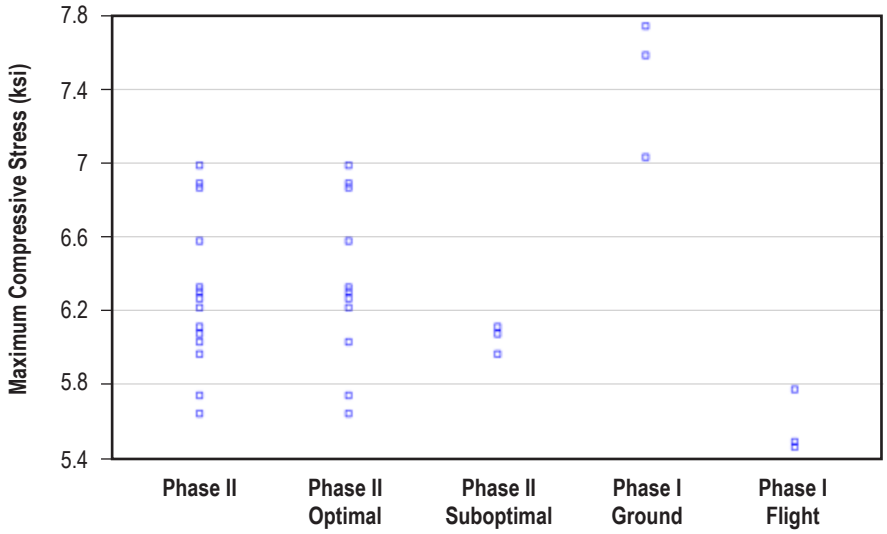

Figure 32. Scatterplot of maximum compressive stress values for phases II and I specimens (20% strain).

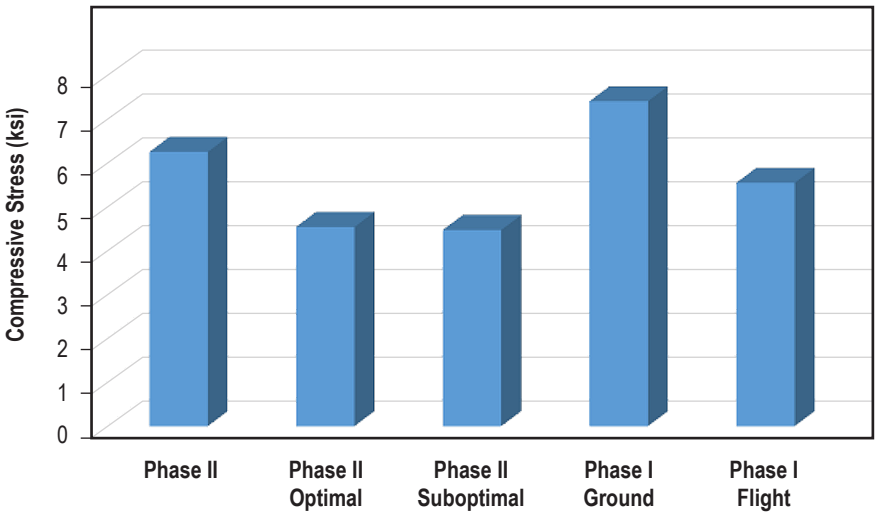

Figure 33. Bar chart comparing average compressive stress values (20% strain).

Table 19. Summary of compressive stress data.

Specimen Set	Compressive Stress at 20% Strain (ksi)	Coefficient of Variation (%)
Phase II	6.29	6.6
Phase II optimal	4.57	9.8
Phase II suboptimal	4.5	1.7
Phase I ground	7.45	5
Phase I flight	5.58	3.1

4.3.1.2 Comparison of Compressive Yield Stress. Compressive yield stress across all specimen sets is summarized in figures 34, 35, and table 20. For this metric, ground and flight specimens are again somewhat distinct from one another and all other groups, although it is recognized that these specimens are at the extremes of the manufacturing processing envelope in terms of extruder stand-off distance. There is some overlap in data sets for the lower range of the phase II specimens and the phase I flight specimens, which again suggest that all the data may be part of the same family. Variability among the sets may be compounded by differences in manufacturing process settings.

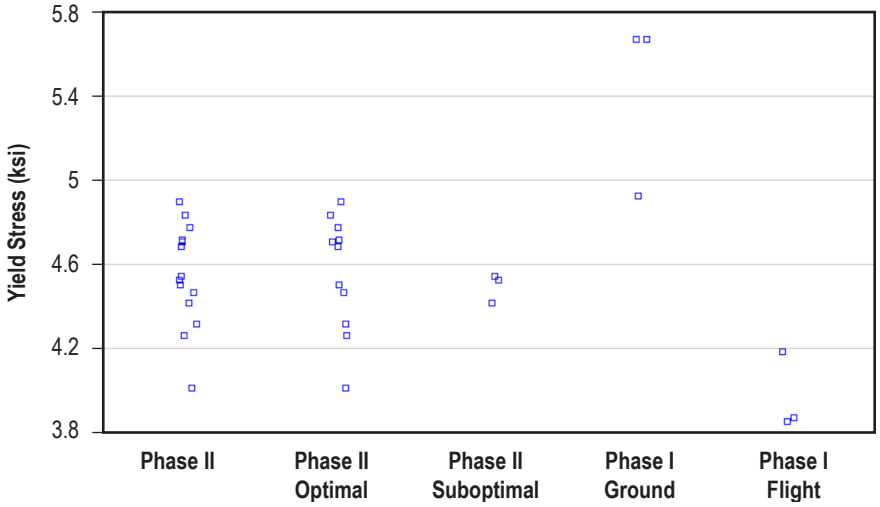

Figure 34. Scatterplot of compressive yield stress values for phases II and I specimens.

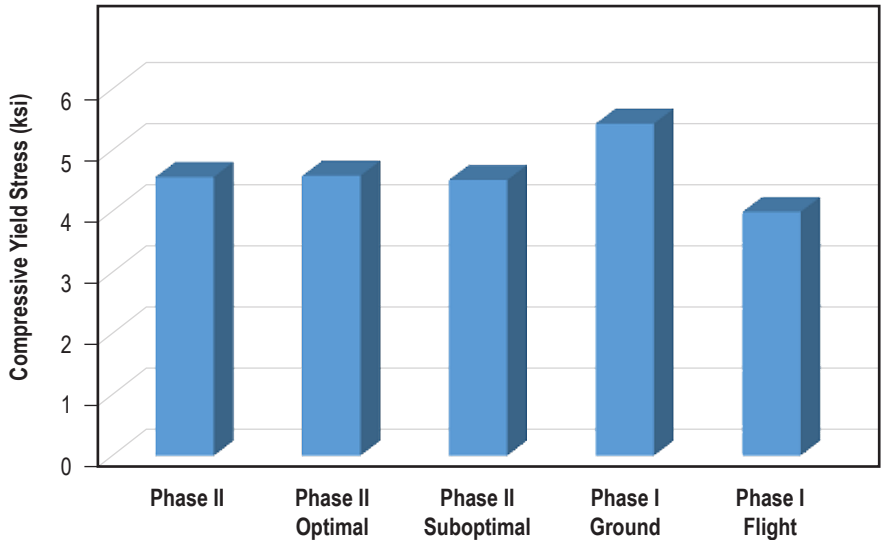

Figure 35. Bar chart comparing average compressive yield stress values.

Table 20. Summary of compressive yield strength data.

Specimen Set	Yield Stress at 20% Strain (ksi)	Coefficient of Variation (%)
Phase II	4.55	5.4
Phase II optimal	4.57	6
Phase II off-nominal	4.5	1.6
Phase I ground	5.42	7.9
Phase I flight	3.98	4.7

4.3.1.3 Comparison of Compressive Modulus. Comparative evaluation of compressive modulus data (figs. 36, 37, and table 21) indicate ground specimens lie slightly outside the data ranges of all other specimen sets in terms of compressive modulus. These specimens were manufactured at a farther extruder standoff distance than any other specimens considered in the study. However, the ground tensile specimens, also manufactured at this distance, were largely in family with other data sets from phase II. The trends and amount of variability observed in the data with known changes in manufacturing process settings may also be specific to the geometry of the test coupon. This finding is corroborated by the extruder standoff distance study in reference 10, which considered tensile, compression, and layer quality specimens produced at various extruder standoff distances. Comparative evaluation of internal material structure with CT sheds additional light on the differences noted in mechanical testing.

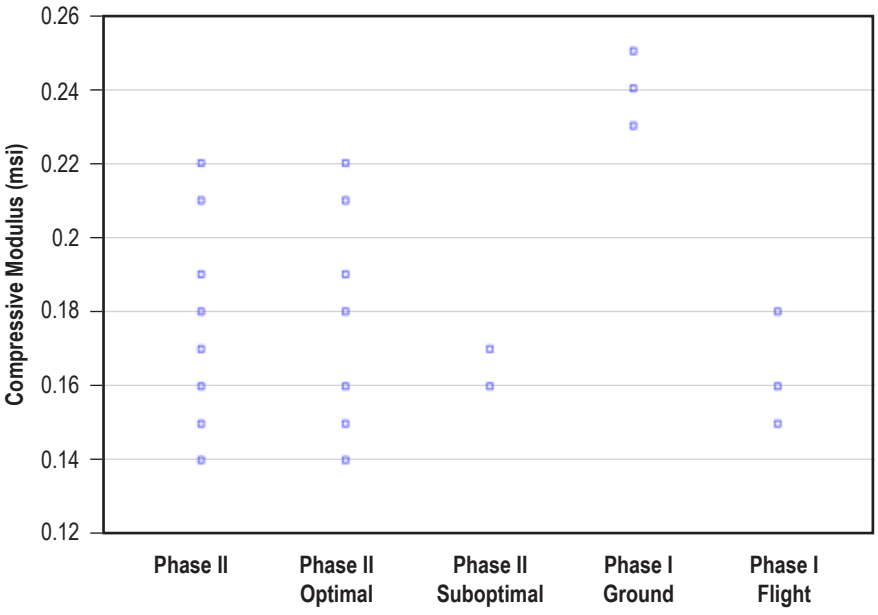

Figure 36. Scatterplot of compressive modulus for phases II and I specimens.

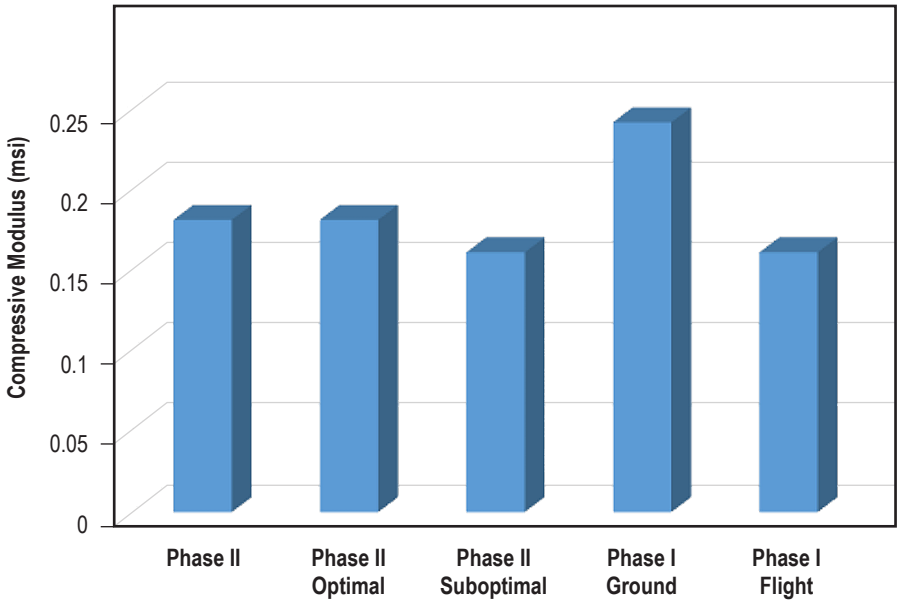

Figure 37. Bar chart comparing average compressive modulus.

Table 21. Summary of compressive modulus data.

Specimen Set	Compressive Modulus (msi)	Coefficient of Variation (%)
Phase II	0.18	13
Phase II optimal	0.18	13.5
Phase II off-nominal	0.16	4
Phase I ground	0.24	4.2
Phase I flight	0.16	9.4

4.4 Summary of Findings From Mechanical Testing

In general, all tensile data appear to be broadly part of the same family. Compression data sets exhibit more variability, with the ground compression specimens manufactured as part of phase I remaining somewhat distinct in terms of mechanical behavior from all other data sets. These specimens were manufactured at the largest extruder standoff distance. Subsequent studies have failed to shed much additional light on the compression behavior observed in the phase I ground specimens, as a strong relationship between compression strength and extruder standoff distance was not indicated in reference 10. Additionally, there is little change in compression performance among the flight prints with a change in the extruder setting. Structured light scanning and CT scanning have shown, based on phases I and II and ground-based study data with the flight equivalent printer, that compression specimen geometries have a higher incidence of voids, changes in density within the

specimen, and misruns than other specimen types. It is possible that manufacturing process variability associated with this particular geometry may result in a more variable data set. At the time of this writing, the relationship between manufacturing process settings and the potential impact on compression specimen performance is not well understood. Overall, mechanical test data are not strongly suggestive of a microgravity effect on material outcomes.

5. STRUCTURED LIGHT SCANNING

Structured light scanning was conducted to create a detailed 3D rendering of the specimens. These data were used to characterize surface geometric variations between the printed part and the CAD model as well as to facilitate dimensional comparison across specimen sets of the same geometry. Point cloud data from structured light were also used to obtain a value for the volume of the closed part surface used in the gravimetric density calculation in section 3.

5.1 Methodology

The scanning was conducted at MSFC using the ATOS II Triple Scan blue light-emitting diode (LED) scanner. The scanner has an accuracy of ±12.7 mm at these volumes and the capability to capture stereoscopic images at a resolution of 5 million pixels per scan. The samples were coated in dry talcum powder (nonreactive with the ABS plastic) to reduce the reflectivity of the sample surfaces, thereby improving scan accuracy. The talcum powder grain size is ≈10 mm in diameter, and thus had little effect on the measurements made by the scanner. The software package that accompanies the ATOS scanner uses the stereoscopic images to capture the fringe pattern sent out from the central LED projector. The software triangulates all of the surface data using the grayscale pixels and black and white contrast from the fringe pattern to determine the shape of the geometry. Through this process, the software generates a complete 3D model of the object being scanned. The software also provides real-time feedback to indicate missing surface data which are captured during subsequent scans. The software package Geomagic was used to compare the virtual objects generated from the scans with both the corresponding CAD model used to make the print and corresponding geometries from other specimen sets. Geomagic reports dimensional variations from the reference specimen, which may be the CAD model or a part from another scan. Geomagic also calculates the volume of the printed parts from the scan data and makes geometric measurements of part features (length, height, diameter, etc.).

For each specimen geometry, the data from the scans were compared in the following manner:

- CAD to optimal. In this analysis, specimens of a particular geometry manufactured at the optimum setting were compared with the CAD (reference) model. This analysis provides insight into how well the as-built specimen manufactured at the optimal extruder distance approximates the intended coupon geometry.

- CAD to suboptimal. Specimens of a particular geometry manufactured at the suboptimal setting were compared with the CAD (reference) model. This analysis quantifies how much the as-built specimen manufactured at the suboptimal extruder standoff distance differs from the nominal CAD geometry.

- Optimal to optimal. This analysis compares specimens of a particular coupon type to other specimens built at the same (optimal) manufacturing distance in a pairwise manner. It also provides an assessment of build-to-build repeatability in terms of dimensional accuracy for this particular process setting.

- Suboptimal to suboptimal. This compares specimens of a particular coupon type built at the suboptimal extruder distance to other specimens also built at this condition in a pairwise manner. Data provide a way to assess build-to-build repeatability in terms of dimensional accuracy for the closer extruder setting.

- Suboptimal to optimal. This analysis compares dimensions of specimens of the same geometry built at the suboptimal manufacturing setting to those produced at the optimal setting in a pairwise manner. It indicates to what extent dimensional variation for a particular geometry may be impacted by a small change in the extruder distance.

In addition to these analyses specific to the phase II prints, structured light scan data from phase I will also be compared with these results. Phase I results indicated warping of many specimens, an effect particularly noted in the tensile geometries, which have a larger plan surface area in contact with the build tray. This is likely a result of uncontrolled cooling of the print on the build tray (3DP has an unheated bed). ABS also has a relatively high coefficient of thermal expansion, which allows internal stress relief to occur prematurely. Within the context of the phase I data, a farther extruder standoff distance seemed to exacerbate this effect, so slightly more warpage of the material was observed in the ground prints from phase I. At the closer standoff distance commensurate with the phase I flight prints, many of the tensile specimens exhibited protrusions (material deposited beyond the nominal CAD dimensions) in the vicinity of the first layers of the print. This was again observed in the extruder standoff distance study at the closer extruder settings. Based on SEM analyses from phase I, these protrusions served as reinforcing structures which served to artificially strengthen the flight tensile and flexure specimens, built at a closer distance than the ground prints. Protrusion can be seen as red spots around the bottom edge of the flight tensile sample in figure 38. Structured light scanning results from phase I and the subsequent ground-based study suggested most of the differences in geometry between flight and ground samples observed in phase I may be attributable to variation in the extruder standoff distance between the two phases of operation as well as differences in cooling rate, the latter finding suggested by the variable microstructures of the phase I specimens.

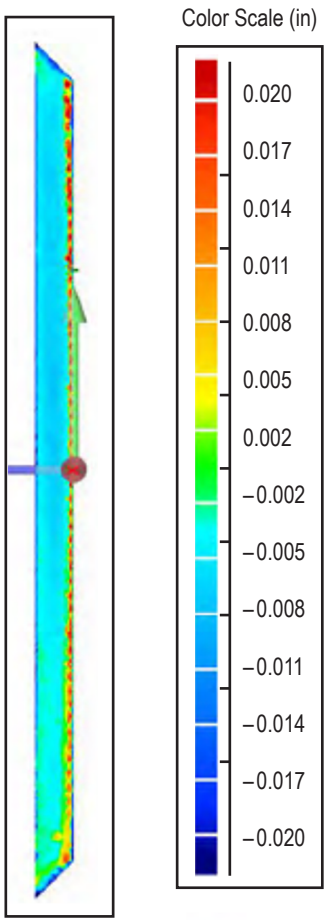

Figure 38. Flight flexure specimen from phase I. Protrusions (excess of material) appear as red regions on the structured light scanning color map.

5.2 Scan Data Comparisons

A summary of data and findings from phase II structured light scanning are summarized in this section. Characteristic values for geometric variation are reported and compared for each specimen set and subsets. The maximum upper deviation and average (+) deviation correspond to the deviation of the geometry from the CAD model in the positive direction; i.e., outside the bounds of the model defined as the reference. The maximum deviation and average (–) refer to the deviation of the geometry from the model in the negative direction; i.e., to what extent the geometry falls inside the bounds of the model defined as the reference. The reference model, in many cases, is the CAD model. In instances where specimens are being compared directly with one another rather than the CAD model, the optimal manufactured specimen is usually defined as the reference. For comparison of suboptimal specimens with one another, the choice of the reference model is arbitrary.

5.2.1 Tensile Specimens

In general, the optimal tensile specimens from phase II show reasonably good agreement with the CAD model for the type IV tensile geometry from which they were constructed. As shown in figure 39, the largest variations from the nominal geometry are noted at the ends of the specimen (the grip section) and at the top of the gauge section. A positive deviation (yellow and red shading) indicates the as-built specimen extrudes outside the boundaries of the CAD model, while a negative deviation (blue) indicates the specimen is undersized relative to the CAD geometry. Green shading indicates the geometries are in agreement. Deviations are reported in inches.

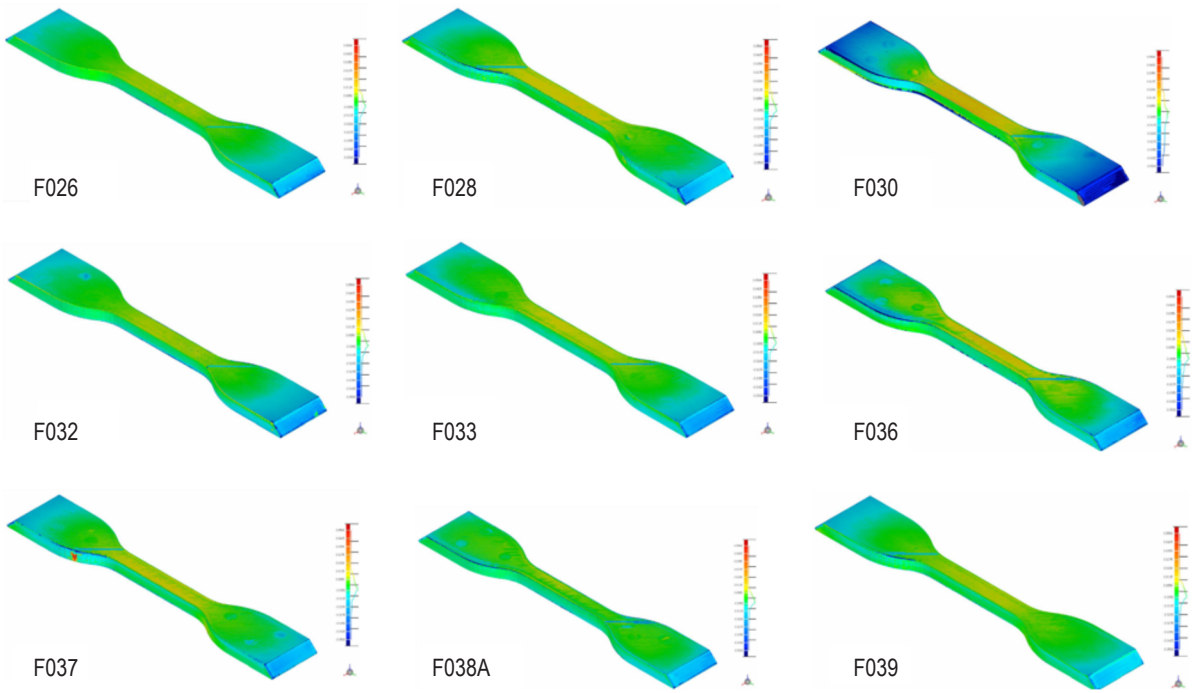

Figure 39. Phase II optimal tensile geometries.

While tensile specimens produced at the optimal manufacturing settings (fig. 39) are remarkably consistent with the CAD model, specimen F037 shows one larger protrusion relative to other specimens near the start of the print. (The point at which the print begins for a tensile specimen is indicated by the diagonal band of material near the transition from the grip section to the narrower cross section of the gauge.) The vast majority of the optimal tensile specimens show good agreement with the CAD model, although there is some negative deviation in the grip sections.

The tensile specimens from phase II manufactured at the closer extruder standoff distance (shown in fig. 40) do not exhibit the same degree of warping and/or protrusions observed in the phase I flight data set and the subsequent ground-based study. While this closer setting did yield a suboptimal geometry in the initial calibration print for phase II operations, which led to the reduction in the *z*-calibration distance/increase in extruder standoff distance at which the 'optimal' prints were subsequently performed, the material produced in the subsequent tensile specimens at the closer

setting does not exhibit these same features. This is an unusual finding and is somewhat inconsistent with previous results, although SEM, discussed in a subsequent section, did reveal a densification of lower layers consistent with the phase I flight tensiles. In general, the deviations from the CAD model are approximately the same for the optimal and suboptimal manufacturing process setting. However, due to limited operations and constraints on crew time, only two tensile specimens were able to be built at the closer extruder setting. As with all flight data, the limitations imposed on the number of specimens that can be produced in an operations window make it difficult to draw conclusions and definitively assess dependencies.

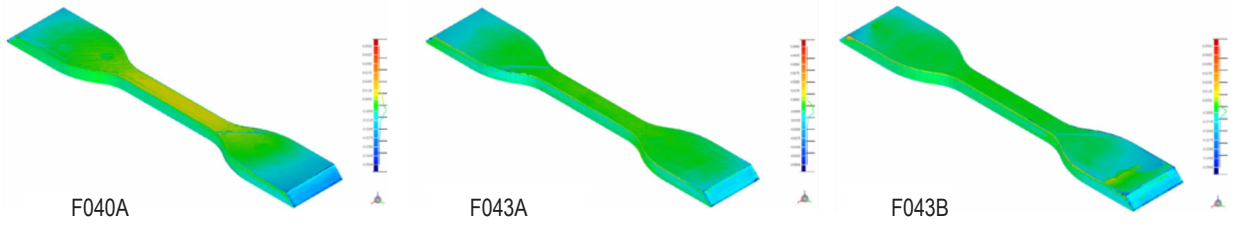

Figure 40. Phase II suboptimal tensile specimens.

Comparisons of specimens made at the optimal distance with other specimens produced at the same setting show a high degree of similarity. A characteristic image from the optimal to optimal comparative analysis is shown in figure 41. The same is true for specimens produced at the suboptimal condition (fig. 42).

Figure 41. Example of a comparison of two optimally manufactured tensile specimens from phase II.

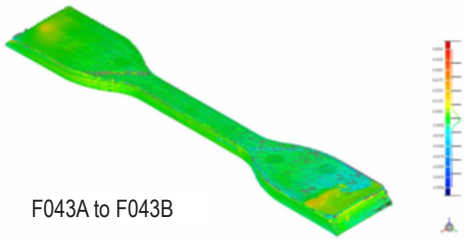

Figure 42. Example of a comparison of two tensile specimens from phase II manufactured at the suboptimal manufacturing setting.

The suboptimal to optimal specimen analyses provide a 'between class' assessment of dimensional variation and is the analysis best poised to assess the variation in geometry, which can result from variation in the extruder standoff distance (fig. 43). Changes in specimen geometry as a result of changes in the commanded position of the build tray relative to the extruder tip in phase I were hypothesized to create protrusions and additional material buildup for some specimens which enhanced the strength of the flight parts. This was not clearly observed in the phase II structured light scanning data but is indicated in other analyses (refer to the sections on SEM and CT). Some representative images from this analysis shown in figure 43 indicate a reasonably good correlation between geometries produced at the suboptimal and optimal settings for phase II.

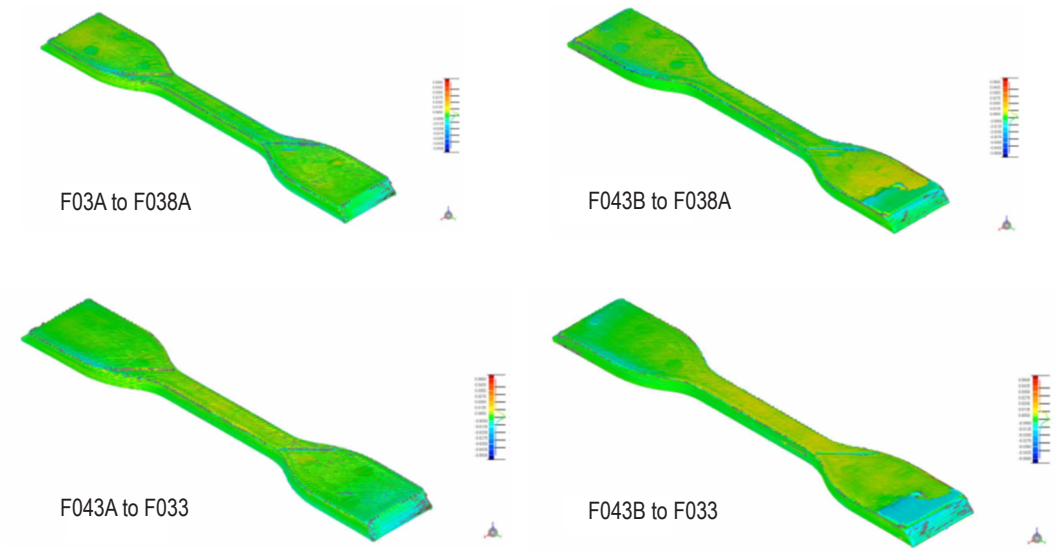

Figure 43. Comparison of specimens manufactured at the optimal condition to specimens manufactured at the suboptimal specimen from phase II.

An isometric view of the structured light scans of the phase I ground tensile specimens appear in figure 44 and the flight tensile specimens are shown in figure 45. Comparing the phase I specimens with phase II, it is evident that the phase I prints in some instances exhibit greater dimensional variation from the CAD model. The additional geometric variation may be attributable to small, nonsystematic changes in extruder distance in the phase I flight prints and the unoptimized extruder setting for the ground prints. Build-to-build variability inherent in operation of any manufacturing hardware is also a contributing factor.

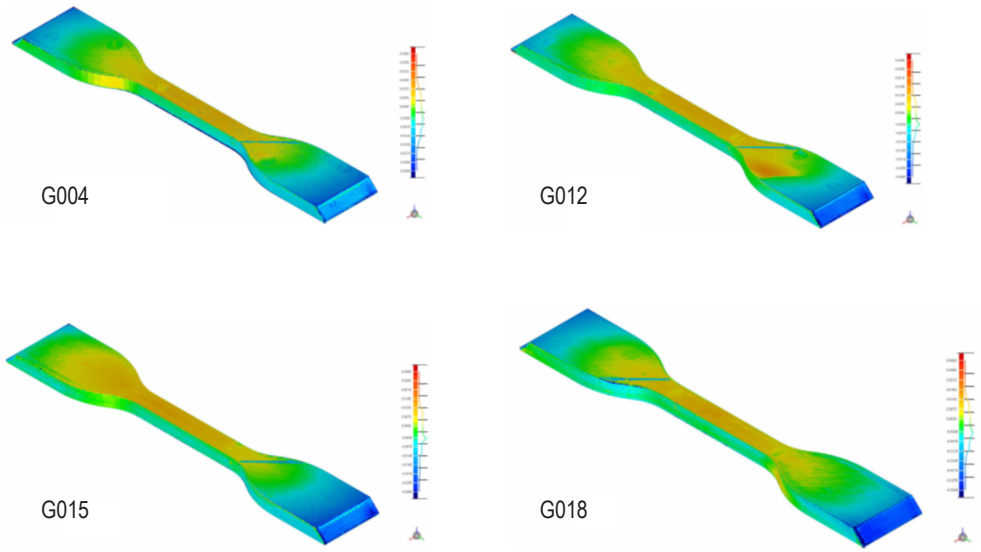

Figure 44. Ground tensile specimens from phase I.

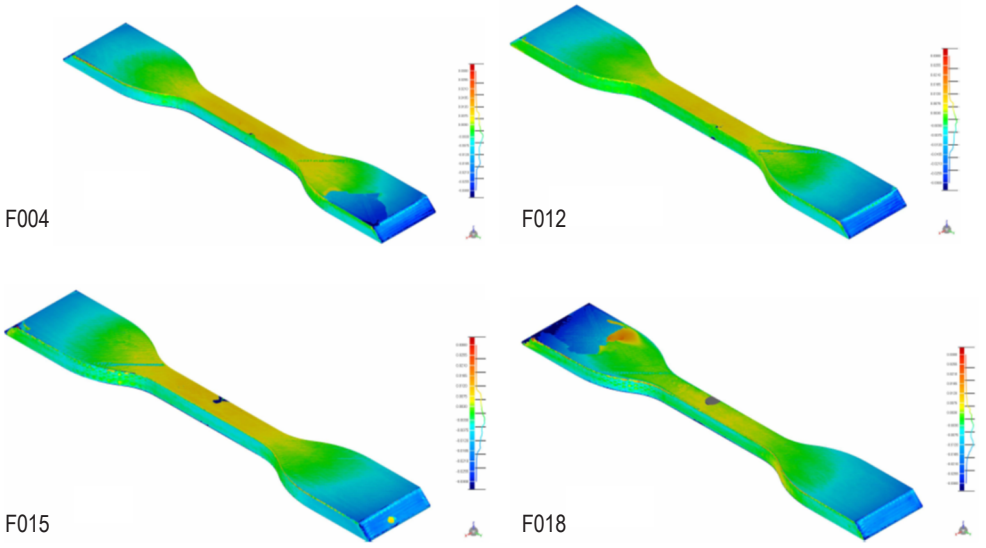

Figure 45. Flight tensile specimens from phase I.

A quantitative analysis of dimensional variation across various data sets is summarized in table 22. While there are differences between specimen sets in terms of the distribution of deviation, as evidenced by the structured light scanning color maps discussed above, the average quantitative metrics are remarkably consistent across specimen sets.

Table 22. Summary of quantitative tensile scan data from structured light scanning.

Specimen Set	Average Maximum Upper Deviation (in)	Average Maximum Lower Deviation (in)	Average Deviation (+) From CAD (in)	Average Deviation (–) From CAD (in)
Optimal tensile to CAD, phase II flight	0.189	–0.224	0.005	–0.012
Suboptimal tensile to CAD, phase II flight	0.146	–0.224	0.005	–0.001
Ground specimens to CAD, phase I	0.147	–0.218	0.007	–0.009
Flight specimens to CAD, phase I	0.198	–0.223	0.005	–0.01

5.2.2 Compression Specimens

Specimens manufactured at the optimal extruder setting during phase II flight operations are shown in figure 46. The large areas of blue shading indicate that many specimens are very slightly undersized (on the order of 0.01 in) relative to the CAD model. Closer examination of the top of some cylindrical specimens show evidence of voids (missing material) and misruns (errors in filament layup), also noted in the CT and SEM analyses. The largest deviations from the CAD model are typically at the top, or sometimes the base, of the cylindrical specimen.

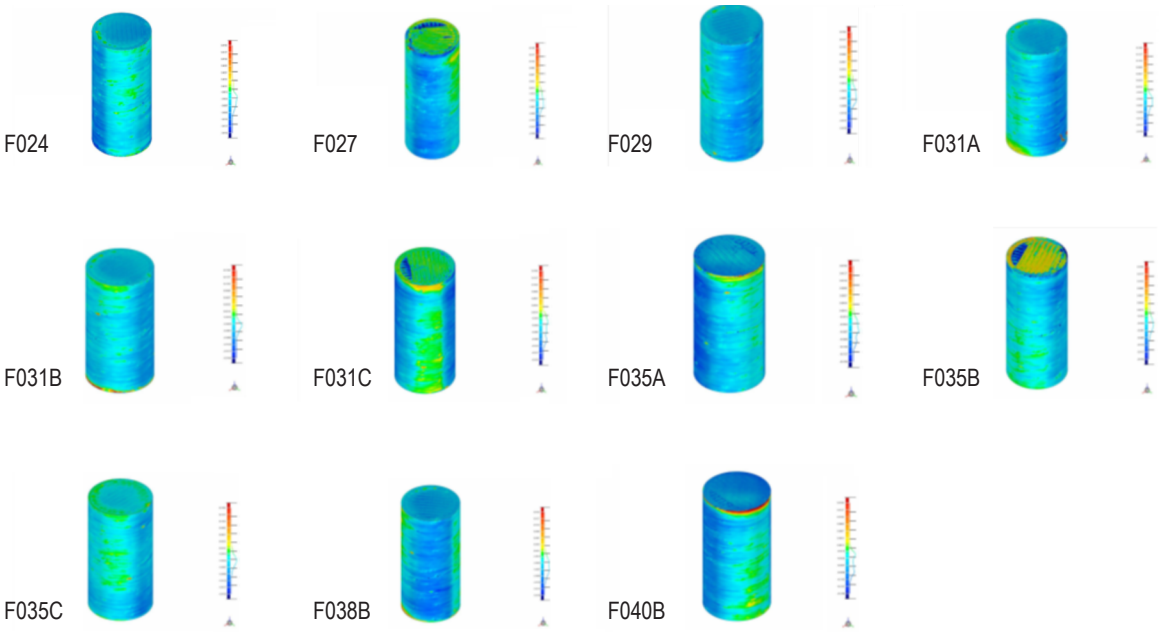

Figure 46. Comparison of compression specimens built at the optimal distance with the CAD model.

Scan data from compression specimens built at the suboptimal manufacturing condition are shown in figure 47.

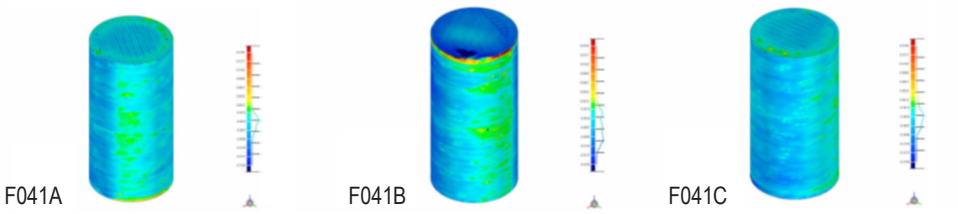

Figure 47. Comparison of phase II compression specimens built at the suboptimal distance with the CAD model.

Comparison of specimens built at the optimal condition to one another demonstrate good correlation, with deviations observed primarily at the outer contours of the cylinder faces at the base and top of the specimens. Figure 48 shows two images from scan data that are characteristic of this analysis.

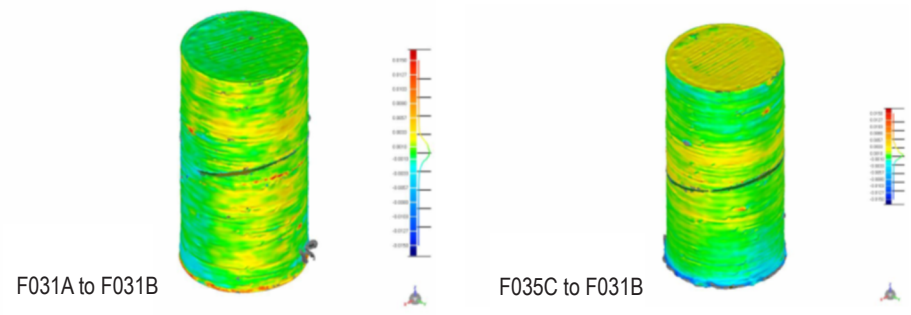

Figure 48. Comparison of compression specimens from phase II built at the optimal manufacturing setting.

Suboptimal specimens (specimens produced at the slightly reduced extruder standoff distance) were also compared with one another. The color mappings (the image in fig. 49 is characteristic) showed strong within-class similarity.

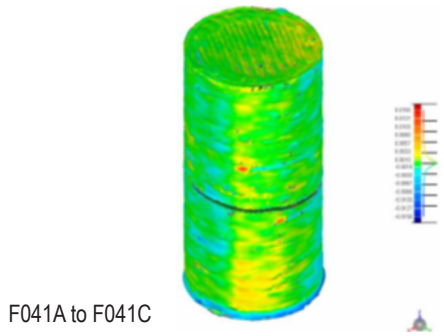

Figure 49. Comparison of compression specimens from phase II, both of which were built at the suboptimal manufacturing setting.

The suboptimal to optimal specimen comparisons showed larger deviations in geometric data than the tensile specimens (fig. 50). Regions of red, yellow, and blue in these images suggest that extruder standoff distance may have a stronger influence on compression specimen geometry than other specimens considered in the phase I and phase II flight prints.

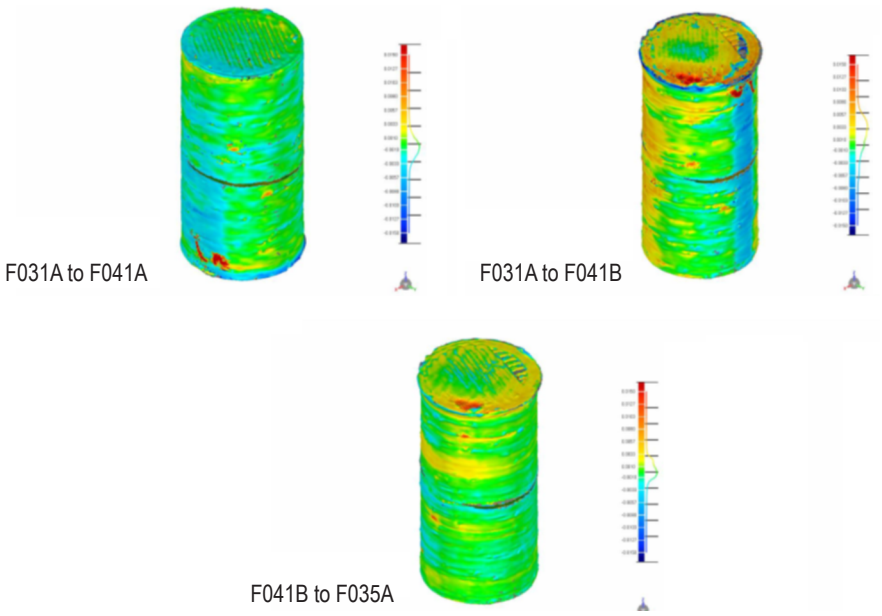

Figure 50. Geometric comparison of specimens manufactured at the optimal and suboptimal manufacturing settings for phase II.

Compression specimens from phase I ground and flight prints with the CAD model are shown for comparison in figures 51 and 52, respectively.

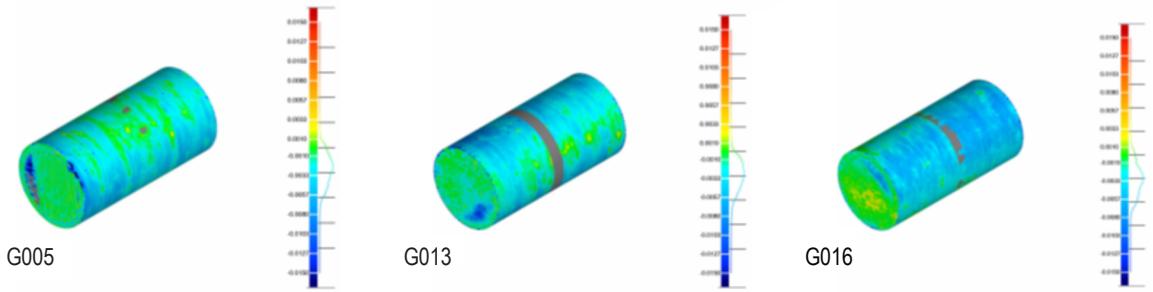

Figure 51. Comparison of ground specimens with the CAD model.

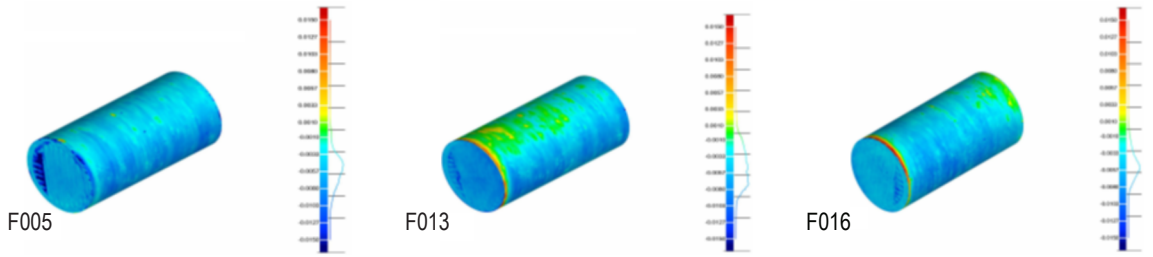

Figure 52. Comparison of phase I flight specimens with the CAD model.

Quantitative data for the compression specimen geometric analysis is summarized in table 23. While the distribution of deviations; i.e., the regions where peak deviations occur, is slightly different for each specimen set, overall average dimensional variation is consistent across specimen sets.

Table 23. Summary of quantitative compression scan data from phases I and II.

Specimen Set	Average Maximum Upper Deviation (in)	Average Maximum Lower Deviation (in)	Average Deviation (+) From CAD (in)	Average Deviation (–) From CAD (in)
Optimal compression to CAD, phase II flight	0.045	–0.05	0.003	–0.004
Suboptimal compression to CAD, phase II flight	0.048	–0.05	0.004	–0.005
Ground specimens to CAD, phase I	0.012	–0.05	0.001	–0.003
Flight specimens to CAD, phase I	0.037	–0.049	0.003	–0.005

5.2.3 Layer Quality Specimens

Figure 53 shows the structured light scanning color maps of phase II specimens produced at optimal conditions (top row) as well as those produced at suboptimal conditions (bottom row). As with the compression specimens, which are geometrically similar to layer quality specimens in height and their footprint on the build tray, the layer quality specimens manufactured at the optimal conditions show good agreement with the CAD model. The blue areas on the structured light scan plots correspond to a slightly undersized geometry on the vertical seams/corners of the specimen. The lack of a heated bed may contribute to this material shrinkage. Specimen F034A has some protruding material along the edges of the specimen at the top layer, which is reflected quantitatively in the specimen's larger upper deviation measurement relative to other specimens in this set.

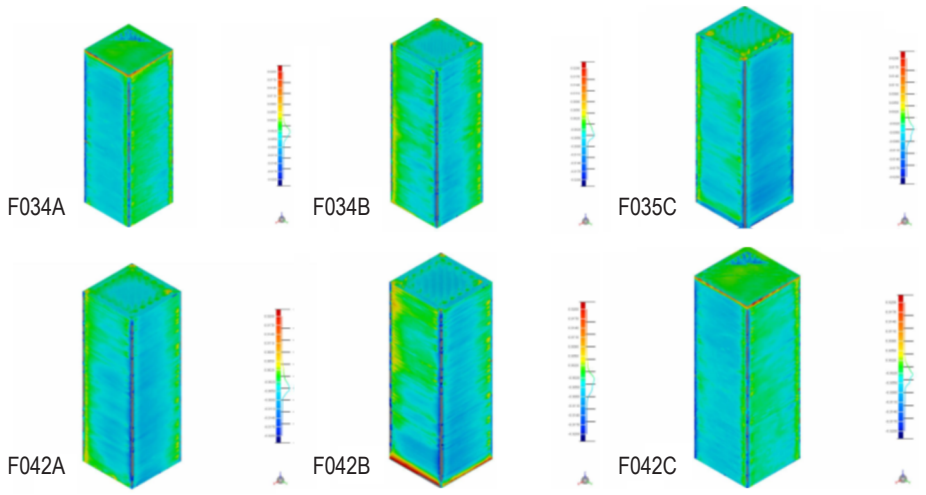

Figure 53. Comparison of layer quality specimens from phase II with the CAD model: Top row: Comparison of layer quality specimens manufactured at the optimal extruder settings to the prescribed geometry. Bottom row: Comparison of layer quality specimens manufactured at the slightly closer extruder settings to their intended geometry.

The layer quality specimens F042A, F042B, and F042C, manufactured at the suboptimal extruder setting, also show good agreement with the CAD model. Overall, layer quality specimens from phase II do not demonstrate significant dimensional differences between the suboptimal and optimal manufacturing settings. Areas of red shading, indicating larger deviations, were observed at the base of specimen F042B.

Specimens produced at the optimal extruder setting exhibit dimensions that are generally consistent with other specimens built at this distance (fig. 54 is characteristic).

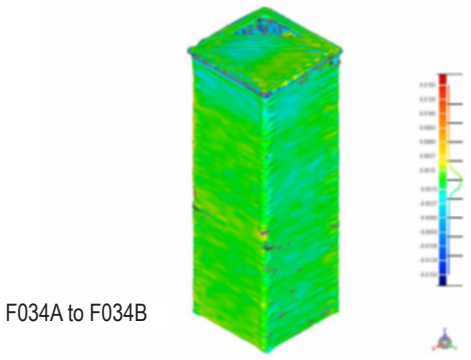

Figure 54. Characteristic comparison of phase II layer quality specimens manufactured at optimal settings to one another.

Specimens built at the suboptimal condition also have strong dimensional correlation with other specimens in this subclass. Relatively larger deviations in alignment of the models are concentrated at the specimen base (fig. 55).

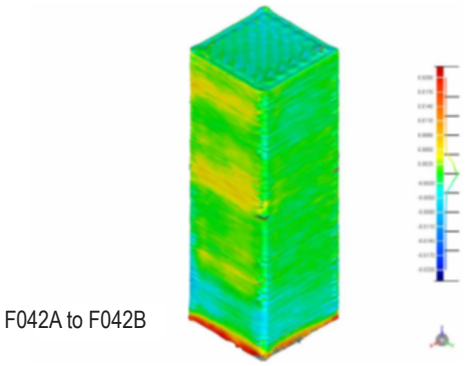

Figure 55. Characteristic comparison of phase II layer quality specimens manufactured at suboptimal extruder distances with one another.

The comparison of specimens built at the closer extruder setting with those constructed at the nominal value shows some dimensional variation between the specimens, with the most significant variations present in the base layers (fig. 56).

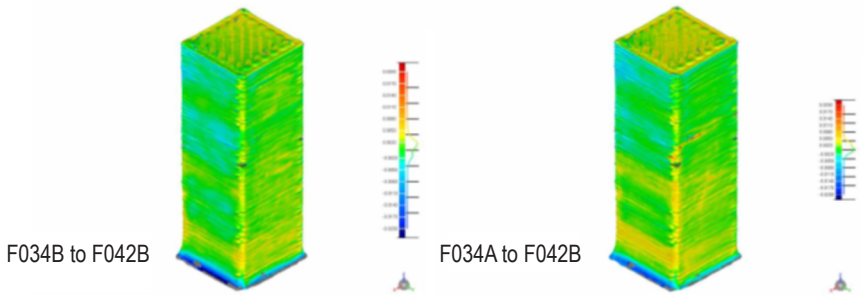

Figure 56. Geometric comparison of specimens from phase II manufactured at the optimal condition to those manufactured at a closer extruder setting.

Structured light scans of ground and flight specimens from phase I are shown in figure 57 for comparison. Specimens are plotted against the CAD geometry. Only a single-layer quality specimen was produced as part of each ground and flight printing campaign in phase I. Table 24 summarizes phases I and II qualitative layer quality scan data.

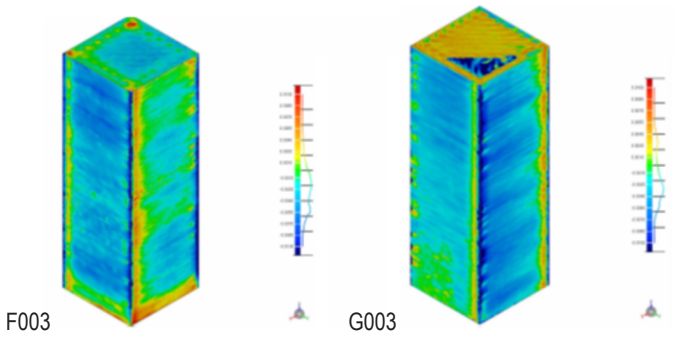

Figure 57. Comparison of layer quality specimens from phase I with the CAD model. F003 is a flight specimen and G003 is a ground-manufactured specimen.

Table 24. Summary of quantitative layer quality scan data from phases I and II.

Specimen Set	Average Maximum Upper Deviation (in)	Average Maximum Lower Deviation (in)	Average Deviation (+) From CAD (in)	Average Deviation (–) From CAD (in)
Optimal layer quality to CAD, phase II flight	0.015	–0.056	0.002	0.004
Suboptimal layer quality to CAD, phase II flight	0.048	–0.05	0.004	–0.005
Ground specimens to CAD, phase I*	0.011	–0.06	0.002	–0.004
Flight specimens to CAD, phase I*	0.02	–0.58	0.002	–0.004

* Only one specimen printed as part of phase I operations.

5.3 Key Findings

Overall, structured light scanning results suggest the geometry of the parts is part of a single family of data. For the phase II prints, geometric variation of the resulting specimen relative to the CAD model is not incredibly sensitive to differences in manufacturing processing conditions changed during the course of operations. There are some inconsistencies in the incidence and magnitude of features such as surface voids and misruns among compression specimens. However, these inconsistencies are present in all data sets and are not specific to the compression specimens produced in microgravity. Any subtle variations in geometry are thus likely attributable to differences in extruder distance and build-to-build variability rather than the influence of microgravity on the printing process.

6. COMPUTED TOMOGRAPHY

Results of CT scans of phase II specimens are detailed in this section. Data are compared to scans of phase I specimens where appropriate.

6.1 Methodology

As with the phase I samples, CT imaging was performed using a microfocus x-ray tube and digital detector panel. Computed tomography is a volumetric inspection method that produces images of cross sections of the inspected material. Each 'CT slice' provides a visual depiction of material structure and density at a specific plane in the part. For example, CT slices taken on a plane parallel to the face of a cube will be square images, while CT slices taken perpendicular to the long axis of a cylinder would be a circular image. Individual slices taken at successive steps through the volume of the inspected part can be reconstructed into a data volume depicting the 3D structure and density of the inspected part, and subsequently manipulated to reveal internal configuration of the part.

For phase II, only a subset of tensile and compression specimens was analyzed using CT. Specifically, three optimal compression specimens (F028, F033, and F038A) were compared with one another and with three specimens manufactured at a suboptimal extruder distance (F043A, F043B, and F043C). For the tensile specimen analysis, three tensile specimens were compared with one another (F028, F033, and F038A) and with two specimens (F043A and F043B) manufactured at the suboptimal (closer extruder) setting. Each specimen required two scans to capture the full volume due to CT scanner size limitations. Scans A and B each correspond to half of the specimen. Phase II specimen CT data were compared with phase I data where appropriate.

Direct quantitative comparisons between phases I and II were largely precluded by a software upgrade to the microfocus CT unit that occurred between the phase I and phase II evaluation, although an algorithm to convert between scales was developed and the phase II data were reanalyzed to facilitate comparison. In the CT software module used to scan the phase I specimens, each discrete CT number was on a scale of zero—no density, full x-ray penetration to 65,535—impenetrable density, no x-ray penetration. These numbers represent a gray level among the 16-bit data that form the image. For phase II, the scale was reduced to a very small fraction of 1. The original equipment manufacturer for the microfocus CT unit has indicated that no precise conversion factor is readily available to map these two numbers onto the same relative scale. For this reason, phase I and phase II comparisons are primarily qualitative, although quantitative comparisons enabled by the conversion algorithm are reported for completeness.

The output of the phase II analysis consists of CT slices and a reconstructed data volume representing the radiographic density and geometric configuration of each specimen. Each sample's data set was analyzed using Volume Graphics VGSTUDIO software. For phase II specimens, solid ABS disks of known density were scanned along side each sample to provide a reference value for the CT density number (a unitless measurement corresponding to the combined influence of physical density and x-ray absorption in the cross section of the sample material). In addition to the mean CT number, density for each specimen is expressed as a proportion of known physical density of the solid ABS. For phase I samples, only the mean CT (raw value output by the software) was considered, as a specimen of known density was not scanned alongside the part. While mean CT is valuable for relative comparisons between specimens, it does not readily permit comparison of the specimen to a 'true' bulk density value for the base material. In the phase I data, only mean CT values were considered since a conversion from mean CT to gravimetric density was not possible for the phase I specimen set.

The procedure for analysis of a specimen and calculation of relative density of the specimen compared to solid ABS is as follows (used for all specimens in phase II, and with the exception of scanning the bulk ABS disc of known density alongside the part, does not differ significantly from phase I analysis procedures):

(1) A region of interest in the CT volume image of the specimen, drawn to encapsulate the maximum possible volume within the specimen without including surrounding air or supporting material, is selected.

(2) VGStudio's volume analyzer tool measures the mean CT number of the selected volume in the specimen and records the mean value.

(3) A region of interest in the CT volume image of the solid ABS reference disk, drawn such that the volume is contained within the ABS disk without including the volume of the test specimen, supporting structures, or inherent artifacts in the outer perimeter of the CT image, is selected. The mean CT value for this volume is recorded.

(4) The ratio of the mean CT number of the specimen volume to the mean CT number of the solid ABS reference disk is calculated. To estimate the physical density of the specimen, this ratio is multiplied with the known physical density of the ABS reference disk.

(5) Each CT slice is visually reviewed. Images of identified anomalies are recorded. Regions of anomalies and trends in images are also noted.

The output of the CT analysis was a calculated ratio of CT numbers of each sample and the reference ABS disk and images in 2D, 3D, or both, as appropriate to describe the type and location of anomalies detected in the course of the analysis.

6.2 Results of Computed Tomography Analysis

The analyzed samples for phase II were in two categories:

(1) Cylindrical compression test specimens (F031B, F035B, F035C, F041A, F041B, and F041C). F041 specimens were manufactured at the suboptimal manufacturing process setting.

(2) Rectangular tensile test specimens (F028, F033, F038A, F043A, and F043B). Specimens F043A and F043B were manufactured at the suboptimal manufacturing process setting.

In an analysis step, distinct from phase I, as noted previously, the procedure included comparison of the CT numbers output by the CT software to those collected from a solid, conventionally manufactured disk of ABS that was scanned in the same CT scan as the specimens for categories (1) and (2). The ratio of CT numbers for the printed material to those for the solid material should correlate approximately linearly to the difference in bulk physical densities between the two materials. An estimate of the bulk physical densities of the printed part can then be obtained by multiplying the calculated ratio of CT densities by a known density of the solid ABS obtained by other methods.

Review of the individual CT slices revealed a large number of features that may not be detrimental to performance or integrity of the printed hardware. Because their impact on material performance is unknown, they have not been characterized as defects. Rather, they are considered evident irregularities or anomalies that are visible in CT and fall into one of a few categories:

(1) Voids—rounded gaps in printed layers that may persist vertically in the *z*-direction (usually the symmetry axis of the printed part).

(2) Misruns—print lines that cross over adjacent lines.

(3) High-density inclusions—particles of higher density than the baseline ABS density.

It must be emphasized that none of these features are known to be a defect but were instead identified for their apparent deviation from observed baseline material uniformity and/or geometry. They have been documented in this TP for the purpose of assisting either diagnosis of performance variations in mechanical testing or characterizing performance of the varying printing parameters used to produce the specimens.

6.2.1 Computed Tomography Analysis of Phase II Tensile Specimens

Table 25 summarizes the quantitative CT data for analysis of the phase II tensile specimens. The specimens range from 93% to 98% of ABS's injection molded density (calculation based on the mean CT value of a disc of conventionally manufactured ABS scanned alongside each specimen), which stands in good agreement with the gravimetric density measurements derived from structured light scanning, which provides a closed part volume, and mass measurement. There is very little change noted in relative density values from the average density of the specimen set. The density of all the phase II tensile specimens is remarkably consistent with only a 1% standard deviation in the bulk sample values. Comparing relative densities between the tensile sets produced at the optimal

setting (F028, F033, and F038A) and suboptimal setting (F043A and F043B), there was a slight trend toward lower-than-average relative density in the former set and higher-than-average density in the latter set. This is consistent with the phase I findings, where parts produced at closer extruder distances exhibited slightly higher densities and mechanical performance. While specimen sets are small, this provides further supporting evidence that the differences observed in phase I were an artifact of differences in manufacturing process settings rather than a microgravity effect.

Table 25. Summary of CT scan data for phase II tensile specimens.

Specimen ID No.	Bulk Sample*	Bulk ABS*	Ratio to ABS	Delta From Average	Voids	Misruns	Inclusions
F028 side A	0.0215218	0.02273989	0.946434	–0.01146526	10	1	–
F028 side B	0.0212206	0.02273989	0.933188	–0.024710706	12	–	–
F033 side A	0.0216829	0.02273989	0.953518	–0.004380793	11	2	3
F033 side B	0.0216467	0.02273989	0.951926	–0.005972709	9	–	–
F038A side A	0.0217699	0.02273989	0.957344	–0.000554917	8	2	–
F038A side B	0.0218956	0.02273989	0.962872	0.004972814	10	–	1
F043A side A	0.0219159	0.02273989	0.963765	0.005865518	8	2	1
F043A side B	0.0222339	0.02273989	0.977749	0.019849754	8	1	1
F043B side A	0.0220158	0.02273989	0.968158	0.010258679	6	1	6
F043B side B	0.021922	0.02273989	0.964033	0.006133769	5	–	8

* Values are relative and unitless and indicate the x-ray absorption. Higher values correspond to more absorption; thus, a higher value indicates higher physical density.

Variation of the number of features (voids, misruns, or inclusions) for the tensile specimens was also small across the phase II tensile data set. Perhaps most importantly, there was no evident trend in the number of voids or misruns when comparing sample set F028, F033, and F038A to set F043A and F043B. This is illustrated in figure 58. The number of inclusions (higher density material imbedded within the sample or on its outside surface) was small except for sample F043B, which had 14 detected inclusions. There is no other observable trend in the number of inclusions in the tensile samples.

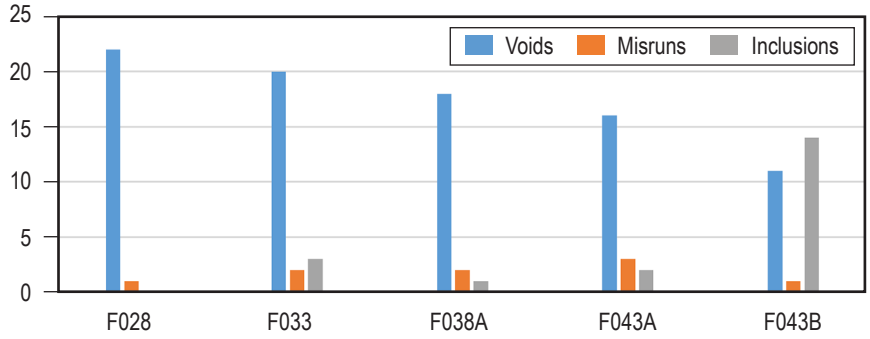

Figure 58. Comparison of the number of voids, misruns, and inclusions detected in the subset of the phase II tensile specimens.

Characteristic images of the tensile specimens considered in the phase II CT analysis are shown in figure 59 (*x*-*y* plane) and figure 60 (*x*-*z* plane). While there are no noticeable differences in tensile specimens in figure 59, the specimens manufactured at the closer extruder distance in figure 60 (F043A and F043B) exhibit slight protrusions at the base of the specimens and densification of lower layers, a finding consistent with SEM results and phase I flight specimens, manufactured at a similar process setting. There is no known change in the process for specimen 43B that could explain the much greater incidence of inclusions (defined as the presence of particles of higher density than the known ABS density) for this specimen relative to other specimens (both tensile and compression) analyzed. Additional images of CT slices from the tensile specimens appear in figure 61.

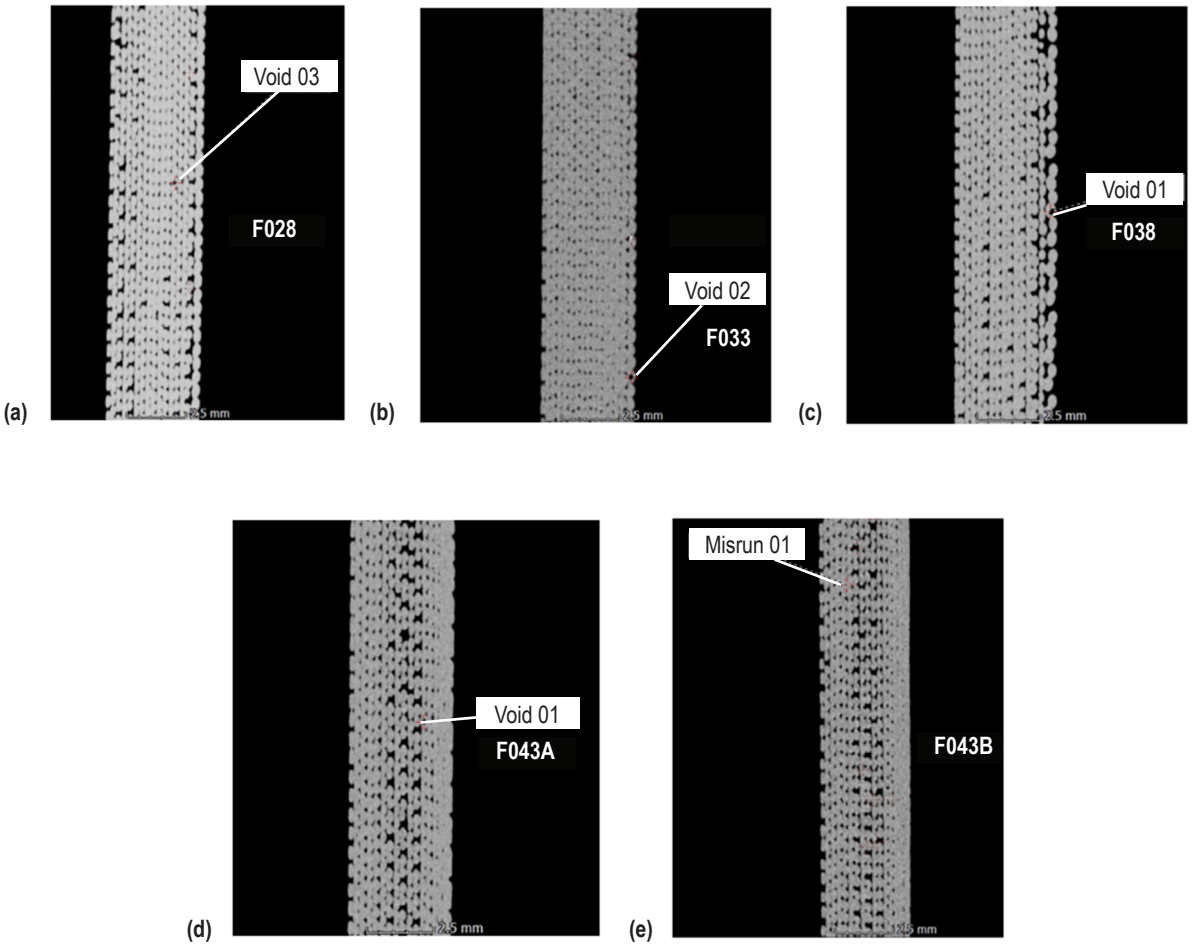

Figure 59. Characteristic cross-sectional images of tensile specimens in the *x*-*y* plane. Void or misrun number identifies the *n*th void or misrun found in that particular specimen. Specimens (a)–(c) were manufactured at the optimal extruder distance, while specimens (d)–(e) were intentionally manufactured at a closer extruder setting.

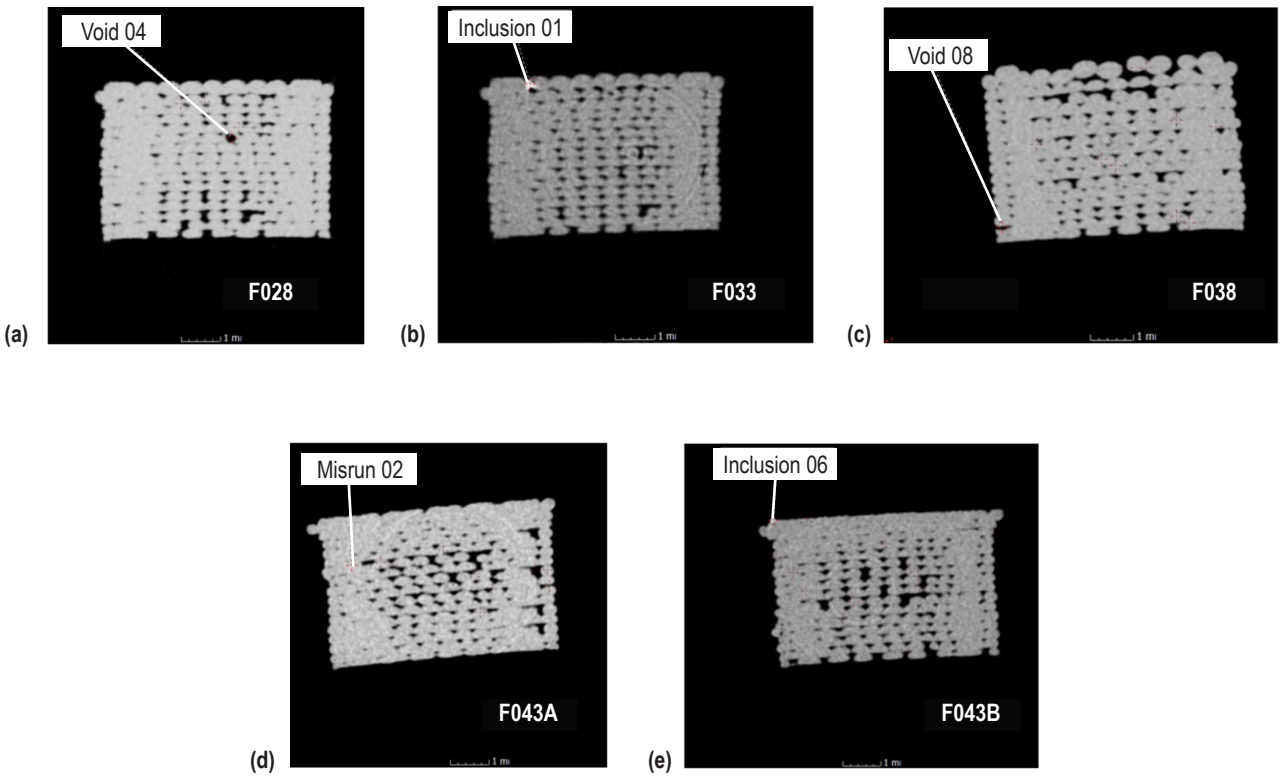

Figure 60. Characteristic cross-sectional images of tensile specimens in the *x*-*z* plane. Void, misrun, or inclusion number identifes the *n*th void, misrun, or inclusion found in that particular specimen. Specimens (a)–(c) were manufactured at the optimal extruder distance, while specimens (d)–(e) were intentionally manufactured at a closer extruder setting. The base of the specimen lies near the top of the image.

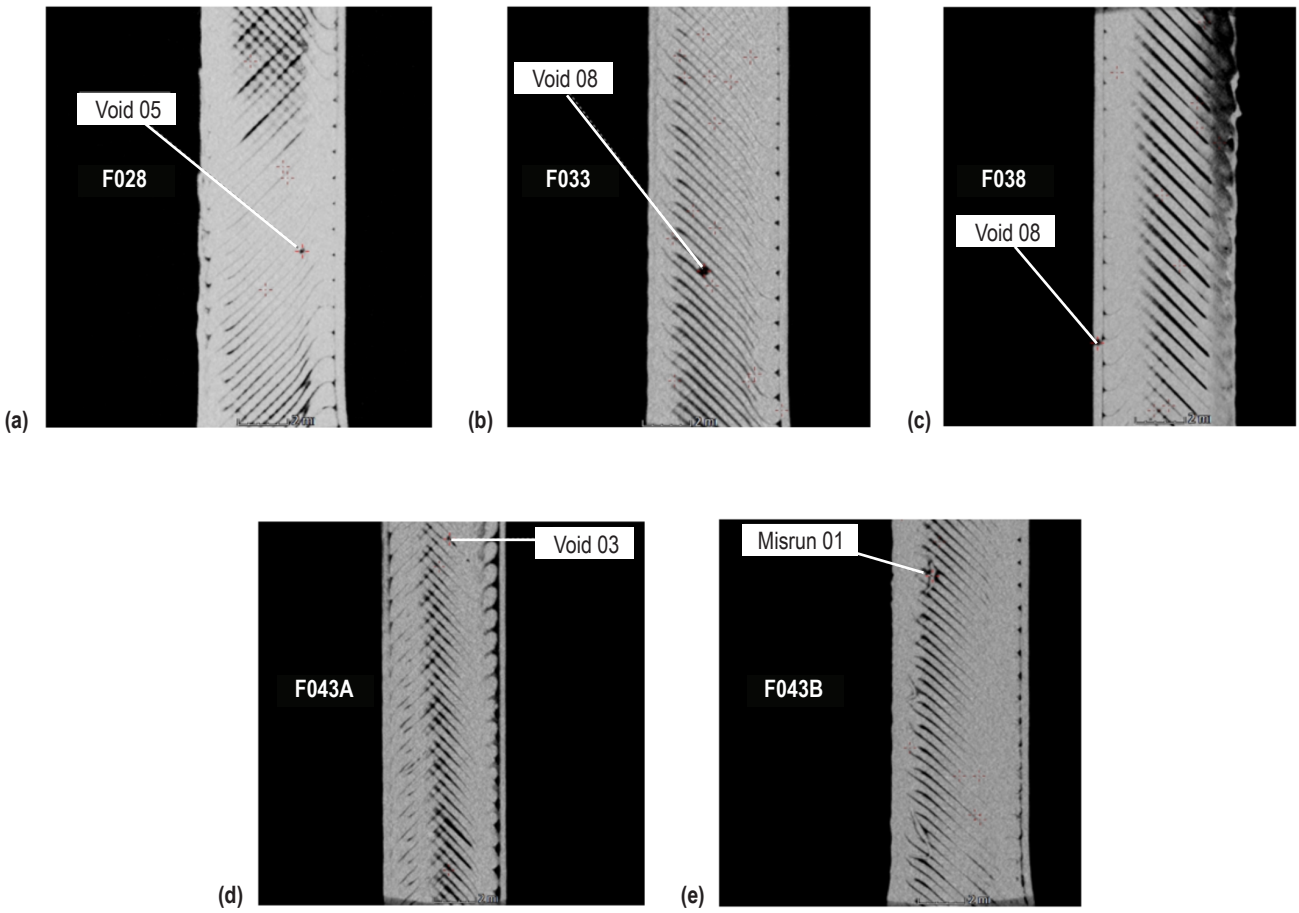

Figure 61. Characteristic cross-sectional images of tensile specimens in the *y*-*z* plane. Void or misrun number identifies the *n*th void or misrun found in that particular specimen. Specimens (a)–(c) were manufactured at the optimal extruder distance, while specimens (d)–(e) were intentionally manufactured at a closer extruder setting. No clear trends in the specimens are noted.

6.2.2 Computed Tomography Analysis of Phase II Compression Specimens

Table 26 summarizes the quantitative data from CT analysis of the compression specimens. The ratio to density of injection molded ABS for the compression specimens ranges from 0.92 (92% of bulk ABS density in the printed specimen) to 0.99. In contrast to the tensile specimens, there was a discernable trend of different numbers of voids and misruns in the two sets of compression samples (fig. 62). Comparing the set F031B, F035B, and F035C to F041A, F041B, and F041C, a larger number of both voids and misruns were noted in the latter set. In comparing relative density with respect to solid ABS between sets of samples, there was a slight trend in comparing the optimally manufactured compression set F031B, F035B, and F035C to suboptimal F041A, F041B, and F041C, with relative densities slightly higher than the overall average in the former set and slightly lower than the overall average in the latter set. This is consistent with the phase I finding, suggesting that compression specimens produced at a too close extruder distance are slightly less dense and slightly weaker on the metric of compressive strength than specimens produced at a farther extruder distance.

Table 26. Summary of CT scan data for phase II compression specimens.

Sample ID No.	Bulk Sample*	Bulk ABS*	Ratio to ABS	Delta From Average	Voids	Misruns	Inclusions
F031B side A	0.0212304	0.0227312	0.933976209	–0.01478495	29	14	1
F031B side B	0.0212718	0.0227469	0.935151603	–0.013609556	33	19	5
F035B side A	0.0224517	0.0226597	0.990820708	0.042059549	31	9	5
F035B side B	0.0213097	0.0221156	0.963559659	0.0147985	26	14	1
F035C side A	0.0220072	0.0230108	0.956385697	0.007624538	32	29	6
F035C side B	0.0218651	0.0228215	0.95809215	0.009330991	39	20	3
F041A side A	0.0212412	0.0230395	0.921947091	–0.026814068	46	27	1
F041A side B	0.0218558	0.0228031	0.958457403	0.009696244	48	24	2
F041B side A	0.0212098	0.0226815	0.935114521	–0.013646638	45	23	2
F041B side B	0.0214367	0.0228406	0.93853489	–0.010226269	42	21	1
F041C side A	0.0214168	0.022743	0.941687552	–0.007073607	51	23	5
F041C side B	0.0215896	0.0226923	0.951406424	0.002645265	47	27	1

* Values are relative and unitless and indicate the x-ray absorption. Higher values correspond to more absorption; thus, a higher value indicates higher physical density.

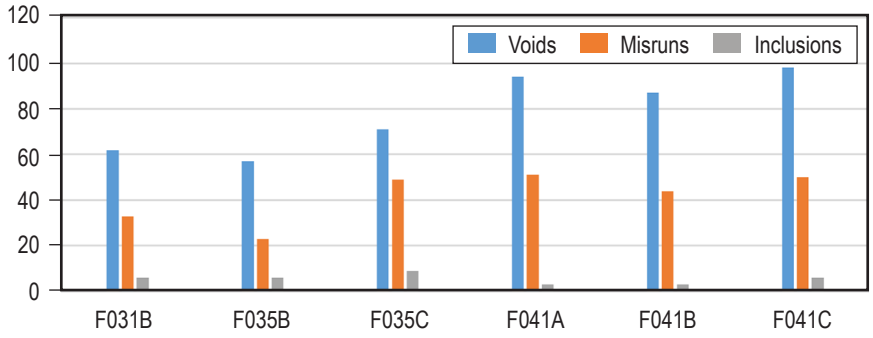

Figure 62. Comparison of number of voids, misruns, and inclusions detected in a subset of the phase II compression specimens.

Characteristic images of the compression specimens considered in the phase II CT analysis are shown in figure 63 (circular cross sections of specimens in the *x*-*y* plane) and figure 64 (rectangular cross section in the *x*-*z* plane). No clear trends are noted expect for an increase in the number of misruns for specimens manufactured at the closer extruder setting. These misruns are more prevalent in the *x*-*y* plane.

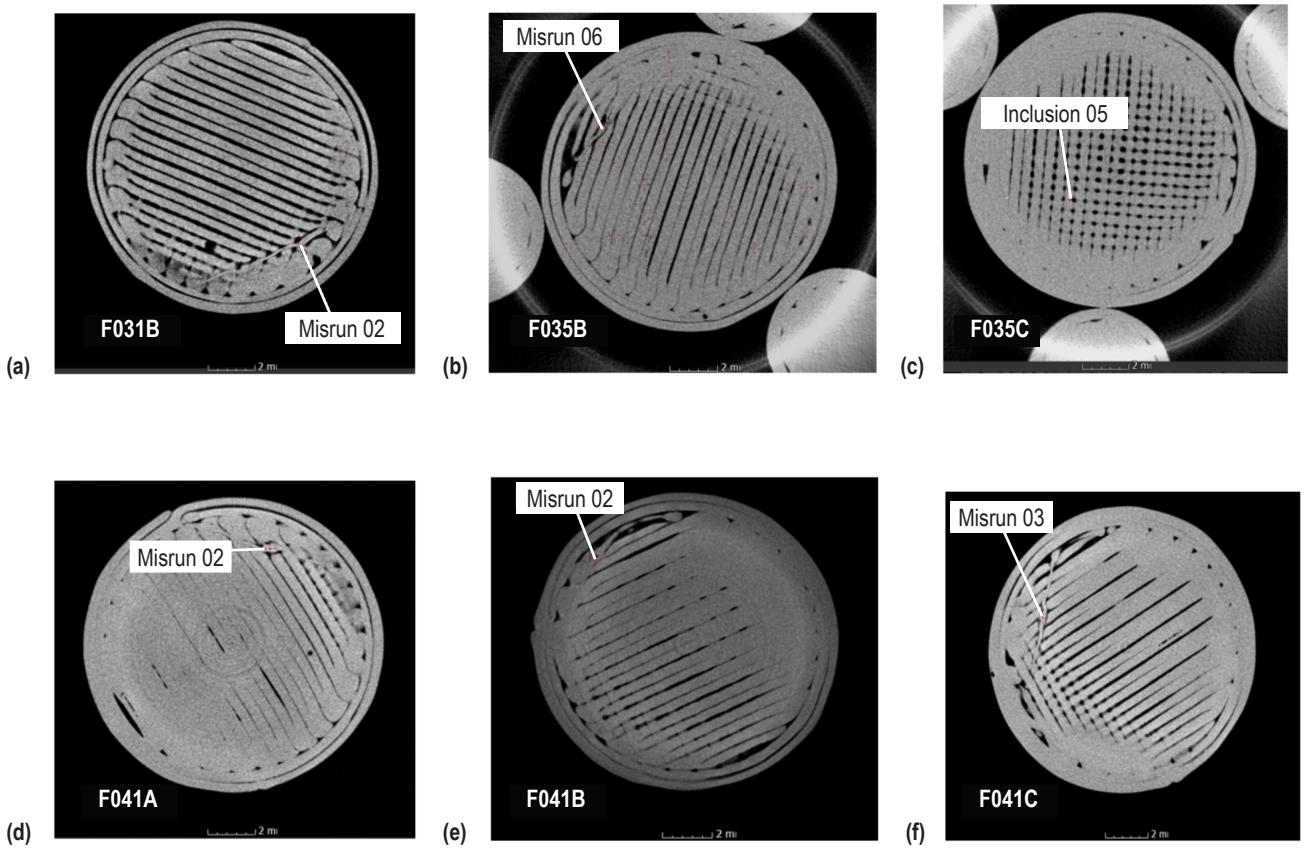

Figure 63. Characteristic cross-sectional images of compression specimens in the *x*-*y* plane. Numbers associated with a void, inclusion, or misrun identify the *n*th feature found in that particular specimen. Specimens (a)–(c) were manufactured at the optimal extruder distance, while specimens (d)–(f) were intentionally manufactured at a closer extruder setting.

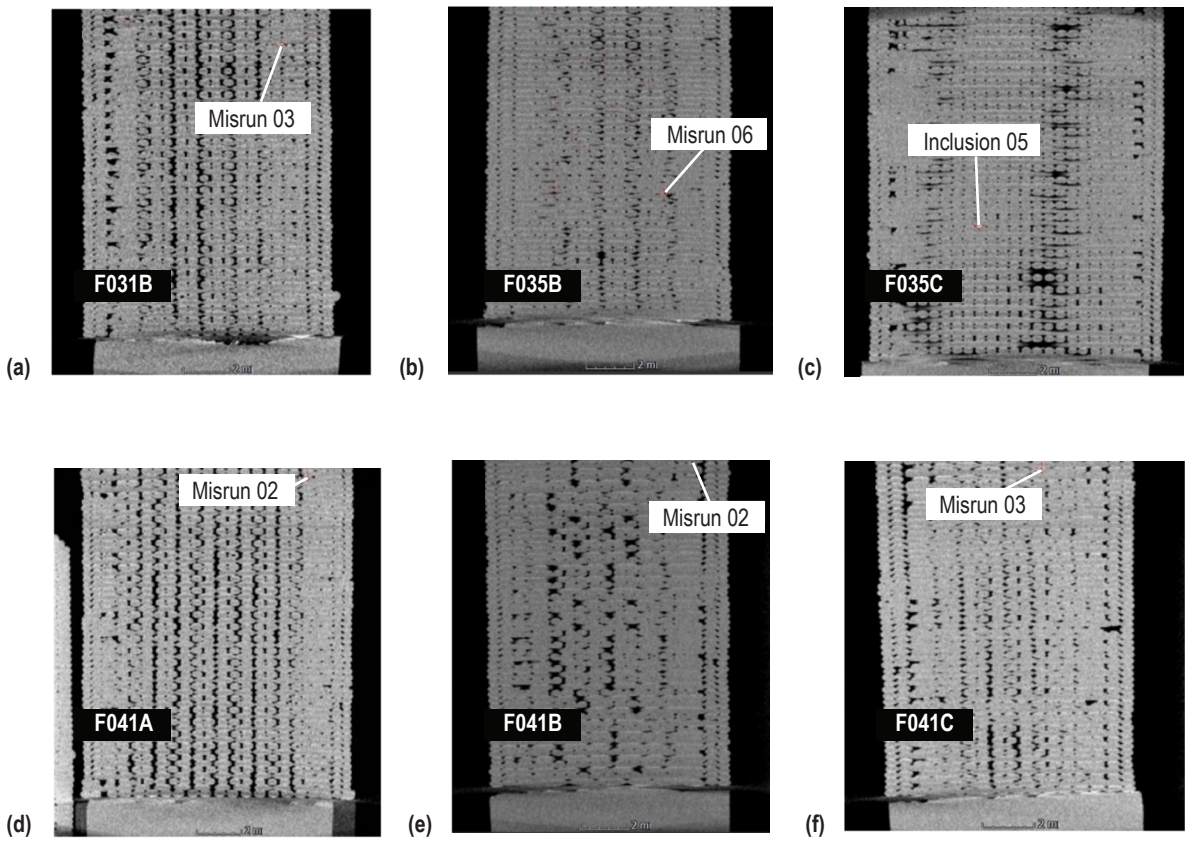

Figure 64. Characteristic cross-sectional images of compression specimens in the *x*-*z* plane. Numbers associated with a void, inclusion, or misrun identify the *n*th feature found in that particular specimen. Specimens (a)–(c) were manufactured at the optimal extruder distance, while specimens (d)–(f) were intentionally manufactured at a closer extruder setting.

6.2.3 Comparison With Phase I Computed Tomography Data

Computed tomography analysis was performed for all flight and ground specimens from 3DP phase I. The key finding from CT analysis from the first phase of operations was that the bulk densities of the flight and ground articles (mean CT value) did not differ significantly. Density gradients in the through-thickness of specimens in the build direction were observed, and this variation seemed to be more pronounced for flight tensile specimens built at a closer extruder standoff distance than the ground specimens. For some phase I specimens, the bottom half of specimens were generally more dense than the top half, but the density variation between these regions was not found to be statistically significant. Review of the initial raw images from the CT scans (shown in fig. 65) confirm that the density of the material decreased as vertical distance from the build start point increased. Observation of this feature in the phase II specimens was not noted during the analysis. Its absence could be attributed to improved process controls for phase II operations, which represent more of a 'locked' manufacturing process than procedures executed in phase I.

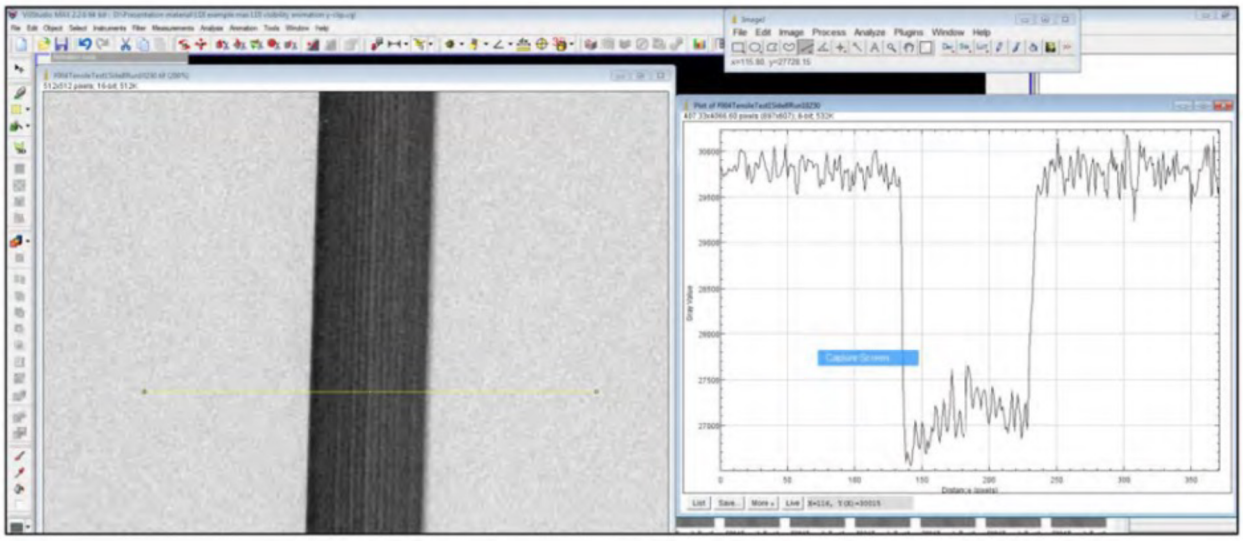

Figure 65. Raw image from CT scan of flight tensile coupon (F004) showing density differences between the upper and lower half of the specimen.

The phase II compression and tensile sets were compared with analogous specimens from the previous sample set. Phase I includes both flight prints and ground prints, the latter made with the printer prior to its launch to the ISS. Quantitative comparison of density between phase I and phase II specimens was complicated by software upgrades to the microfocus CT unit between phase I and phase II specimen analysis, which resulted in the raw density data (mean CT) being reported on dramatically different scales. A method to readily convert between the mean CT range output by the previous software (zero for no density and full x-ray penetration to 65,000 for impenetrable density) and the range output in phase II (on a 1.0 scale) was developed to facilitate comparison of specimen sets of the same geometry. Table 27 summarizes the mean CT values for all tensile specimens analyzed to date. Group comparisons are shown in the bar chart in figure 66. When considered on the same scale (the zero to 65,000 scale used in phase I analysis), phase II specimens have slightly lower mean CT values than phase I specimens and the suboptimal specimens have a significantly lower mean CT value. This is inconsistent with gravimetric density results reported in section 3 and may call into question the efficacy of the scale conversion method. (The most robust technique would be to rescan phase I specimens using the upgraded software.)

Table 27. Mean CT values for tensile specimens from phases I and II.

Specimen ID No.	Specimen Type	Mean CT
G004 side A	Ground phase I	44,111
G004 side B	Ground phase I	35,964
G012 side A	Ground phase I	35,207
G012 side B	Ground phase I	39,667
G015 side A	Ground phase I	22,582
G015 side B	Ground phase I	38,424

Table 27. Mean CT values for tensile specimens from phases I and II (Continued).

Specimen ID No.	Specimen Type	Mean CT
G018 side A	Ground phase I	36,747
G018 side B	Ground phase I	35,439
F004 side A	Flight phase I	45,717
F004 side B	Flight phase I	38,777
F012 side A	Flight phase I	36,113
F012 side B	Flight phase I	39,452
F015 side A	Flight phase I	34,640
F015 side B	Flight phase I	39,153
F018 side A	Flight phase I	40,201
F018 side B	Flight phase I	40,288
F028 side A	Flight phase II—optimal	40,988
F028 side B	Flight phase II—optimal	45,707
F033 side A	Flight phase II—optimal	10,031
F033 side B	Flight phase II—optimal	38,658
F038A side A	Flight phase II—optimal	42,283
F038A side B	Flight phase II—optimal	31,452
F043A side A	Flight phase II—suboptimal	41,182
F043A side B	Flight phase I—suboptimal	12,211
F043B side A	Flight phase II—suboptimal	18,552
F043B side B	Flight phase II—suboptimal	28,090

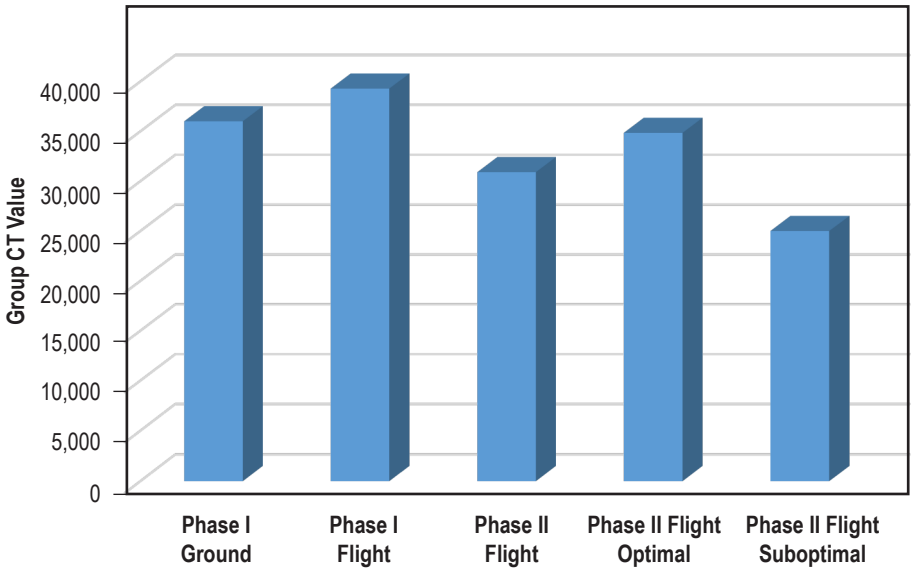

Figure 66. Comparison of characteristic mean CT values for tensile specimens across specimen sets.

Table 28 tabulates the mean CT values (converted to the same scale) for phase I and phase II compression specimens. In addition to differences in the software scale, which required development of a sophisticated conversion technique for the phase II data set to facilitate comparisons, phase II compression specimens were scanned in two sections to increase the fidelity of the data. Figure 67 compares the average CT value for specimen groups. Phase II flight specimens have lower mean CT values than phase I specimens. Specimens manufactured at the suboptimal setting also have lower mean CT values than other compression specimens. These findings are somewhat inconsistent with gravimetric density comparisons, where the phase I flight specimens had a lower density than all other groups. There is also substantially greater variation in the CT numbers for the phase II parts after conversion to the original scale (zero to 65,000, with the latter corresponding to full x-ray penetration). The reason for this is not well understood and was not noted in the phase II data prior to scale conversion.

Table 28. Mean CT values for compression specimens from phases I and II.

Specimen ID No.	Specimen Type	Mean CT
G005	Ground phase I	29,238
G013	Ground phase I	26,709
G016	Ground phase I	27,369
F005	Flight phase I	28,332
F013	Flight phase I	29,704
F016	Flight phase I	29,739
F031B side A	Flight phase II—optimal	22,022
F031B side B	Flight phase II—optimal	14,244
F035B side A	Flight phase II—optimal	27,369
F035B side B	Flight phase II—optimal	18,641
F035C side A	Flight phase II—optimal	17,704
F035C side B	Flight phase II—optimal	21,232
F041A side A	Flight phase II—suboptimal	16,546
F041A side B	Flight phase II—suboptimal	19,173
F041B side A	Flight phase II—suboptimal	5,507
F041B side B	Flight phase II—suboptimal	6,576
F041C side A	Flight phase II—suboptimal	19,626
F041C side B	Flight phase II—suboptimal	30,119

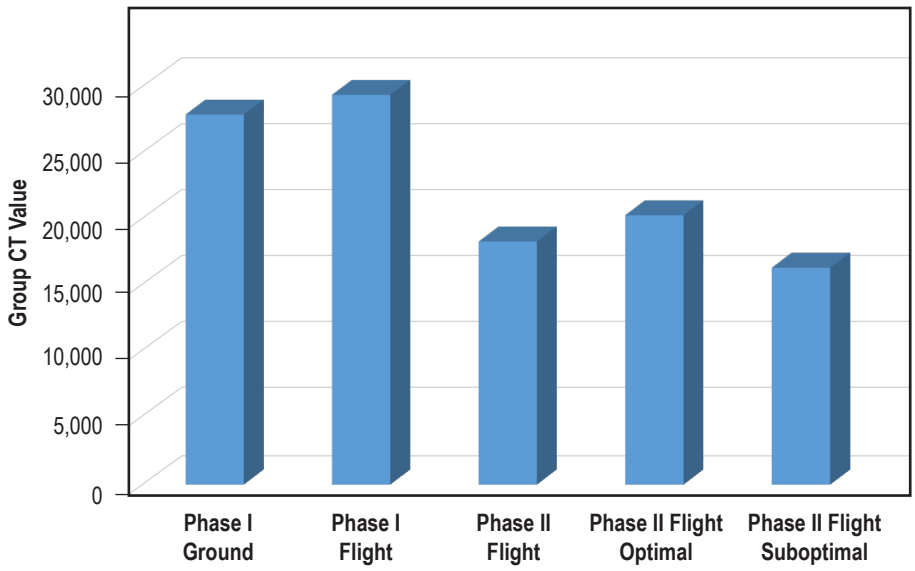

Figure 67. Comparison of characteristic mean CT values for compression specimens across specimen sets.

Given the differences in scale, equipment, and scanning techniques between phase I and phase II specimen analysis, qualitative comparisons are, in this instance, more meaningful. Qualitative comparisons of phase II compression and tensile specimens with phase I specimens reveal several important similarities. Type II voids, which are observed between infill and contour and occur when the infill material does not fully attach to the contour material, are common to the FDM process. Type I voids, also noted in all specimen sets, are created by machine error in the placement of extruded filament. Since voids are detected in all specimen sets and there does not appear to be a clear, discernable trend in the size or frequency of voids among specimens, their presence cannot be definitively attributed to operation of the FDM process in the microgravity environment. Instead, any slight differences in the number of voids (e.g., the increase in voids observed for compression specimens manufactured at a closer extruder distance in phase II specimens) are hypothesized to be related to changes in process settings or, in other cases, simply build-to-build variability. In phase I, the type, number, and distribution of voids was not significantly different between ground and flight specimen sets. Additionally, variations in density are small across the data sets (phase I ground, phase I flight, and phase II flight).

Computed tomography is a powerful tool for analysis of additively manufactured specimens and provides insight into the internal structure of material produced with the FDM process, both on Earth and in a microgravity environment. Ultimately, the CT analysis work conducted in support of phases I and II is not suggestive of engineering significant microgravity effects on material outcomes.

7. MICROSCOPY

As for phase I, SEM analysis was performed on the phase II flight tensile, layer quality specimens, calibration coupons, and compression specimens. Previous SEM work on 3DP (using ground and flight specimens from phase I operations) appears in reference 7, but a summary is also included here since it was not part of the volume I TP and was instead published as an academic journal article.

7.1 Review of Phase I Scanning Electron Microscopy Findings

Stress-strain plots of the phase I ground- and ISS-processed samples in tension revealed two distinct classes of data.[6] The flight specimens were stronger and stiffer than their ground counterparts, with one anomalous flight specimen (F004) that exhibited behavior somewhat in family with the ground specimens. Weights and densities of the ground and flight specimens, however, showed only minimal variations. A comparison of the top surfaces of tensile specimens showed structural differences within both the terrestrially processed and ISS-built specimens. In general, ground sample surfaces were more open, an indication that these specimens were built with the extruder tip too far from the build tray (fig. 68). For two of the flight tensile specimens (F004 and F018), the part clearly stuck to the build tray, and subsequent removal resulted in a layer or two delaminating from the sample at a paddle end.

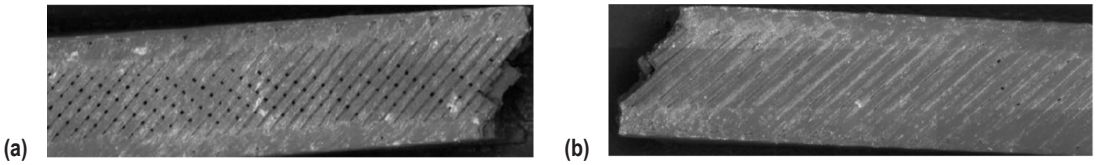

Figure 68. Image of (a) G012 which has an open surface structure compared with image of (b) F012, which has a closed surface structure.

A general comparison of the fracture surfaces of the ground and flight tensile specimens in SEM revealed the presence of open, central fibers in the ground specimens with a dense fiber agglomeration on the sides. For the flight specimens, the fiber structure was less open (more bonded) in the central cross section and the dense fiber agglomeration was noted on the sides and the bottom of the specimens (fig. 69). The fiber fracture surfaces appear typically glassy brittle in nature. These structural variations within and between ground and flight specimens likely account for differences in measured mechanical properties and are likely a result of different processing conditions (notably the *z*-calibration value) between the ground and flight specimens. The difference in processing conditions precludes ascertaining subtle microgravity influences between Earth and ISS specimens.

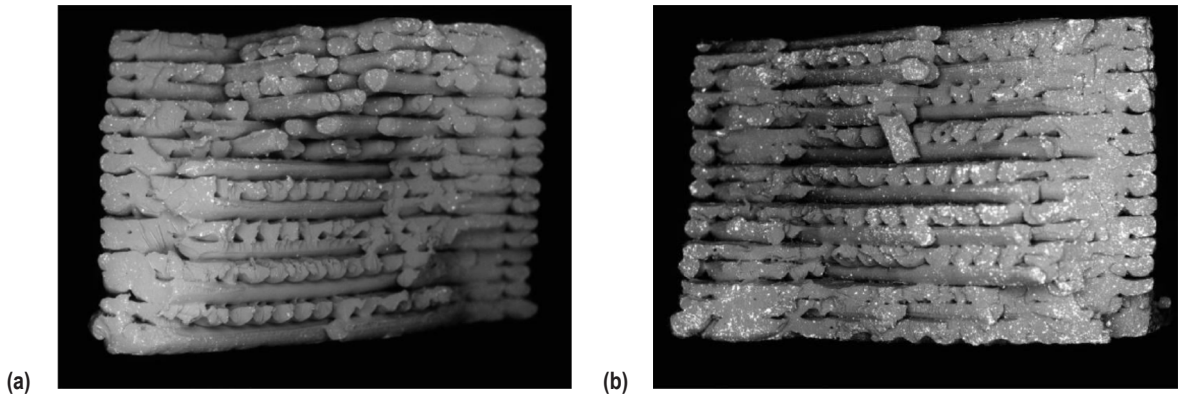

Figure 69. Cross sections of (a) G004 and (b) F012, which reveal the more densely bonded cross section and dense fiber agglomeration noted on the sides and bottom of the specimen for the flight tensile specimens.

The higher performance of the flight tensile specimens may be explained by fiber orientation and strength considerations. Zieman et al. found that parts with a longitudinal raster orientation (0) have a greater mean yield strength than those with other layups (45/–45, 45, 90).[11] The ground and flight tensile specimens were made in a 45/–45 orientation, but the bonding on the edges of the flight specimens creates a zero degree fiber orientation (fig. 70). More fiber bonding on the bottom of the flight specimens also helps to strengthen the part, likely a consequence of the closer extruder stand-off distances for the flight prints.

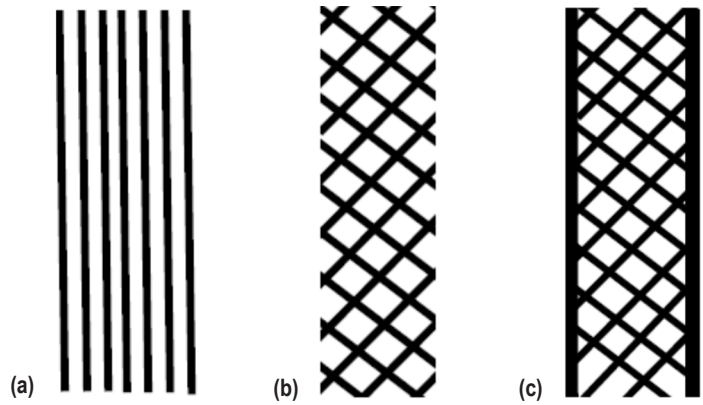

Figure 70. Illustration of fiber orientation of flight prints: Prints were built at (b) 45º/–45º layup, but agglomeration on sides is similar to (a) 0º degree orientation. Result is a structure that is closer to (c) and could potentially explain the greater strength and reduced ductility of the flight prints.

The lower percent elongation and the greater strength of the flight specimens may be explained based on the initial state of the material and its structure. The tensile strength of F004, which was in family with the ground specimens, was hypothesized to be attributable to the irregularity of the specimen cross section. The protrusion at the bottom of the specimen and the dense fiber agglomerations for the flight prints made it difficult to obtain a characteristic cross-sectional area to be used in strength calculations. If a revised cross section is defined based on SEM, the flight specimen exhibits a strength that is in family with the ground specimens.

7.1.1 Phase I Calibration Coupons

The calibration coupons, which had a sparser fill than the other specimens, were better poised to answer the question of microgravity effects. External examination of the surface specimens showed differences in layup, although the edge morphology was reasonably similar for both specimens. Like the tensile samples, the flight specimen evaluated had a larger base buildup than the corresponding ground specimen, likely a consequence of the closer extruder standoff distance. Cross sections of both calibration specimens evaluated reveal 'fiber slump' (sagging of a deposited fiber) and variation in fiber diameter (fig. 69). If a significant microgravity effect on the FDM process were present, it would likely manifest itself in the cross section of specimens with sparser fill, where differences in fiber slump between ground and flight processed parts can be observed more readily. Fiber slump of the same degree is present in both ground and flight specimens, as illustrated in the images being compared in figure 71. If there were a significant microgravity effect on processing, the filament slump in the ISS-manufactured specimens would be less pronounced. This is not the case for any ground and flight specimens from phase I compared in the SEM analysis.

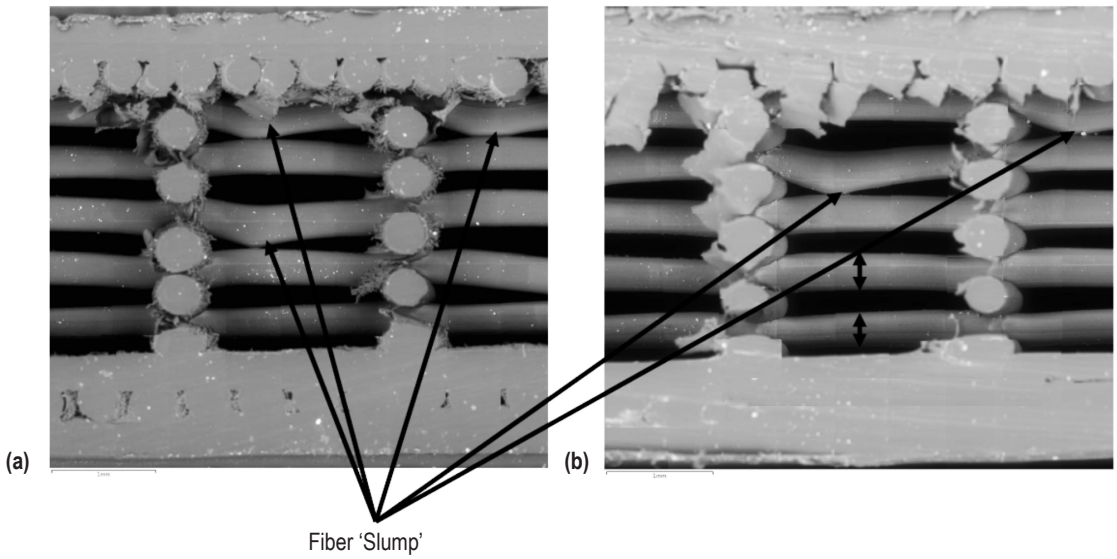

Figure 71. Section view of fiber slump and variations in fiber diameter for (a) ground specimens (G001) and (b) flight specimens (F001C).

Differences in densification between the flight and ground calibration specimens are attributable to differences in processing conditions discussed previously. Slight variations in filament diameter noted in the part cross sections (observed for both ground and flight calibration specimens) may be due to slight variations in nozzle/build plate speeds, slight induced variations in nozzle height, variations in ABS flow rate, or variations in ABS extruded volume during the printing process. Since these variations are equally present in both classes of specimen, there is no indication that they stem from operation of the hardware in microgravity.

7.1.2 Phase I Compression Specimens

Compression specimens were analyzed using SEM postdestructive testing. Both flight and ground specimens exhibit typical failure along the 45-degree shear plane. The flight specimens exhibited significantly poorer bonding than the ground specimens (fig. 72). For ground specimens, melding of fibers is observed, but visible separation is present between fibers in flight samples. This marked difference in structure explains the weakness of the flight specimens relative to their ground counterparts, but provides little indication as to the root cause of the discrepancy in bonding between specimen classes. Differences in bonding are most likely a result of differences in build procedures between Earth- and ISS-manufactured samples, but could also point to differences in the cooling rate for specimen classes or, less likely, given the magnitude of the structural differences between flight and ground, a microgravity influence.

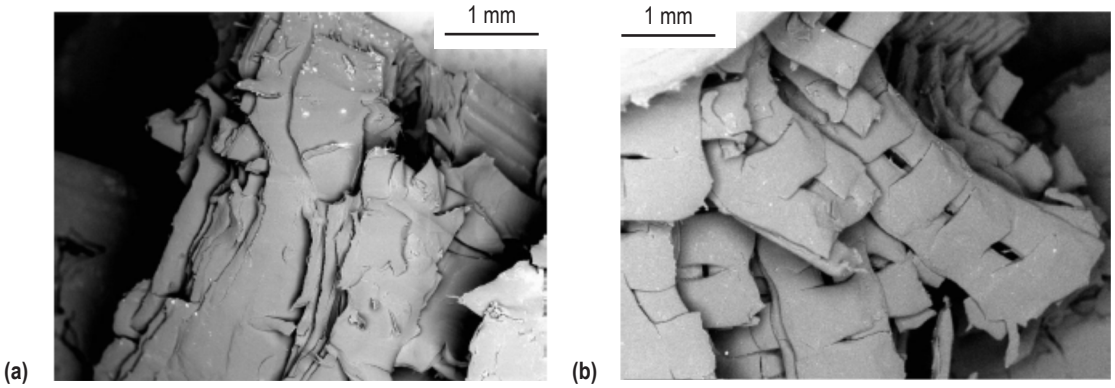

Figure 72. Comparison of internal structure for (a) ground compression specimen G013 and (b) flight compression specimen F016 postdestructive testing. G013 exhibits better fiber bonding.

7.2 Summary of Phase II Scanning Electron Microscopy Findings

7.2.1 Phase II Tensile Specimens

ABS samples for phase II operations were manufactured with the goal of observing variations in tensile strength with differences in the print head offset (*z*-height). Two series of samples were printed: optimum (2.54-mm *z*-height) and suboptimum (2.64-mm *z*-height, where the build tray

was translated upward by 0.1 mm, rendering the extruder tip 0.1 mm closer to the build tray and mimicking the conditions of the phase I prints). Optical images were taken of each tensile fracture surface for specimens from the suboptimal and optimal tensile specimen sets. These images were then compared to the tensile strength for the samples.

Representative cross-sectional images of specimens produced at the optimal *z*-height appear in figure 73. The corresponding tensile curves are plotted in figure 74.

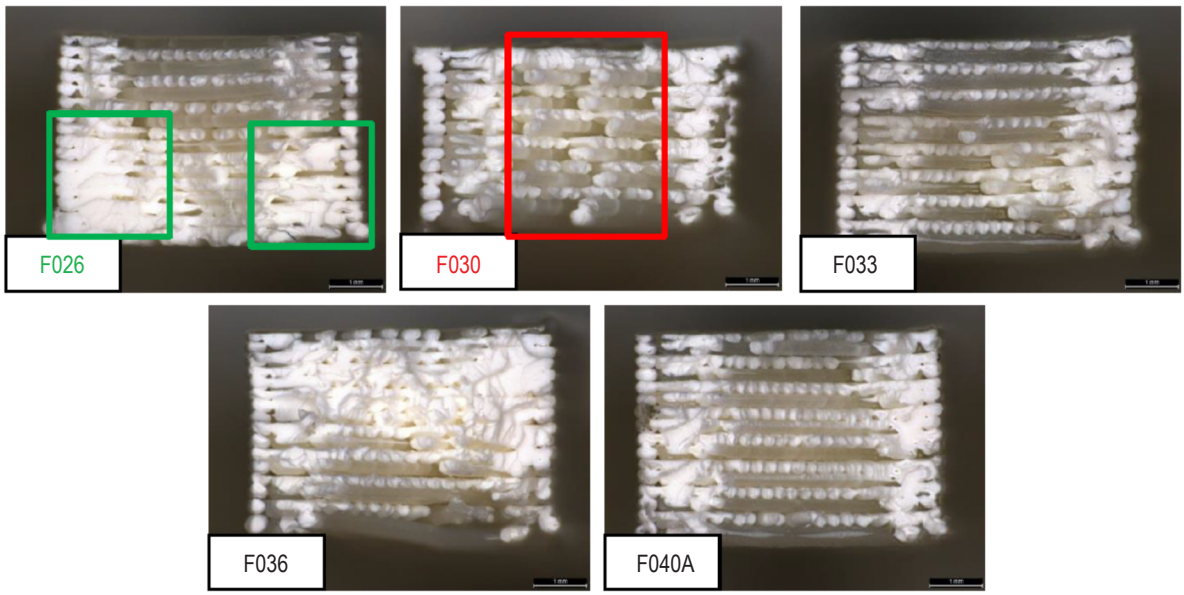

Figure 73. SEM images of cross sections from optimally manufactured settings. F030 has a characteristically open structure, while F026 shows some densification of lower layers, despite being produced at the optimal manufacturing setting.

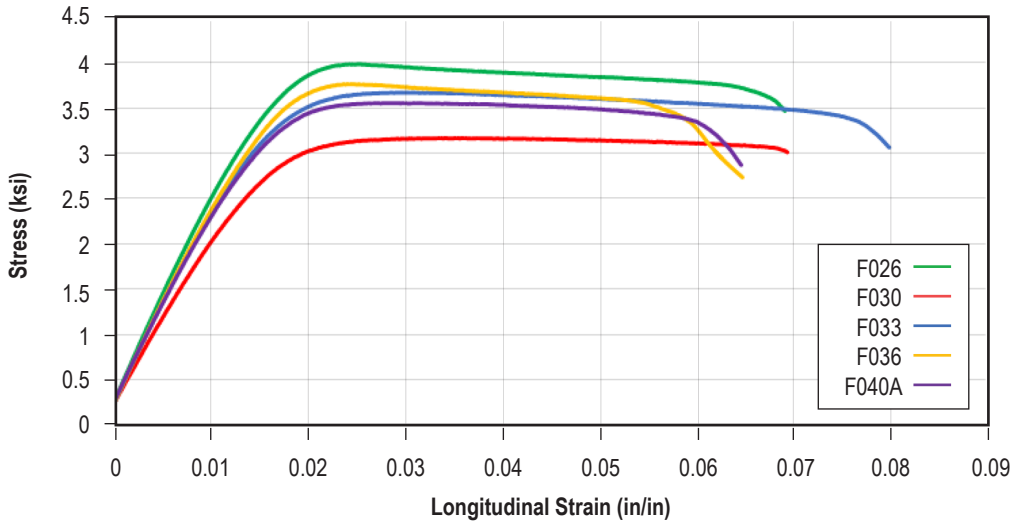

Figure 74. Stress/strain plot for optimal tensile specimens considered in SEM analysis.

For the five optimum samples considered in this analysis, the sample with the highest tensile strength (F026) had a fracture surface that appears to be the most dense (highlighted in green). Comparatively, the sample with the lowest tensile strength (F030) had the least dense fracture surface (highlighted in red) as well as thickness measurements showed this sample was approximately 0.2 in (~5 mm) thinner than the other samples.

The suboptimal specimens produced at the closer extruder standoff distance that were analyzed appear in figure 75. Corresponding stress-strain curves appear in figure 76.

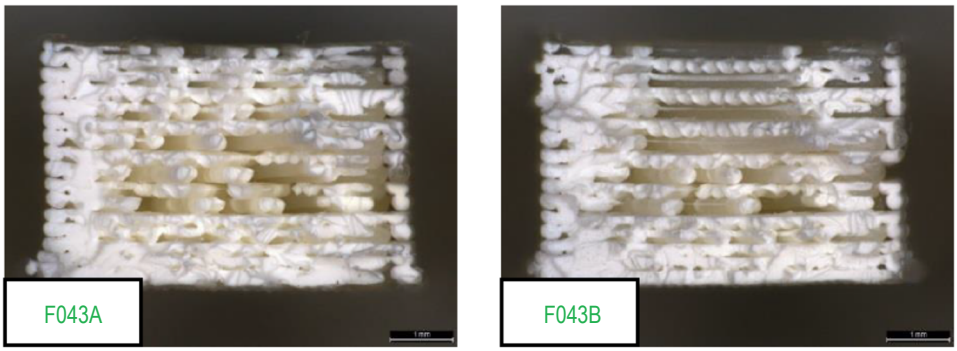

Figure 75. SEM images of cross sections of phase II tensile specimens produced at a closer extruder standoff distance.

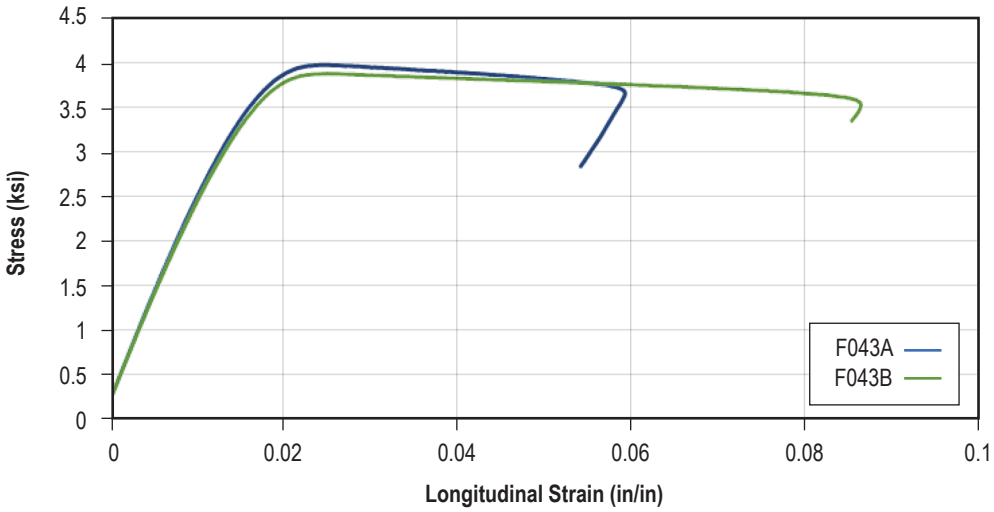

Figure 76. Stress/strain plot for suboptimal tensile specimens considered in SEM analysis.

For the two suboptimum samples analyzed, both have approximately the same tensile strength. As observed in the optical images, the fracture surfaces appear similar with approximately the same percentage of dense and less dense areas.

The average tensile strength of the optimum samples was 3.63 ± 0.3 ksi. The average tensile strength of the suboptimum samples was 3.93 ± 0.07 ksi. As expected, a correlation was observed with the highest and lowest tensile strengths and the percentage of dense material observed in the samples. Overall, the suboptimal samples appear to be more dense (hypothesized to be an artifact of the closer extruder standoff distance) and the lower strength samples consistently have a less dense open structure. In the less dense structures, the fibers appear to not be strongly bonded to the surrounding fibers. This may be indicative of the original structure of the specimen or the fibers may have slid along one another during the tensile experiment. Ultimately, the tensile data from phase II are consistent with phase I findings, that a closer extruder standoff distance can create densification in the first layers of the specimen. This observation supports the hypothesis that a closer standoff distance in manufacturing the phase I flight prints relative to the ground was responsible for the differences in the strength of the parts rather than a microgravity effect.

7.2.2 Phase II Compression Specimens

ABS compression specimens for phase II were manufactured with the goal of observing variations in compressive strength with differences in the print head offset (*z*-height). Two series of samples were printed: optimum (2.54-mm *z*-height) and suboptimum (2.64-mm *z*-height). The compression samples were compressed to 20% strain. Optical images were taken of the top and edge surfaces. Backscatter electron (BSE) images were taken of the top and edge surfaces to compare to the optical images. After initial analysis, the samples were cross sectioned and polished. BSE images were taken of the cross sections to show any internal defects such as voids.

The optimal images are shown in figure 77. Rows A and B compare the optical (row A) and BSE (row B) images of the top surface. Rows C, D, and E compare the optical (rows C and D) and BSE (row E) of the side surface. On each sample, imperfections are shown on the optical samples as a reflected 'X' shape. The BSE images show these imperfections closer, which appear to be printing defects where the fiber is distorted. Fiber distortions and evidence of 'misruns' were also observed in the phase I and phase II data (x-ray/CT) and in the extruder standoff distance study using the ground test unit for 3DP. Distortion overall is not linked to a particular process setting.

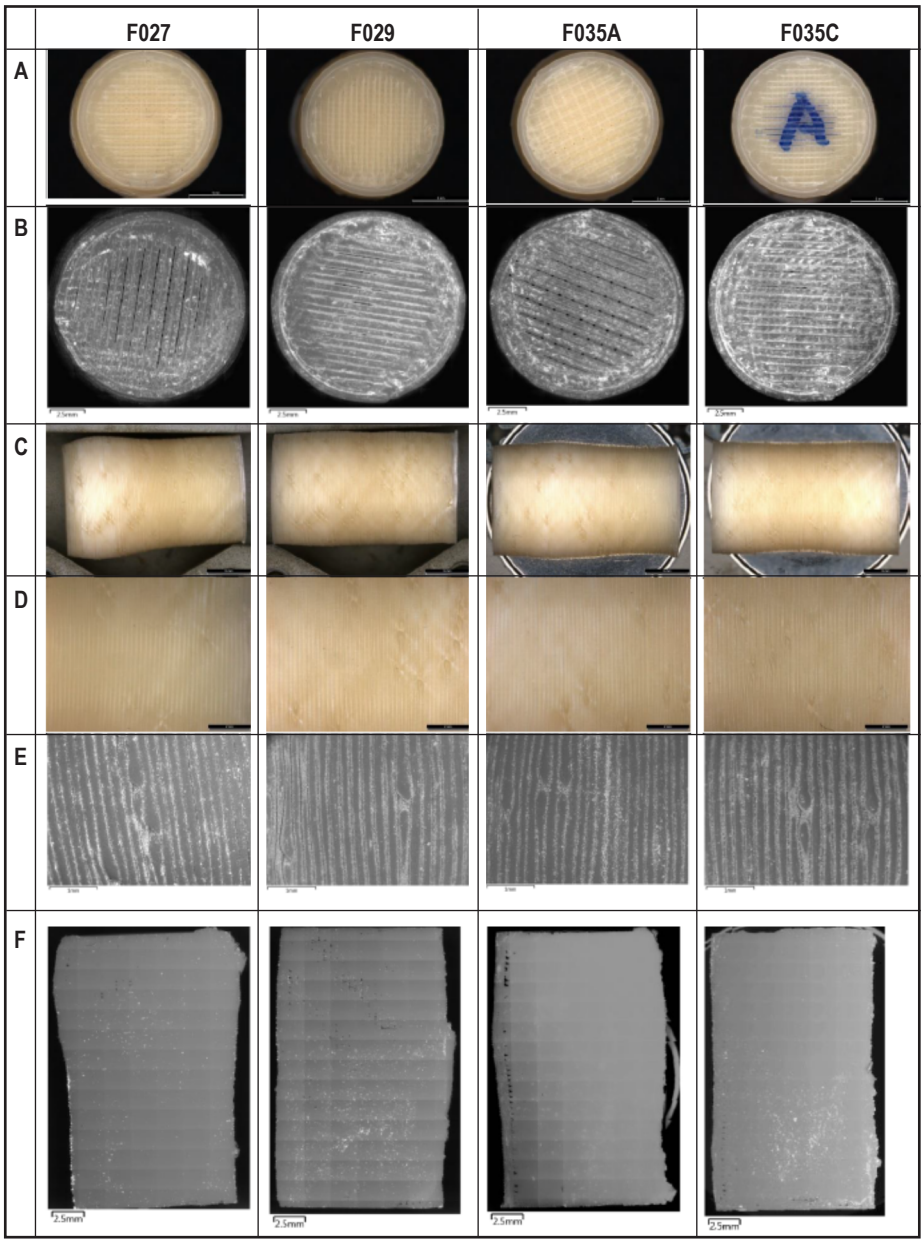

Figure 77. Optical microscope images of phase II compression specimens manufactured.

Images from compression specimens at the suboptimum setting are captured in figure 78. Rows A and B compare the optical (row A) and BSE (row B) images of the top surface. Rows C, D, and E compare the optical (rows C and D) and BSE (row E) of the side surface. On each sample, imperfections are again shown on the optical samples as a reflected X shape. The BSE images show these imperfections closer, which appear to be printing defects where the fiber is distorted. Row F is a BSE image of the cross section showing voids within each sample. These appear to be separation between the fiber layers where the sample is not fully dense.

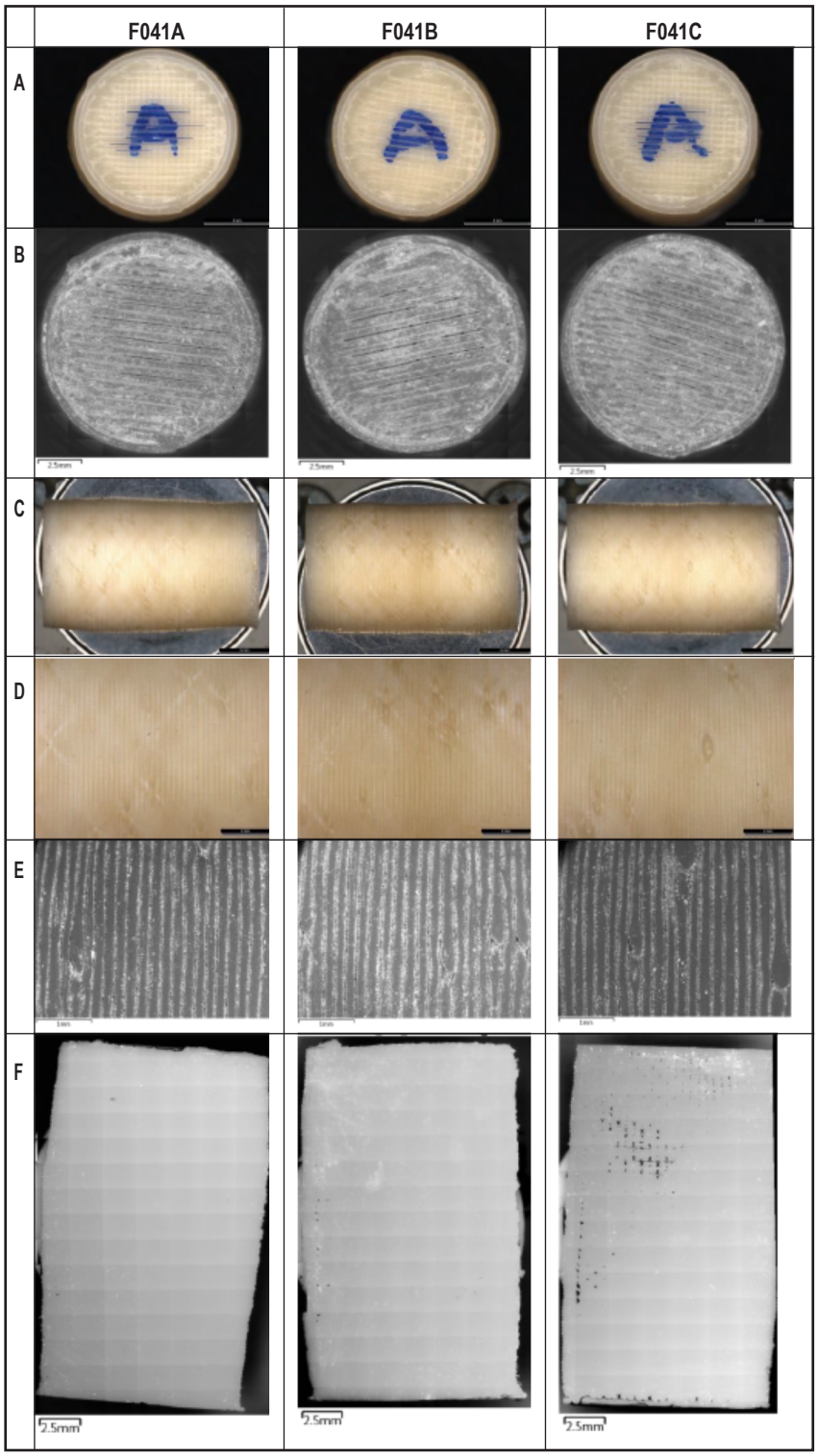

Figure 78. Optical microscope images of phase II compression specimens manufactured at the closer extruder setting.

Visually, it is difficult to compare the phase II compression specimens directly with phase I data. (While phase II compression specimens were truncated at 20% strain, in part, to preserve the internal structure for posthoc microscope analysis, phase I specimens were run to 100% strain.) For phase II, each sample set is similar. Both contain surface defects along the sides that appear to be printing defects where the fiber is distorted. Each cross section—regardless of the phase II set it originated from—showed voids in the center of the sample. These are likely due to separation between the fiber layers and result in a sample that is not completely dense, although gaps in the fibers are slightly more pronounced in the phase II suboptimal specimens relative to the optimally manufactured samples. Some variations were also observed on the top face of both sets. Material structure is highly variable within each part. Some of the fibers appear to have contact with the fibers on either side throughout the entire surface, but on other specimens, there is some separation between the fibers. These features may be a result of subtle variations in printing and dispensation of filament that are inherent to the hardware.

7.2.3 Layer Quality Specimen Analysis

Phase II layer quality specimens were manufactured with the goal of observing variations in geometry and layer spacing with differences in the print head offset (z-height). Two layer quality specimens at each extruder distance were selected for SEM analysis: optimum (2.54-mm z-height) and suboptimum (2.64-mm z-height). Optical images were taken of all six surfaces of each block. BSE images were taken of the top and left surfaces to compare to the optical images. The top surfaces were polished on the specimens selected for analysis to reveal any internal defects. Optical and BSE images were taken of the polished surfaces. Images from samples F034A and F034B, part of the optimum group, are shown in figure 79. These images are very similar to specimens F041A and F042B, manufactured at the suboptimal setting. Figure 80 compares a specimen from the optimal set (F034B) with a specimen from the suboptimal set (F042A). Some gaps and voids along the length of the specimens were noted (as seen in specimen 34B in fig. 80), but these are not specific to a particular manufacturing condition.

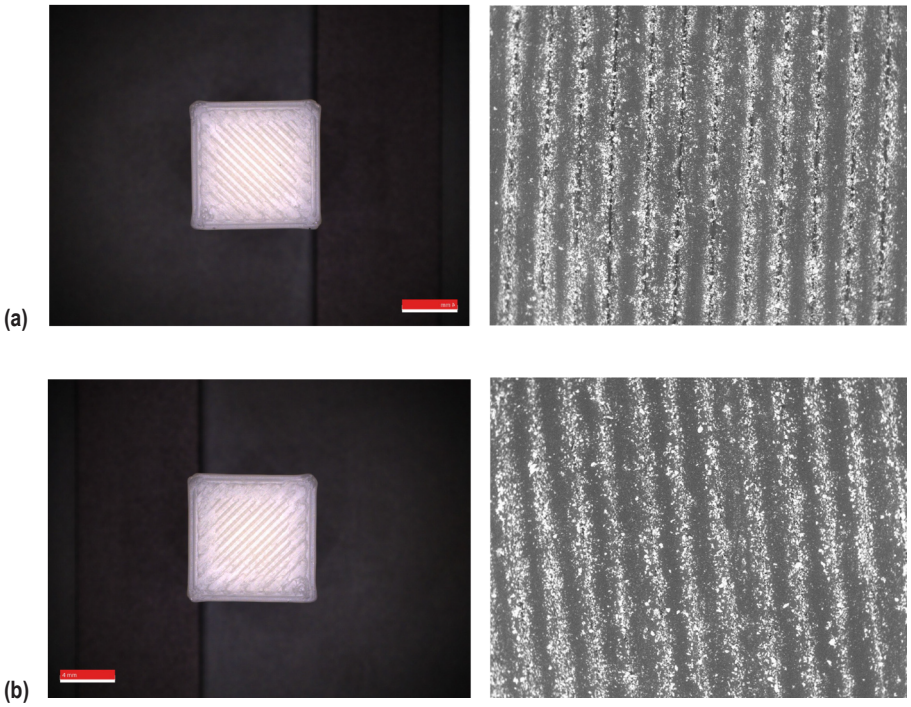

Figure 79. Optical microscope images of specimens (a) F034A and (b) F034B from phase II (manufactured at the optimal extruder setting).

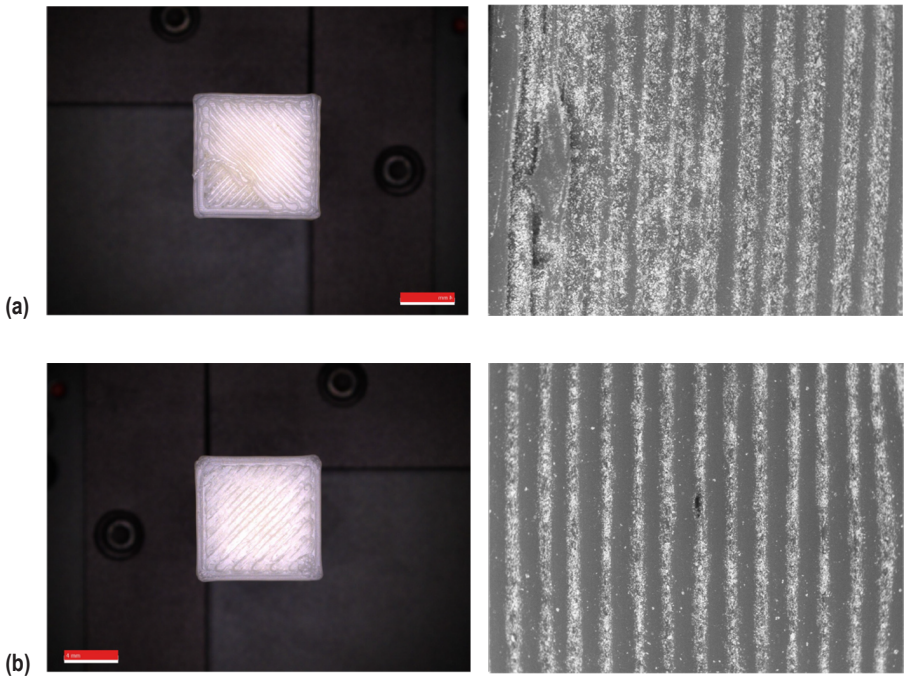

Figure 80. Optical microscope images of specimens (a) F034B and (b) F042A from phase II. F042A was manufactured with the extruder tip closer to the build tray.

7.3 Summary of Microscope Analyses

Considering both phase I and phase II data, the differences in the internal material structure of between ground and flight specimen sets are not suggestive of microgravity effects on the manufacturing process. Overall, some degree of variability is observed in the internal structure of the specimens, even for specimens produced at identical manufacturing settings. This variation does not always translate into differences in mechanical performance of a corresponding magnitude but does suggest that the uncontrolled cooling rate (the printer does not have a heated bed) may create material structures and impede the repeatability of the manufacturing process. Dinwiddie et al. conducted a study of real-time temperature monitoring in FDM, finding that temperature variation in parts as they are being built may be substantial and strongly impacted by their location on the build tray.[12] This thermal variation, which is linked closely to resulting material structure, may be exacerbated by printing on an unheated build tray and may explain some of the variability in material structure noted in the 3DP specimen analysis.

Compression specimen structure for phase II specimens were preserved by truncating the testing at 20% strain, which enabled an evaluation of material structure that was not possible for the phase I specimens (run to 100% strain). The mechanism for the reduced fiber bonding observed in some of the phase II flight prints for compression is not well understood. Overall, the tensile specimens evaluated further substantiate the hypothesis that moving the extruder tip closer to the part create densification in the first few layers and sides of the specimen. It is believed to be these features, and not operation of the hardware in the microgravity environment, that contributed to enhanced tensile performance of the flight prints in phase I. This hypothesis has been validated by two subsequent studies.[7,10]

8. CHEMICAL ANALYSIS

Infrared (IR) analysis was performed on ABS flight samples F029 and F042C from phase II operations and further compared to spectra collected from prior samples. These samples included flight samples F004 and F005 from phase I operation, ground samples G004 and G005 (printed prior to the printer's launch to the ISS), and filament feedstock materials identified as flight and nonflight samples. This work was performed to determine if any IR spectral differences exist between these samples that are indicative of chemical changes in the feedstock due to aging and/or moisture absorption. For phase II operations, the feedstock was 18 months older than the feedstock at the time of the phase I prints and 21 months older than the feedstock at the time of the phase I ground prints. For the phase I analysis, feedstock and printed samples from phase I ground and flight prints were compared and no substantive chemical differences were noted.

8.1 Methodology

The analysis conditions for FTIR were as follows:

- Single-bounce attenuated total reflectance (ATR) analysis accessory purged with nitrogen gas.
- Sixty-four scans per sample at a resolution setting of 4 cm^{-1}.
- Replicate spectrum collected for each sample.
- Polystyrene reference spectrum collected prior to and following the last test sample analyzed to verify instrument performance.

As for phase I analysis reported in reference 7, each sample was prepared for ATR analysis by excising a small, thin area from the surface using a scalpel blade. This work was performed using a dissecting scope to aid in material separation and assure that the sample area was free of extraneous material. Once removed, the sample was placed, unexposed surface side down, on the ATR crystal surface for spectral analysis.

The ATR accessory used for this analysis consists of an IR transparent germanium crystal with a pressure device located above the crystal surface, the latter intended for collection of solid sample IR spectra such as these. A sample is placed on the crystal surface, pressure applied, and the IR signature collected from the crystal contact side of the sample. This is largely considered a surface-based analysis as the IR penetration is equivalent to only a few microns, and thus independent of sample thickness in general. Spectra collected by this method are sensitive to the amount of pressure applied, with increasing pressure translating into primarily greater peak heights. The pressure device being used for this testing has a locking mechanism that ensures a constant pressure, such that a semi-quantitative comparison between samples is possible under most conditions.

Replicate IR spectra for each sample were collected and a manufacturer software program designed to compare peak-to-peak similarity (QC Compare) between spectra was employed. This was intended to provide replicate variability data for the current samples and for comparison to prior tested materials described above.

8.2 Results

Figures 81 and 82 include replicate spectra from F029 and F042C, respectively. Each indicated a high similarity index within replicate samples, with a value of 0.99 for both materials (maximum 1).

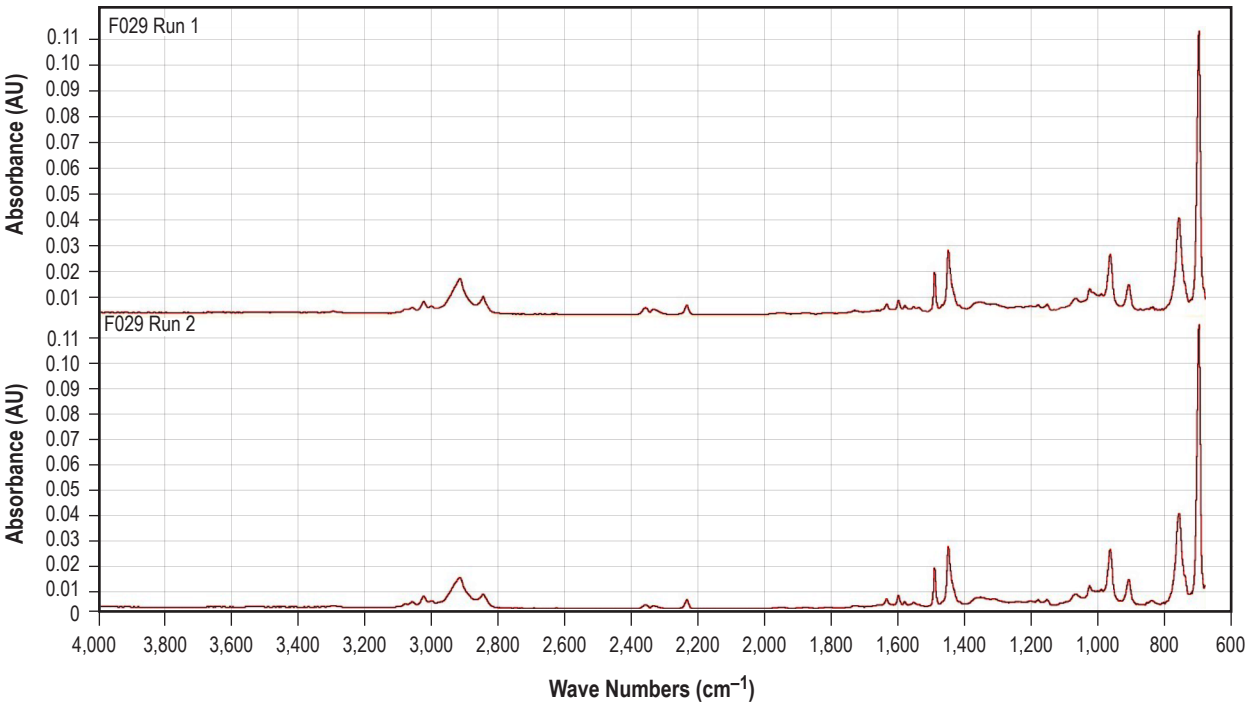

Figure 81. F029 replicate spectra.

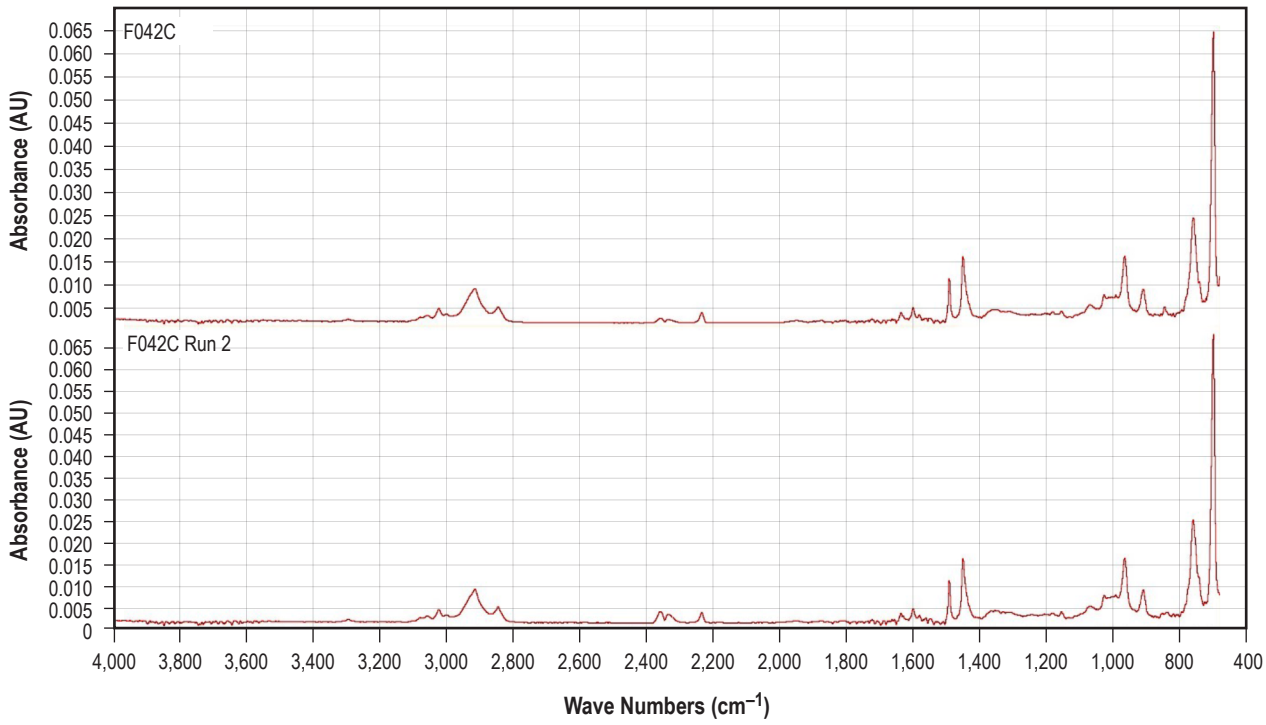

Figure 82. F042C replicate spectra.

Figure 83 presents a direct comparison between phase II samples and again shows a high correlation value between these samples (0.99). Due to the high similarity value between current materials, only one (F042C) was chosen for direct comparison to previously collected spectra.

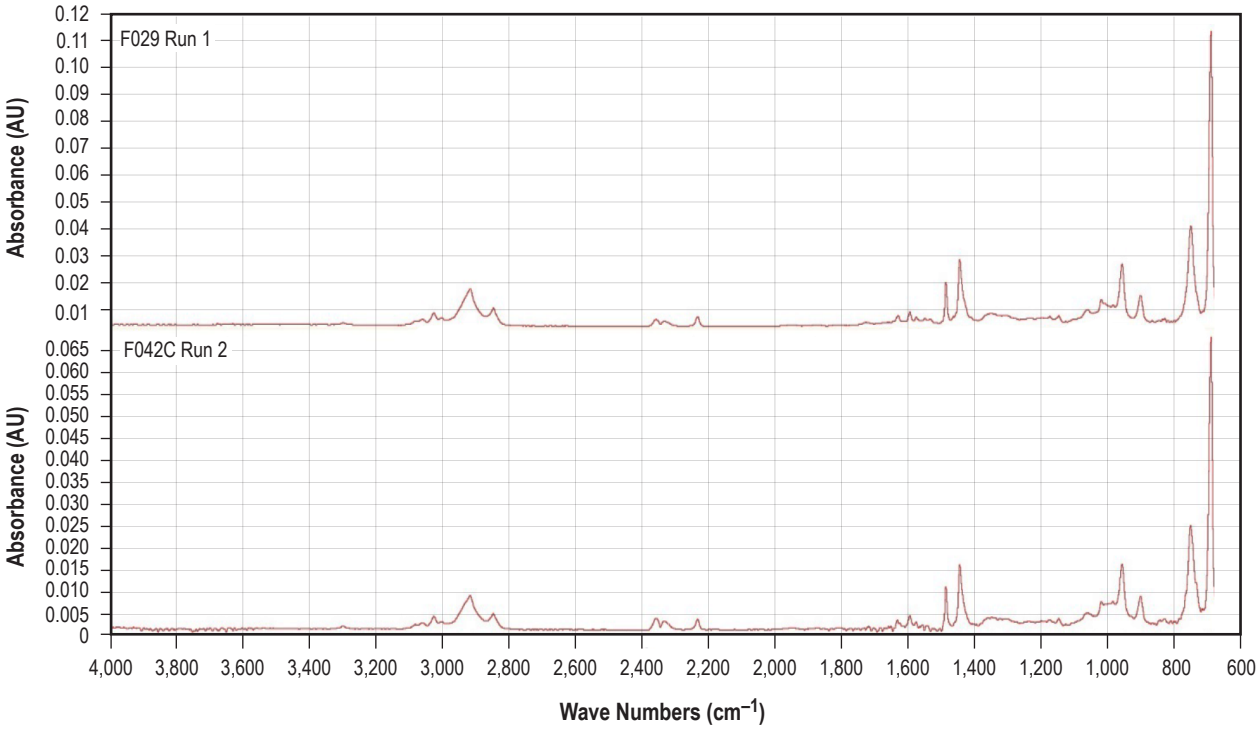

Figure 83. Spectral comparison between F029 and F042C.

The data in figure 84 represent comparison of current (phase II) material spectra to previously provided flight (middle plot) and nonflight feedstock of the same material and from the same manufacturer (bottom plot) samples. High correlation values were seen when compared to these materials, with values approaching 0.98.

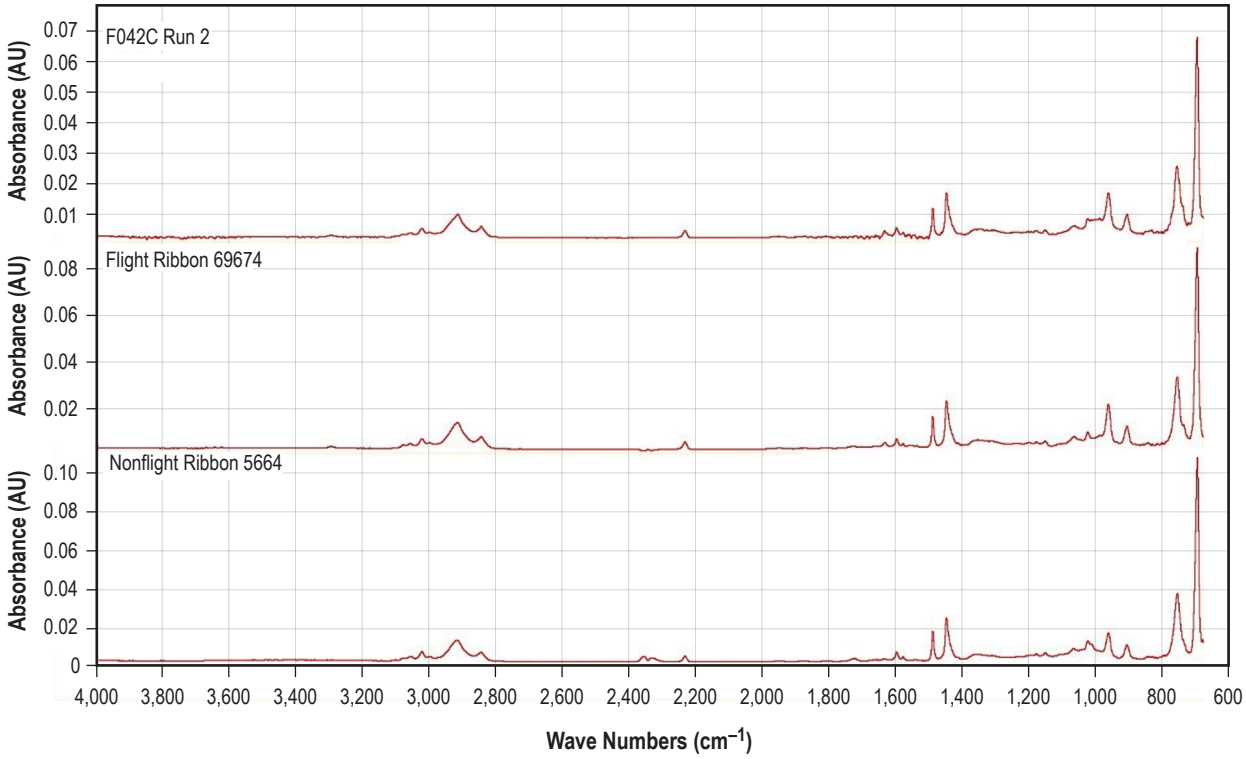

Figure 84. Spectral comparison of F042C and flight/nonflight feedstock materials.

Figures 85 and 86 represent comparative spectra between F042C and the flight samples F004/F005 and ground samples G004/G005, respectively. As discussed in prior reports, these samples indicated, in addition to the characteristic peaks associated with the acrylonitrile, butadiene, and styrene of ABS, the presence of a peak at approximately 1,000 cm^{-1}. The current samples do not indicate the presence of this peak, and as expected, provide somewhat lower correlation values when compared to current material. Even so, good similarity values were noted between current samples and these previously analyzed materials, with correlation values approaching 0.86 and 0.83 for F004/F005 and G004/G005 materials, respectively.

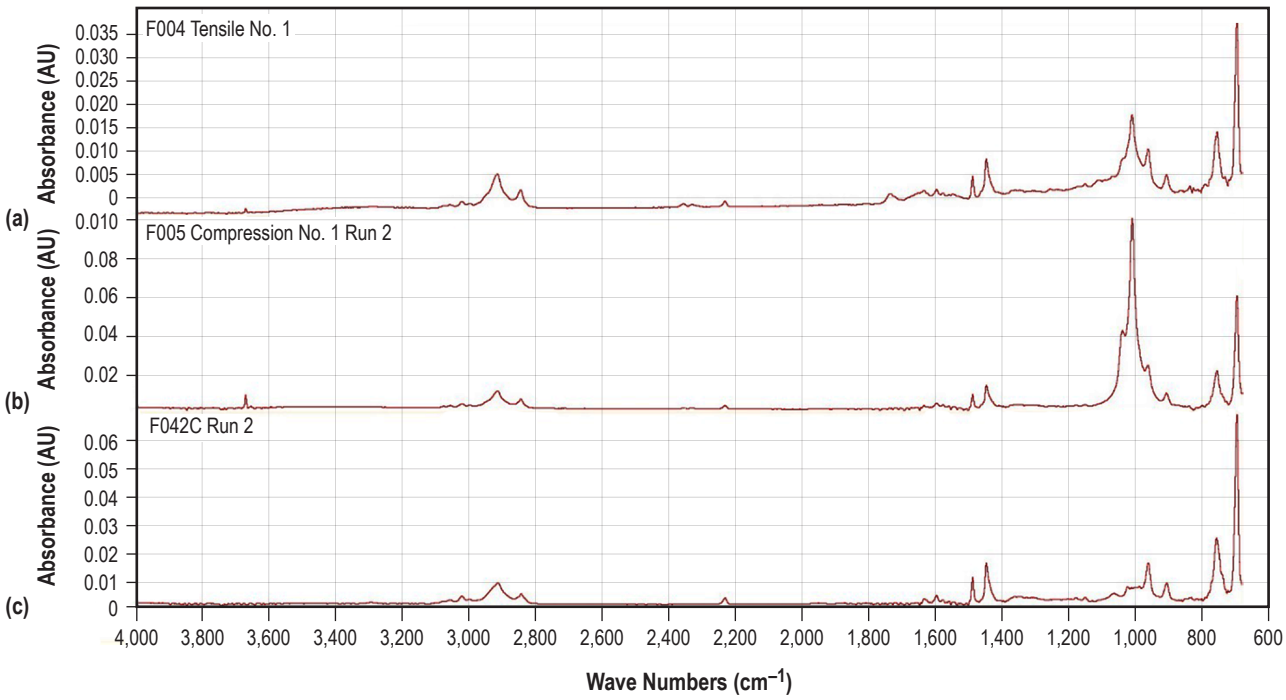

Figure 85. Spectral comparison of (a) F004 and (b) F005 with (c) F042C materials.

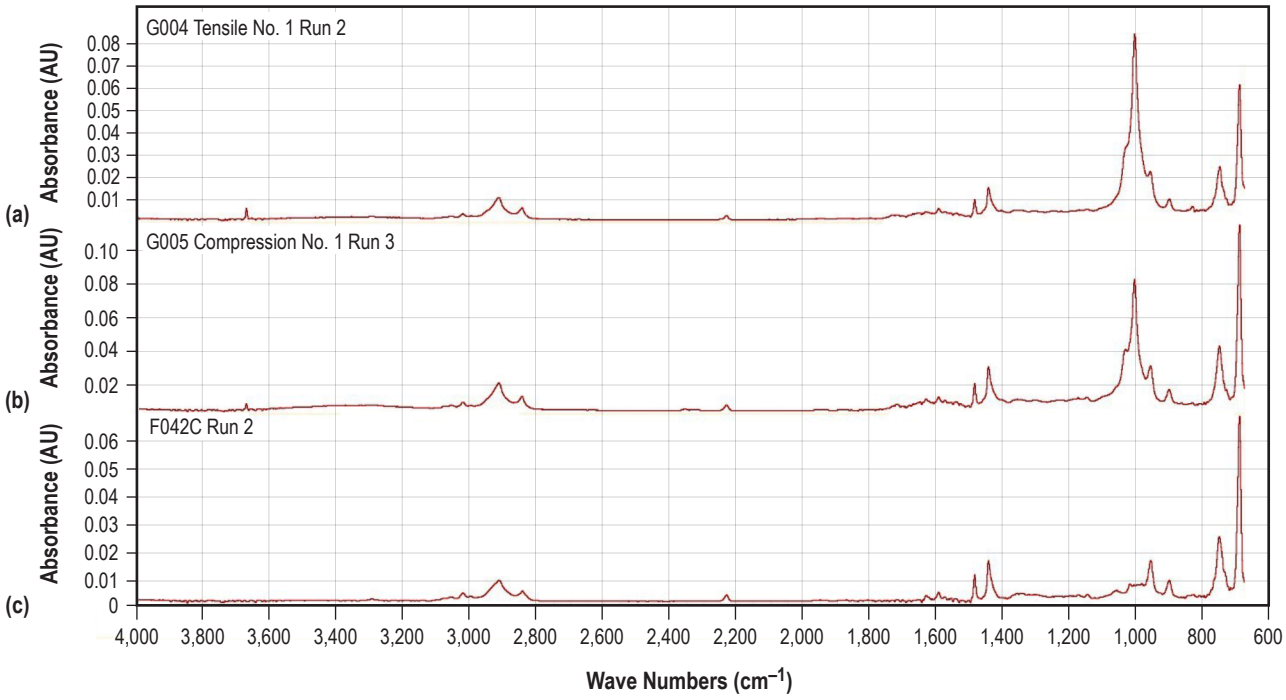

Figure 86. Spectral comparison of (a) G004 and (b) G005with (c) F042C materials.

While a subtle difference between phase II spectra and previously collected spectra was noted, it is not significant enough to consider the phase II spectra 'out of family' with previous collected specimens. All sample spectra collected to date will be imported into a user-specific database to provide a searchable resource to compare spectral properties of future material. This has been done previously for other programs and has proven useful as a chemical fingerprinting tool.

9. PHASE II ANALYSIS SUMMARY AND CONCLUSIONS

The ability to manufacture parts in space, rather than launch them from Earth, represents a critical and exploration-enabling transition for human spaceflight operations. Additive manufacturing technologies, in particular, with their flexibility in part design and feedstock, have the potential to provide an on-demand part replacement capability for long-duration, long-endurance missions where cargo resupply is not readily available and reduce initial upmass requirements. The purpose of the 3D Printing in Zero-G Technology Demonstration Mission was to evaluate the feasibility and potential of polymer additive manufacturing, specifically, the FDM process, to produce parts and tools on orbit. The printer for this mission was developed by Made in Space, Inc. in Mountain View, California, under a Small Business Innovative Research (SBIR) grant. The 3D printer technology demonstration unit was integrated into the MSG on the ISS in November 2014, and phase I printing operations took place from November to December of that year, yielding 21 specimens (mostly mechanical test coupons) for comparison with ground-processed specimens manufactured with the printer prior to its launch to the ISS.

Phase I operations demonstrated the ability to safely operate the polymer printing process in a microgravity environment, remove parts from the printer, remotely command the printer from the ground, and uplink new files for printing, and ultimately produce tools that could be evaluated for form/fit/function. Phase I specimens were downmassed from the ISS in February 2015 and underwent evaluation at MSFC's Materials and Processes Laboratory from April to October 2015.

The phase I specimens went through an extensive test regime: photographic/visual inspection, mass and density evaluation, structured light scanning (to characterize dimensional variation by comparing specimens with their corresponding CAD model and other specimens of the same geometry), x-ray and CT, mechanical testing, and both optical and SEM. FTIR analysis was later performed on the flight and ground specimens to look for aging effects that may have contributed to chemical degradation of the feedstock material. (At the time of specimen manufacture, feedstock for flight prints was 6 months older than feedstock used for ground prints.) There were some differences in mechanical properties noted between the flight and ground data sets, but the small size of the phase I sample set made it difficult to definitively assess the source of the variability. Based on detailed material analysis and a subsequent ground-based study which examined the impact of variations in a process setting (the distance between the extruder and the build plate, which was varied for phase I prints) on material outcomes, it was determined that differences noted in the flight and ground specimens were most likely attributable to differences in operational settings between the specimens as well as inherent build-to-build variability. Phase I results were published in references 7, 10, and 13.

A second round of operations with the technology demonstration printer took place in June and July 2016. The purpose of this print campaign was primarily to gain greater insight into sources of variability in the 3DP phase I data set. For the last 9 prints of the 34-print series, the build tray

was moved slightly closer to the extruder tip, mimicking manufacturing process conditions present in the phase I flight prints. The controlled manufacturing settings implemented for the first 25 prints of the series, where the distance between the extruder and the build tray was locked at an optimal setting, both enable an assessment of build-to-build variability of the system in microgravity and permit a closer examination of microgravity on the FDM process by adding additional specimens to the overall data set. Phase II operations also offered an opportunity to collect data on aging of the printer feedstock and its potential impact on material outcomes. While all feedstock originated from the same manufacturing lot, there were differences in the age of the feedstock at the time of printing among specimen sets. For phase I, flight feedstock was 6 months older than the feedstock used to produce the ground specimens. Due to a lapse in operations between phases I and II, the feedstock had aged another 18 months and was now beyond the 12-month recommended shelf life specified by the manufacturer. However, feedstock was stored in a sealed container with desiccant prior to use, which should mitigate the potential for moisture absorption. Ultimately phase II operations were intended to provide additional data to ascertain whether trends, biases, and characteristic mechanical properties noted in the phase I analysis are consistent with further flight operation of the printer and determine the degree to which differences in material outcomes can be attributed to the effect of microgravity on the FDM process.

Like phase I specimens, phase II specimens underwent an extensive testing regime at MSFC from September 2016 to October 2017. Evaluation included photographic/visual inspection, mass and density, structured light scanning, CT, FTIR, and SEM. Results of the testing and comparison with phase I data are discussed extensively in previous sections of this TP. Key findings are summarized below:

- Mass evaluation. No substantial mass differences were noted in comparison of the tensile, layer quality, and calibration prints across manufacturing settings. The total mass of extrudate across a range of manufacturing conditions for a particular specimen geometry is remarkably consistent, which agrees with phase I findings. Limiting the comparative analysis to only phase II specimen sets, the change in the extruder standoff distance does not seem to substantively impact the mass of the specimens produced for any specimen geometry considered in the microgravity environment.

- Density evaluation. Density values were calculated using the closed part volume measured in structured light scanning. Derived gravimetric density values show a high degree of similarity across all specimen sets and suggest all data are part of the same family. An apparent engineering significant relationship between part density and extruder distance is not strongly evident here, as ground prints for tensile and compression (manufactured at the farthest extruder setting) are both in family with phase II prints.

- Mechanical properties. Phase II specimens underwent tensile and compression testing. Flexure specimens, which were a part of the phase I data set, were not included in the phase II print matrix. When considered in a holistic manner, overlap in mechanical performance between specimen sets suggests that data are part of a single large, albeit variable, family of data.

  – Tensile properties. Two of the phase I flight tensile specimens exhibit mechanical properties (UTS, yield strength, and fracture elongation) which are still somewhat distinct from other data

sets. The four phase I flight specimens constitute the upper range of tensile properties across all specimen sets. However, there is some overlap in the phase I flight data subset with the phase II specimens manufactured at a suboptimal extruder setting, which mimics the phase I flight process settings as well as the general phase II tensile data. Overall, the consideration of the phase I and phase II tensile data in a holistic manner suggests that all specimens are part of the same family of data.

– Compression properties. Compression data sets exhibit more variability, with the ground compression specimens manufactured as part of phase I remaining somewhat distinct in terms of mechanical behavior from all other data sets. Phase I flight compression specimens, manufactured at a closer extruder setting, represent the lower bound of the phase I and phase II data. There is some overlap between phase I flight compression properties considered (ultimate compressive strength, compressive yield strength, and compressive modulus) with those of phase II specimens.

• Structured light scanning. Structured light scans were performed on all specimens to provide an estimate for closed part volume (used in density calculations) and to assess geometric variation of a particular specimen relative to other specimens of the same type and the CAD model.

– Tensile specimens. As expected, phase II tensile specimens manufactured at the optimal setting show reasonably good agreement with the CAD model. Specimens manufactured at the closer extruder standoff distance do not exhibit the degree of warping and/or protrusions observed in the phase I flight specimen data set. Deviations from the CAD model are thus generally similar for the phase II suboptimal and optimal specimens. This finding is somewhat inconsistent with previous results (phase I flight specimens and the subsequent ground-based study in ref. 10), but the phase II suboptimal specimen set is small ($n = 2$) and it may be that the differences in specimen structure induced by any changes in this manufacturing process setting are more readily apparent in CT or SEM.

– Compression specimens. As with the tensile specimens, comparisons of specimens made at the optimal setting show a high degree of similarity to the CAD model and one another. For the compression specimens manufactured at the suboptimal condition, closer examination of the top of the cylindrical specimens show evidence of voids (missing material) and misruns (errors in filament layup). The largest deviations from the CAD model for these specimens are typically at the top or base of the cylinder. Overall, compression specimens show similar dimensional variation regardless of the manufacturing condition.

– Layer quality. Layer quality (square column specimens) show little variation across the phase II data set and do not demonstrate significant dimensional differences between the suboptimal and optimal manufacturing settings. Layer quality specimens for phase II are also similar to the phase I specimens.

• Computed tomography analysis. A subset of phase II tensile and compression specimens was scanned using a microfocus CT capability. Specimens were compared with phases I and II specimens of the same geometry type. A software modification to the equipment between phase I and phase II analysis largely prevented direct quantitative comparison of phase I and phase II data.

Qualitative comparison of the volumetric reconstruction of specimens indicates that voids and misruns (errors in filament layup) are observed throughout the specimen sets and are not specific to specimens manufactured in microgravity. These features are not characterized as defects since their impact on mechanical performance is unknown.

  – For phase II tensile specimens, there was no observable trend in the frequency, number, or size of voids with changes in extruder distance.

  – For phase II compression specimens, no clear trends are noted except for a slight increase in the number of voids for specimens manufactured at the closer extruder setting. Misruns (errors in filament layup) were also noted in the *x*-*y* plane.

- SEM analysis. SEM analysis of a subset of tensile, compression, and layer quality specimens was performed for phase II.

  – Tensile specimens. SEM analysis of phase I specimens revealed a more densely bonded cross section and dense fiber agglomeration noted on the sides and bottom of the specimen for the flight tensile specimens. These specimen features were hypothesized to be an artifact of differences in distances in extruder distance for the phase I flight prints, ultimately resulting in the creation of reinforcing material that enhanced the mechanical performance of the flight specimens. (This hypothesis was substantiated by a subsequent ground-based study varying extruder standoff distance and using the flight backup hardware.[10]) Phase II specimens manufactured at the suboptimal process setting in phase II also exhibited these features. Together, these results strongly indicate that enhanced strength of the tensile specimens observed in phase I was not a microgravity effect, but rather a result of changes in manufacturing process settings.

  – Compression specimens. No significant, discernable differences in internal material structure across the phase II specimen set were noted. For compression specimens, a direct comparison with phase I internal structure is precluded by slight differences in test procedures. For phase I, compression specimens were run to 100% strain, which made examination of the internal structure difficult posthoc. In phase II, specimens were truncated at 20%, which better preserved the specimen for posttest evaluation.

  – Layer quality specimens. These specimens exhibit some gaps and voids along the length of the specimen, but are not specific to a particular manufacturing condition.

- Chemical analysis. FTIR was performed to look for signs of feedstock material degradation due to aging or exposure to the environment; i.e., humidity, radiation. Phase I FTIR analysis showed no chemical differences between flight and ground feedstock (originating from the same lot), despite a 6-month difference in feedstock age at the time of manufacturing. For phase II, flight feedstock had aged 18 months beyond the phase I flight prints. While some subtle shifts in spectral peaks were noted, the phase II flight print spectra are considered in family with both the phase I flight and ground specimens.

In a holistic consideration of the data from phases I and II discussed in this TP, it appears likely to originate from the same family. Based on this extensive analysis, mechanical property differences noted in the phase I analysis cannot be linked to operation of the FDM process in microgravity but are instead likely attributable to changes in manufacturing process settings and build-to-build variability. This variability is also likely influenced by uncontrolled cooling of the specimens. (The 3DP hardware did not have a heated build tray or a heated volume, a feature that has been incorporated into its successor hardware, the Additive Manufacturing Facility (AMF).)[14]

With the completion of phase II operations, the 3DP mission has successfully demonstrated the first step toward manufacturing in space. As a follow-on to the technology demonstration mission, Made in Space developed the AMF. AMF provides a multimaterial polymeric printing capability for the ISS and currently serves as the utilization printer for the Space Station. Over 100 parts for NASA and other customers have been printed to date. A materials characterization plan for AMF is currently being executed by Made in Space, MSFC, and the Southern Research Institute. The results of this work will provide baseline design values for materials produced with AMF and will be subsequently published. Comparison of specimens produced on orbit with specimens manufactured using a ground-equivalent printer provide another opportunity to evaluate the impact of microgravity on material outcomes for fused filament fabrication processes.

As the ISM project at NASA continues to use the ISS as a testbed to explore other manufacturing processes, including recycling with the Refabricator Payload developed by Tethers Unlimited in 2018,[15] work performed under the ISM umbrella may serve to accelerate the shift from traditional Earth-dependent approaches to logistics for long-duration crewed missions to a space where manufacturing systems operated inside the crew habitat provide spares on demand, enable adaptive and rapid response to unforeseen operational scenarios, and facilitate the use and repurposing of nuisance materials, such as trash recyclables. Manufacturing will be a critical part of any space-based economy and the ISM project continues to enable commercial space efforts through its work with small businesses under the helm of NASA's SBIR program.[16] Through the SBIR program, ISM is supporting work on development of custom packaging materials for the ISS which are designed to be recycled,[17,18] hybrid additive and subtractive manufacturing systems capable of processing aerospace-grade metallics,[16] and space-based printing systems for electronics. In 2017, the ISM project released a Next Step Technologies for Exploration Partnerships Broad Agency Announcement for a multimaterial fabrication laboratory on board the ISS.[19] The fabrication laboratory will provide an exploration-grade capability for the ISS which integrates multiple manufacturing processes into a single unit in the 2021 timeframe.[20] The overlap between ISM and in situ resource utilization will also be explored more fully in the coming years. 3DP and the ISM activities stemming from it represent the first steps on the path toward sustainable, truly Earth-independent exploration initiatives. Manufacturing capabilities deployed in the space environment have the potential to fundamentally change exploration architectures and enable space settlement.

REFERENCES

1. Owens, A.; de Weck, O.; Stromgren, C.; et al.: "Supportability Challenges, Metrics, and Key Decisions for Human Spaceflight," AIAA 2017–5124, AIAA Space and Astronautics Forum and Exposition 2017, Orlando, FL, doi.org/10.2514/6.2017-5124, September 12–14, 2017.

2. Owens, A.; and DeWeck; O.: "Systems Analysis of In-Space Manufacturing Applications for the International Space Station and the Evolvable Mars Campaign," AIAA 2016–5394, AIAA Space and Astronautics Forum and Exposition 2016, Long Beach, CA, doi.org/10.2514/6.2016-5394, September 13–16, 2016.

3. ASTM D638-14, "Standard Test Method for Tensile Properties of Plastics," ASTM International, West Conshohocken, PA, doi.org/10.1520/D0638-14, 2014.

4. ASTM D695-15, "Standard Test Methods for Compressive Properties of Rigid Plastics," ASTM International, West Conshohocken, PA, doi.org/10.1520/D0695-15, 2015.

5. ASTM D790, "Standard Test Methods for Flexural Properties of Unreinforced and Reinforced Plastics and Electrical Insulating Materials," ASTM International, West Conshohocken, PA, 2015.

6. Prater, T.J.; Bean, Q.A.; Beshears, R.D.; et al.: "Summary Report on Phase I Results From the 3D Printing in Zero-G Technology Demonstration Mission, Volume 1," NASA/TP—2016–219101, NASA Marshall Space Flight Center, Huntsville, AL, 156 pp., July 2016.

7. Prater, T.J.; Bean, Q.A.; Werkheiser, N.; et al.: "Analysis of specimens from phase I of the 3D printing in Zero G technology demonstration mission," *Rapid Prototyping Journal*, Vol. 23, No. 6, pp. 1212–1225, doi.org/10.1108/RPJ-09-2016-0142, 2017.

8. Rodriguez, J.F.; Thomas, J.P.; and Renaud, J.E.: "Mechanical behavior of acrylonitrile-butadiene styrene (ABS) fused deposition materials: experimental investigation," *Rapid Prototyping Journal*, Vol. 7, No. 3, pp. 148–158, doi.org/10.1108/13552540110395547, 2001.

9. Sun, Q.; Rizvi, G.M.; Bellehumeur, C.T.; and Gu, P.: "Effect of processing conditions on the bonding quality of FDM polymer filaments," *Rapid Prototyping Journal,* Vol. 14, No. 2, pp. 72–80, doi:10.1108/13552540810862028, 1995.

10. Prater, T.J.; Bean, Q.A.; Werkheiser, N.; et al.: "A Ground-Based Study on Extruder Standoff Distance for the 3D Printing in Zero Gravity Technology Demonstration Mission," NASA/TP—2017–219631, NASA Marshall Space Flight Center, Huntsville, AL, 94 pp., June 2017.

11. Ziemian, C.; Sharma, M.; and Ziemian, S.: Chapter 7, "Anisotropic Mechanical Properties of ABS Parts Fabricated by Fused Deposition Modelling," in *Mechanical Engineering*, Dr. Murat Gokcek (Ed.), InTech, cdn.intechopen.com/pdfs/35261/InTech-Anisotropic_mechanical_properties_of_abs_parts_fabricated_by_fused_deposition_modelling.pdf, 670 pp., 2012.

12. Dinwiddie, R.B.; Love, L.J.; and Rowe, R.C.: "Real-time Process Monitoring and Temperature Mapping of a 3D Polymer Printing Process," *Proc. SPIE 8705, Thermosense: Thermal Infrared Applications XXXV*, 87050L, G.R. Stockton and F.P. Colbert (Eds.), doi:10.1117/12.1518454, May 22, 2013.

13. Prater, T.; Quincy, B.; Werkheiser, N.; and Ledbetter, F.: "NASA's In-Space Manufacturing Project: Materials and Manufacturing Process Development Update," *Proc. National Space and Missile Materials Symposium*, <https://ntrs.nasa.gov/search.jsp?R=20170008163 2018-01-30T15:07:49+00:00Z>, Palm Springs, CA, June 26–29, 2017.

14. *Additive Manufacturing Facility (AMF) User Guide,* Made in Space, <http://madeinspace.us/wp-content/uploads/AMF-User-Guide.pdf>, April 29, 2016.

15. Guthrie, P.: "'Sporks in Space': Bothell firm brings recycling to final frontier," *Herald Business Journal,* <www.heraldnet.com/business/sporks-in-space-bothell-firm-brings-recycling-to-final-frontier/>, August 24, 2016.

16. Prater, T.; Werkheiser, N.; and Ledbetter, N.: "Toward a Multimaterial Fabrication Laboratory: In-Space Manufacturing as an Enabling Capability for Long Endurance Human Space Flight," AIAA Space and Astronautics Forum 2017, Orlando, FL, September 12–14, 2017.

17. Snyder, R.: "Reversible Thermoset Materials for in situ Resource Utilization," *Proc. 2017 National Space and Missile Materials Symposium,* Indian Wells, CA, June 26–29, 2017.

18. "CRISSP— Customizable Recyclable International Space Station Packaging," Abstract from NASA SBIR STTR database, <www.sbir.gov/sbirsearch/detail/1148879>, 2015.

19. "In-Space Manufacturing (ISM) Multi-material Fabrication Laboratory (FabLab)," Broad Agency Announcement, <www.fbo.gov/index?s=opportunity&mode=form&tab=core&id=8a6ebb526d8bf8fb9c6361cb8b50c1f8&_cview=1<>, Solicitation Number: NNHZCQ001K-ISM-FabLab, April 11, 2017.

20. Warner, C.: "NASA Selects Three Companies to Develop 'FabLab' Prototypes," NASA Press Release 17-094, <www.nasa.gov/press-release/nas-selects-three-companies-to-develop-fablab-prototypes>, December 7, 2017.

REPORT DOCUMENTATION PAGE

Form Approved
OMB No. 0704-0188

1. REPORT DATE *(DD-MM-YYYY)*	2. REPORT TYPE	3. DATES COVERED *(From - To)*
01–03–2018	Technical Publication	

4. TITLE AND SUBTITLE

Summary Report on Phase I and Phase II Results From the 3D Printing in Zero-G Technology Demonstration Mission, Volume II

5a. CONTRACT NUMBER

5b. GRANT NUMBER

5c. PROGRAM ELEMENT NUMBER

6. AUTHOR(S)

T.J. Prater, N.J. Werkheiser, and F.E. Ledbetter III*

5d. PROJECT NUMBER

5e. TASK NUMBER

5f. WORK UNIT NUMBER

7. PERFORMING ORGANIZATION NAME(S) AND ADDRESS(ES)

George C. Marshall Space Flight Center
Huntsville, AL 35812

8. PERFORMING ORGANIZATION REPORT NUMBER

M–1457

9. SPONSORING/MONITORING AGENCY NAME(S) AND ADDRESS(ES)

National Aeronautics and Space Administration
Washington, DC 20546–0001

10. SPONSORING/MONITOR'S ACRONYM(S)

NASA

11. SPONSORING/MONITORING REPORT NUMBER

NASA/TP—2018–219855

12. DISTRIBUTION/AVAILABILITY STATEMENT

Unclassified-Unlimited
Subject Category 29
Availability: NASA STI Information Desk (757–864–9658)

13. SUPPLEMENTARY NOTES

Prepared by the Materials and Processes Laboratory, Engineering Directorate
*Wheelhouse Consulting, LLC, Marshall Space Flight Center

14. ABSTRACT

In-space manufacturing seeks to develop the processes, skill sets, and certification architecture needed to provide a rapid response manufacturing capability on long-duration exploration missions. The first 3D printer on the Space Station was developed by Made in Space, Inc. and completed two rounds of operation on orbit as part of the 3D Printing in Zero-G Technology Demonstration Mission. This Technical Publication provides a comprehensive overview of the technical objections of the mission, the two phases of hardware operation conducted on orbit, and the subsequent detailed analysis of specimens produced. No engineering significant evidence of microgravity effects on material outcomes was noted. This technology demonstration mission represents the first step in developing a suite of manufacturing capabilities to meet future mission needs.

15. SUBJECT TERMS

additive manufacturing, in-space manufacturing, microgravity materials processing, polymers, 3D printing

16. SECURITY CLASSIFICATION OF:			17. LIMITATION OF ABSTRACT	18. NUMBER OF PAGES	19a. NAME OF RESPONSIBLE PERSON
a. REPORT	b. ABSTRACT	c. THIS PAGE			STI Help Desk at email: help@sti.nasa.gov
U	U	U	UU	120	19b. TELEPHONE NUMBER *(Include area code)* STI Help Desk at: 757–864–9658

National Aeronautics and
Space Administration
IS02
George C. Marshall Space Flight Center
Huntsville, Alabama 35812